Triaxial octupole deformations and shell structure

W. D. Heiss and R. A. Lynch
Centre for Nonlinear Studies and Department of Physics, University of the Witwatersrand, PO Wits 2050, Johannesburg, South Africa

R. G. Nazmitdinov
Centre for Nonlinear Studies and Department of Physics, University of the Witwatersrand, PO Wits 2050, Johannesburg, South Africa;
Bogoliubov Laboratory of Theoretical Physics, Joint Institute for Nuclear Research, 141980 Dubna, Russia

(Submitted 11 March 1999)
Pis'ma Zh. Éksp. Teor. Fiz. **69**, No. 8, 525–530 (25 April 1999)

Manifestations of pronounced shell effects are discovered when nonaxial octupole deformations are added to a harmonic oscillator model. The degeneracies of the quantum spectra are in good agreement with the corresponding main periodic orbits and winding number ratios which are found by classical analysis. © *1999 American Institute of Physics.* [S0021-3640(99)00108-5]

PACS numbers: 21.60.Cs, 21.10.Ky, 21.10.Gv

The remarkable regularity of the rotational spectra of superdeformed nuclei has prompted many investigations into the contribution of higher multipoles to the formation of shell structure.[1] Related questions have arisen for other mesoscopic systems. In particular, it appears that octupole deformation has the same importance for two-dimensional systems like quantum dots and surface clusters[2] as for three-dimensional systems like nuclei[3] and metallic clusters.[4] Semiclassical analysis based on periodic orbit theory[5–7] provides substantial insight into the role of the octupole deformation for axially symmetric systems.[8–10] Axially symmetric octupole deformation, which leads to soft chaos in the classical case, produces short periodic orbits at particular parameter strengths, and, correspondingly, pronounced shell effects arise in the quantum spectrum.[8,9]

Conservation of angular momentum may increase the regular region for a nonintegrable problem with axial symmetry (see, for example, Ref. 11). The situation becomes more complicated for nonaxial systems with three degrees of freedom, since angular momentum is no longer a constant of motion and the classical dynamics may lead to a stronger degree of chaos.[12] Inclusion of exotic, i.e., nonaxial, octupole deformations renders the finding of pronounced shell effects rather difficult. Results based on the term $Y_{3\pm1}$, which was suggested by Mottelson[13] and studied in Ref. 14, have been questioned in Ref. 15. Other attempts which incorporate nonaxial octupole deformation start with axially symmetric potentials; they have found indications of shell effects using $Y_{3\mu}$ deformations mainly with $\mu=0,2$ (Refs. 15 and 16). The increasing accuracy of measurements of nuclear spectra, due to the new generation of detectors, gives substantial indications of strong octupole correlations.[3,17] This calls for a thorough analysis of non-

axial octupole deformations. A similar question about shell effects in electronic structures and their connection to octupole deformations arises from the *ab initio* calculations of the melting transitions in small alkali clusters.[18] In this letter we demonstrate the existence of strong shell effects which arise in the triaxial harmonic oscillator combined with nonaxial octupole deformations. The model may serve for a simple and transparent study of the effective mean field for mesoscopic systems like nuclei and metallic clusters. In addition, features characteristic of realistic potentials, i.e., a coexistence of regular and chaotic dynamics and the consequences for quantum mechanics, are addressed.

As in the procedure pursued in Ref. 8, we are guided by the study of the classical motion in obtaining the quantum mechanical results. The single-particle Hamiltonian considered reads

$$H=\frac{(\mathbf{p})^2}{2m}+\frac{m\omega^2}{2}\left[\left(\frac{x}{a}\right)^2+\left(\frac{y}{b}\right)^2+\left(\frac{z}{c}\right)^2+r^2\sum_{\mu}\lambda_{3\mu}Y_{3\mu}\right], \tag{1}$$

where the $Y_{\lambda\mu}$ are the usual spherical harmonics. To maintain time reversal invariance, only the combinations $Y_{3\mu}\pm Y_{3-\mu}$ are considered, with a factor i where appropriate. We take into account only one of the deformations $\mu=0,1,2,3$ at a time. For convenience, we express all quantities below in units of $\omega\equiv\omega_x$, i.e., $a=1$. If any of the parameters $\lambda_{3\mu}$ are nonzero, we are faced with a nonintegrable system. In fact, the problem gives rise to chaotic motion even at relatively small values of the octupole parameters. The parameters have to be limited by their respective critical values $\lambda_{3\mu}^{\mathrm{crit}}$ at which the potential no longer binds. The critical values depend on the parameters a, b, c, which can be expressed through standard quadrupole deformations $\epsilon_{2\mu}$, and, if more than one $\lambda_{3\mu}$ is considered, critical surfaces are obtained. It is obvious that a search for shell structure for the corresponding quantum mechanical problem becomes meaningless above the critical values, as then the quantum mechanical spectrum obtained by matrix diagonalization does not relate to the corresponding classical Hamiltonian.

The quadrupole shapes as determined by the parameters a, b, c are illustrated by the hexagonal figure given in Fig. 1. The three axes denoting axially symmetric prolate (oblate) shapes differ by an appropriate permutation of the coordinates x–y–z. For physical consideration it is therefore sufficient to consider just one sector if only quadrupole deformation is being studied.[6] However, the addition of an octupole term defines an orientation, since it refers to a specific z axis. Therefore, when adding, say, the term $r^2\lambda_{30}Y_{30}$, the physical situation is different for two oblate cases, for example, obl/x and obl/z in Fig. 1. Note that the latter case would preserve axial symmetry, thus making it effectively a system with two degrees of freedom. But the former case is now a genuine three-degrees-of-freedom system, since the symmetry axis of the quadrupole shape (the x axis) is different from the symmetry axis of $r^2\lambda_{30}Y_{30}$ (the z axis).

In the same vein, the addition of a term $r^2\lambda_{3\mu}Y_{3\pm\mu}$ to any of the axially symmetric quadrupole shapes gives rise to a three-degrees-of-freedom system for $\mu\neq 0$.

The effect of r^2Y_{30} upon the axes pro/z and obl/z has been dealt with in Ref. 8. In the present paper we begin with the combination $r^2(Y_{33}-Y_{3-3})$. Numerical analysis of the classical equations of motion (see below) reveals that the most regular motion occurs in the vicinity of the pro/x axis. The procedure used to approximate the nonintegrable classical system is the 'removal of resonances' method.[19] To lowest order it consists of

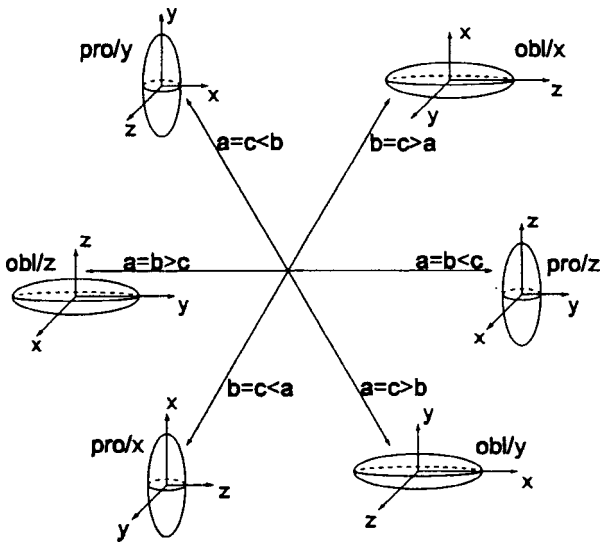

FIG. 1. Shapes in the *a, b, c* plane. Spherical symmetry ($a=b=c$) obtains at the center, while axially symmetric prolate and oblate shapes are obtained along the various axes. A genuine triaxial quadrupole deformation ($a\neq b\neq c$) occurs between the axes.

averaging the Hamilton function over the fastest angle of the unperturbed motion (all $\lambda_{3\mu}=0$) after rewriting the momenta and coordinates in terms of action–angle variables:

$$q_i=\sqrt{\frac{2J_i}{m\omega_i}}\sin\theta_i, \quad p_i=\sqrt{2J_i m\omega_i}\cos\theta_i, \quad \theta_i=\omega_i t, \quad i=x,y,z.$$

On the axis pro/x one would therefore average over θ_z or θ_y and above it over θ_z, since there $\omega_z>\omega_y>\omega_x$ ($a>b>c$). Based on the observation that $r^2(Y_{33}-Y_{3-3})$ is proportional to $x(x^2-3y^2)/r$, we expect the z motion to be weakly affected by this term. In the vicinity of the pro/x axis an averaging over θ_z is thus indicated. Moreover, for the reasons just given, an averaging over θ_z, which yields an effective potential in the x–y coordinates, is expected to make little difference from an effective potential obtained by simply setting $z=0$. This expectation is convincingly confirmed by numerical tests as long as $\omega_z\geqslant\omega_y$. In other words, for $\omega_z\geqslant\omega_y>\omega_x$, the motion effectively decouples into an unperturbed motion in the z coordinate (governed by the potential $mz^2\omega^2/(2c^2)$) and the two degrees of freedom motion in the x–y plane. Averaging now over the fast angle θ_y yields the unperturbed motion in the y coordinate (governed by $my^2\omega^2/(2b^2)$) and the effective potential for x, which reads

$$U_{\rm eff}(x)=\frac{m\omega^2}{2}\left[x^2+\lambda_{33}\frac{\mathrm{sign}(x)}{\pi}\left(2x^2K\left(-\frac{\xi_y^2}{x^2}\right)-3\pi\xi_y^2{}_2F_1\left(\frac{1}{2},\frac{3}{2},2;-\frac{\xi_y^2}{x^2}\right)\right)\right], \quad (2)$$

where K and ${}_2F_1$ denote the first elliptic integral and the hypergeometric function, respectively, and $\xi_y^2=2E_y/m\omega_y^2$, where $\omega_y=\omega/b$. The approximation used here assumes that E_y, the energy residing in the y motion, is constant (and therefore also E_x); note that the effective potential $U_{\rm eff}(x)$ depends on E_y. A numerical comparison between the true

three-dimensional motion and the approximate decoupled motion nicely confirms the validity of the approximation for $\lambda_{33} \lesssim \lambda_{\rm crit}/2$. The crucial test which is relevant for the corresponding quantum mechanical case is the comparison of the winding number ratios $\omega_x^{\rm eff}/\omega_y$ and $\omega_x^{\rm eff}/\omega_z$. Moreover, these ratios are virtually independent of E_y for E_y less than 60% of its maximal value $E_{\rm tot}$. As a result, we may evaluate $\omega_x^{\rm eff}$ analytically by choosing $E_y=0$ in Eq. (2) and obtain

$$\omega_x^{\rm eff}:\omega_y:\omega_z=\frac{2\sqrt{1-\lambda_{33}^2}}{\sqrt{1-\lambda_{33}}+\sqrt{1+\lambda_{33}}}:\frac{1}{b}:\frac{1}{c}. \tag{3}$$

By appropriately tuning the parameters b, c and λ_{33}, we can obtain simple ratios for the winding numbers. They determine short periodic orbits which are expected to occupy a major part of the phase space. For a two-dimensional problem the Poincaré surface of section can be used for estimation of the percentage of phase space occupied by periodic orbits. In the present situation, the five-dimensional phase space renders an understanding of the underlying structure rather difficult. The technique utilized here is essentially a frequency analysis. It is in principle impossible to determine whether a trajectory is quasi-periodic or chaotic merely by looking at the frequency spectra.[20] A pragmatic approach is adopted here in that an initial condition is deemed to yield a chaotic orbit if the associated frequency spectra have sufficiently many discernible peaks. We call an orbit chaotic if any one of the frequency spectra has more than six peaks with intensities greater than 1% of the maximum intensity. These arbitrary choices proved satisfactory for our purpose. If the orbit is quasi-periodic, then the most significant frequency peaks are compared and the approximate winding number and period are obtained. Repeating this procedure many times using different initial conditions in phase space yields a Monte Carlo-type estimate of the portions of phase space characterized by the various different frequency ratios. If a particular simple ratio dominates, as exemplified below, then we expect specific signatures in the quantum spectrum as shell structure. Examples are illustrated in Figs. 2, 3, and 4. We have chosen the numbers $a:b:c=1:0.5577:0.5577$, $1:0.3718:0.5577$ to obtain the ratios 1:2:2, 1:3:2 from Eq. (3), respectively. This ratio is sufficiently simple to make for an easy comparison with the quantum results.

The adiabatic approach predicts orbits with the frequency ratios 1:2:2 and 1:3:2 at $\lambda_{33}=0.5\lambda_{\rm crit}$. The corresponding spectra are displayed in Fig. 4. Classical frequency analysis (CFA) of the exact orbits shows a peak at $\lambda_{33}\approx 0.55\lambda_{33}^{\rm crit}$ for the ratios 1:2:2, 1:3:2, and the quantum shell structure occurring at $\lambda_{33}\approx 0.5\lambda_{33}^{\rm crit}$ has the correct degeneracy pattern for about the first hundred levels.

As a quantitative measure of the shell structure we use the Strutinsky-type analysis introduced in Ref. 8. From the quantity $\Delta E(\lambda,N)=\delta E(\lambda,N+1)+\delta E(\lambda,N-1)-2\,\delta E(\lambda,N)$, where δE is the fluctuating part of the total energy, we obtain the precise location of the magic numbers (see Fig. 4). Similarly, the whole discussion can also be applied to the axis pro/y in Fig. 1 by using the combination $r^2(Y_{33}+Y_{3-3})\sim y(y^2-3x^2)/r$ instead. It turns out that, due to the weak z dependence of the combinations $r^2(Y_{33}\pm Y_{3-3})$, it is mainly the x–y profile of the unperturbed harmonic oscillator that is important. The stronger the deformation in the x–y plane, i.e., the further away from the z-axial symmetry line (pro/z and obl/z), the better the adiabatic approximation and shell

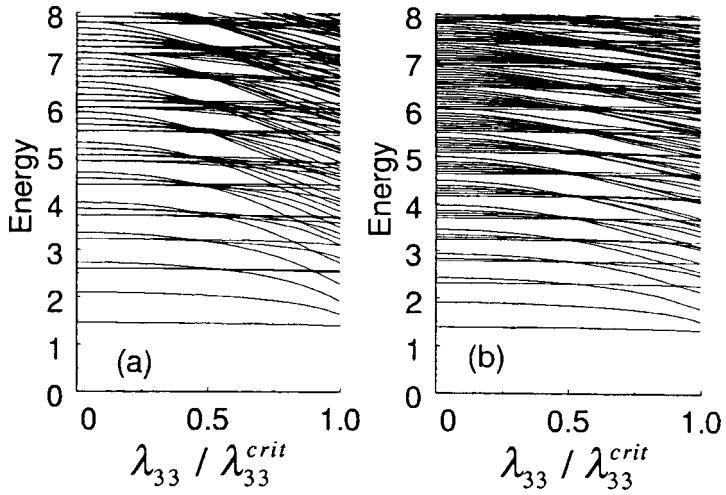

FIG. 2. Two quantum spectra: (a) for the parameters $b=c=0.5577$; (b) for the parameters $b=0.3718$, $c=0.5577$. Energies are given in units of $\hbar\omega$.

structure become. In contrast, along this horizontal line either $Y_{3\pm3}$ combination acts upon a circular potential in the $x-y$ plane and quickly introduces chaos. The CFA, applied to the combination $r^2(Y_{31}-Y_{3-1})\sim x(4z^2-x^2-y^2)$, reveals that the y motion is weakly affected for $\lambda_{31}\lesssim 0.6\lambda_{31}^{\rm crit}$ in the vicinity of the pro/x axis. Applying the analysis described above, we found that this term leads to shell effects similar to those of $r^2(Y_{33}-Y_{3-3})$. In fact, Eq. (3) holds for this combination as well. The plus combination $r^2(Y_{31}+Y_{3-1})$ is simply the minus combination under the interchange of x and y, and thus will produce the same effects near the region pro/y. It is important to note that the addition of a term $\lambda_{30}r^2Y_{30}$ to either situation, pro/x or pro/y, leads to the onset of

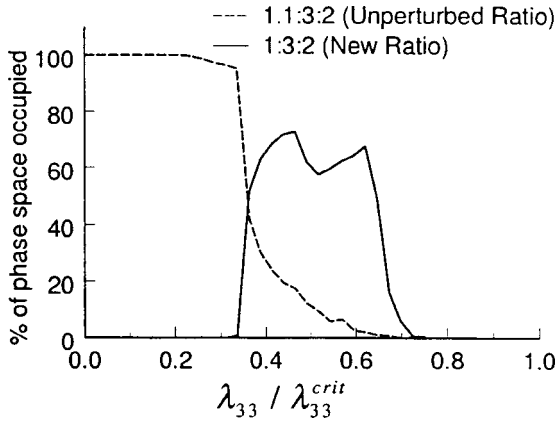

FIG. 3. Classical phase space occupation for the frequency ratios 1.1:3:2 and 1:3:2. The 1:3:2 peak at $\lambda_{33}/\lambda_{33}^{\rm crit}\approx 0.55$ leads to the shell structure displayed in Fig. 2b.

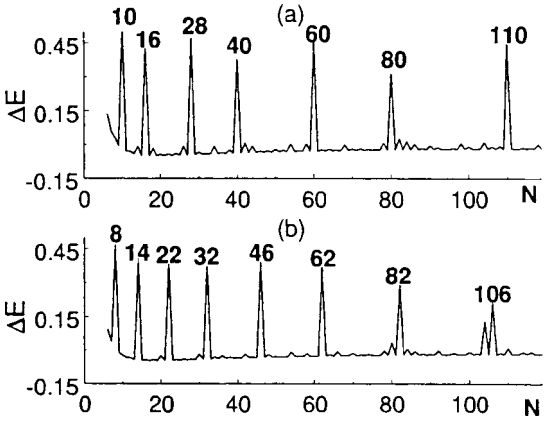

FIG. 4. Magic numbers calculated at the parameter values used for Fig. 2. The magic numbers corresponding to a pure quadrupole deformed harmonic oscillator are indicated in (a) for the ratio 1:2:2 and in (b) for the ratio 1:3:2.

chaos for rather small values of λ_{30}, and accordingly the quantum spectrum does not exhibit shell structure.

The two combinations $r^2(Y_{3\mu}\pm Y_{3-\mu})$ produce the same potential shape for the spherical case.[16] However, according to the analysis above, the plus and minus combinations have different effects for different sectors of the hexagonal figure (Fig. 1). The CFA shows that the adding of the octupole term $\lambda_{32}r^2(Y_{32}+Y_{3-2})$ gives rise to chaotic motion for comparatively small coupling values. In contrast, the term $\lambda_{32}r^2(Y_{32}-Y_{3-2})$ has less impact on the unperturbed motion, chaotic motion only becoming discernible for $\lambda_{32}\gtrsim 0.5\lambda_{\rm crit}$. Since $(Y_{32}-Y_{3-2})$ is symmetric with respect to an interchange of x and y, this result applies to the region above and below the axis pro/z, including the axes obl/x and obl/y. The quantum mechanical results are in accordance with the classical findings: the plain quadrupole spectrum changes weakly over a considerable range of λ_{32} when the term $r^2(Y_{32}-Y_{3-2})$ is added, while the order soon decays when the plus combination is switched on.

The cases considered here represent novel examples of *three-dimensional* nonintegrable systems, which can be well approximated by integrable ones. The results of the current literature are limited primarily to axially symmetric nonintegrable systems.[7,12] Special parameter values, found by the ''removal of resonances'' method, produce potentials conducive to regular classical motion in much of phase space. The various octupole combinations may have different effects on the generation of shell structure, depending on where the unperturbed potential lies in the hexagonal figure (Fig. 1). The effect of r^2Y_{30} upon the axis pro/z is similar to that of $r^2(Y_{33}\pm Y_{3-3})$ and $r^2(Y_{31}\pm Y_{3-1})$ upon the axis pro/x or pro/y. In contrast, the terms $r^2(Y_{32}\pm Y_{3-2})$ do not support shell structure. In this context we mention that the special combination $r^2\tilde{\lambda}(Y_{30}+3(Y_{32}+Y_{3-2}))$, when added to pro/z, is, after suitable permutation of the coordinates, identically equivalent to the adding of $r^2\lambda_{33}(Y_{33}-Y_{3-3})$ to pro/x. Thus we have generalized our previous result[8] to the domain of triaxiality in that the combination of quadrupole and *nonaxial* octupole deformations has been shown to lead to shell effects equivalent to

those from a plain quadrupole deformed potential, at least for the first one hundred levels. More comprehensive details of the classical frequency analysis, the adiabatic approach, and the quantum mechanical analysis will be presented in a forthcoming paper. Finally, we note that negative parity states observed in rare-earth nuclei with neutron number $N\sim 92$, which become yrast at high spins, need an unexpectedly strong degree of triaxiality (see Ref. 21) when described in terms of quadrupole and hexadecapole deformations only. We suggest that inclusion of an octupole deformation $r^2(Y_{33}-Y_{3-3})$ or a banana-type octupole deformation $r^2(Y_{31}-Y_{3-1})$, which effectively gives rise to shell effects of a triaxial oscillator, could yield a more natural explanation of these phenomena.

R. G. N. acknowledges financial support from the Foundation for Research Development of South Africa which was provided under the auspices of the Russian/South African Agreement on Science and Technology.

[1] S. Åberg, H. Flocard and W. Nazarewicz, Annu. Rev. Nucl. Part. Sci. **40**, 439 (1990).
[2] S. M. Reiman *et al.*, Phys. Rev. B **56**, 12147 (1997).
[3] P. A. Butler and W. Nazarewicz, Rev. Mod. Phys. **68**, 349 (1996).
[4] S. Frauendorf and V. V. Pashkevich, Ann. Physik (Berlin) **5**, 34 (1996); B. Montag *et al.*, Phys. Rev. B **52**, 4775 (1995); H. Häkkinen *et al.*, Phys. Rev. Lett. **78**, 1034 (1997).
[5] M. C. Gutzwiller, J. Math. Phys. **12**, 343 (1971); R. Balian and C. Bloch, Ann. Phys. (N.Y.) **69**, 76 (1972); V. M. Strutinsky *et al.*, Z. Phys. F **283**, 269 (1977).
[6] A. Bohr and B. Mottelson, *Nuclear Structure*, Vol. 2, Benjamin, New York, 1975.
[7] For a recent survey see M. Brack and R. K. Bhaduri, *Semiclassical Physics*, Addison and Wesley, Reading, Mass., 1997.
[8] W. D. Heiss, R. G. Nazmitdinov, and S. Radu, Phys. Rev. Lett. **72**, 2351 (1994); Phys. Rev. B **51**, 1874 (1994); Phys. Rev. C **52**, 3032 (1995).
[9] K. Arita and K. Matsuyanagi, Prog. Theor. Phys. **91**, 723 (1994); Nucl. Phys. F **592**, 9 (1995).
[10] S. C. Creagh, Ann. Phys. (N.Y.) **248**, 60 (1996).
[11] W. D. Heiss and R. G. Nazmitdinov, Physica D **118**, 134 (1998).
[12] M. C. Gutzwiller, *Chaos and Classical and Quantum Mechanics*, Springer, New York, 1990.
[13] B. R. Mottelson, *Proceedings of the Conference on High-Spin Nuclear Structure and Novel Nuclear Shapes*, Argonne, Ill., 13–15 April 1998, Argonne National Laboratory Annual Report ANL-PHY-88-2 (1988), p. 1.
[14] R. R. Chasman, Phys. Lett. B **266**, 243 (1991).
[15] J. Skalski, Phys. Lett. B **274**, 1 (1992).
[16] I. Hamamoto *et al.*, Z. Phys. D **21**, 163 (1991); F. Frisk *et al.*, Phys. Scr. **50**, 628 (1994).
[17] J. K. Hwang *et al.*, Phys. Rev. C **56**, 1344 (1997); G. J. Lane *et al.*, Phys. Rev. C **57**, R1022 (1998); J. F. Smith *et al.*, Phys. Rev. C **57**, R1037 (1998).
[18] A. Rytkönen, H. Häkkinen, and M. Manninen, Phys. Rev. Lett. **80**, 3940 (1998).
[19] A. J. Lichtenberg and M. A. Lieberman, *Regular and Stochastic Motion*, Springer, New York, 1983.
[20] R. S. Dumont and P. Brumer, J. Chem. Phys. **88**, 1481 (1988).
[21] K. P. Blume *et al.*, Nucl. Phys. **464**, 445 (1987); J. N. Mo *et al.*, Nucl. Phys. F **472**, 295 (1987); W. Schmitz *et al.*, Nucl. Phys. F **539**, 112 (1992); H. Schack-Peterson *et al.*, Nucl. Phys. F **594**, 175 (1995).

Published in English in the original Russian journal. Edited by Steve Torstveit.

Jump kinetics on the Fibonacci quasilattice. Exactly solvable model of the layer growth and dislocation kinetics in quasicrystals

M. A. Fradkin*
IMRS 6225 Montréal, Québec, H3S 2T5, Canada

(Submitted 5 January 1999; resubmitted 18 February 1999)
Pis'ma Zh. Éksp. Teor. Fiz. **69**, No. 8, 531–536 (25 April 1999)

The jump kinetics on a quasiperiodic pinning potential is analyzed under small external force in a 1D Fibonacci quasilattice model. The model describes planar (layer) growth of stable quasicrystals from the melt and is also relevant to the movement of quasicrystal dislocations under small stress. An exact solution is found for the spectrum of jump length as function of the driving force. The solution describes the supercooling dependence of the spectrum of nucleus heights on the growing surface of a quasicrystal. The spectrum appears to be universal and its shape has a periodic dependence on the logarithm of the supercooling. The resulting quasicrystal growth kinetics agrees well with that found in computer simulations and in the analysis of continuous thermodynamic models. © *1999 American Institute of Physics.*
[S0021-3640(99)00208-X]

PACS numbers: 61.44.Br, 61.72.Lk, 81.10.Aj

The dynamics of crystal growth is usually studied through the kinetic equation for a model Hamiltonian that involves a surface tension along with the pinning term.[1,2] The supercooling is a thermodynamic driving force and the kinetic coefficient corresponds to the surface mobility. The model describes a temperature-induced roughening transition between the smooth and rough states of the equilibrium surface as well as a dynamic roughening transition separating normal and layer growth mechanisms. A layer (planar) growth proceeds through the thermally activated nucleation of 2D nuclei followed by their lateral expansion via the movement of the surface steps.[3] Thus the surface jumps between minima of the pinning potential, the jump length being equal to the period of the pinning potential, i.e., the lattice period in the direction of growth. The growth rate in this case has an exponential dependence on the supercooling, in contrast with normal growth, where this dependence is linear.[2,3]

In the case of quasicrystals the pinning potential is quasiperiodic due to quasiperiodicity of their atomic structure. The thermodynamic roughening temperature appears to be infinite,[4,5] and, hence, the equilibrium surface remains smooth at any temperature. This corresponds to the experimentally observed growth shapes for stable quasicrystals and implies layer growth at sufficiently small supercoolings.[2] On account of the quasiperiodicity, the thickness of the growing layer of a quasicrystal can take values from a

dense set of ''interplane distances'' (Ref. 6). Thus, during growth of a quasicrystal under fixed supercooling there is some spectrum of thicknesses of the growing layer (nucleus heights).

In this paper I present the exact form of this nucleus height spectrum, obtained by solving the pinning problem on the 1D Fibonacci quasilattice. The model is also relevant to the movement of dislocations in quasicrystals under small stress due to the fact that intrinsic ''phason'' contribution to the energy of a dislocation leads to the quasiperiodic Peierls potential. This paper is organized as follows. After description of some features of quasicrystal growth and brief analysis of the dislocation mobility in quasicrystals, the 1D kinetic problem is formulated. The exact solution of this problem is then presented, followed by a discussion of its implications with respect to the available experimental data.

For conventional crystals the energy of any perturbation on a flat solid–liquid interface consists of the bulk supercooling term along with the free energy of a linear step, which has a large entropic contribution.[3] This entropic term makes the step free energy negative at temperatures above the thermodynamic roughening transition for conventional crystals. As the quasicrystal structure is not invariant under translations, there is an additional area-proportional contribution to the nucleus energy due to the difference in the surface energy between old and new positions of the surface.[7] A layer of thickness h can appear during the quasicrystal growth only if the corresponding ''effective supercooling''[7]

$$\Delta\mu_{\rm eff}(h,z)=\Delta\mu-\Delta\sigma(h,z)/h \tag{1}$$

is positive. Here $\Delta\mu=\mu_{\rm solid}-\mu_{\rm liquid}$ is the supercooling and $\Delta\sigma$ is the difference in surface energy. $\Delta\mu_{\rm eff}$ depends not only on the nucleus height h but on the current location z of a surface as well. The nucleus that will appear on the growing surface located at z for a given supercooling $\Delta\mu$ is selected by the smallest height h with positive $\Delta\mu_{\rm eff}(h,z)$ (Ref. 8).

The surface energy $\sigma(z)$ can be expressed[7] as $\sigma(z_{||})\propto z_{\perp}^{\,2}$, with $z_{||}$ and $z_{\perp}$ being the ''physical'' and ''orthogonal'' components of the 6D quasilattice vector $\mathbf{z}$ (Ref. 9). Then the effective supercooling takes the form

$$\Delta\mu_{\rm eff}(h)=\Delta\mu-A\frac{\Delta(z_{\perp}^{\,2})}{h}, \tag{2}$$

where $\Delta(z_{\perp}^{\,2})=(z+h)_{\perp}^{\,2}-z_{\perp}^{\,2}$. This expression for the effective supercooling leads to the power-law dependence of average nucleus height on the bulk supercooling:[7,8]

$$h\propto(\Delta\mu)^{-1/3}. \tag{3}$$

The dislocation movement in crystals is described by the thermodynamic model in a manner similar to the crystal growth. There are terms in Hamiltonian corresponding to a periodic pinning (Peierls barriers) and to the dislocation line tension. The nuclei correspond to dislocation kinks and the stress component in the glide plane plays a role of the supercooling. The dislocations in quasicrystals have a 6D Burgers vector,[10] and their

movement involves ''phason'' displacements which correspond to diffusionlike atomic rearrangement. Thus the dislocation movement in quasicrystals is not a glide but is like a ''creep''[11] accompanied by atomic diffusion.

The formation work for a dislocation kink is proportional to the product of the Burgers vector to the kink normal and the translation vector. As Burgers vector has phason component, contribution proportional to perpendicular component of the translation vector appears. Minimization of this work with respect to both the translation length and the orientation of the kink normal gives an expression for the activation energy similar to that for the nucleation barrier for quasicrystal growth. Thus the results for the planar growth of quasicrystals are relevant to the dislocation problem as well. The quasiperiodic pinning potential for dislocation movement was obtained in a computer simulation of the quasicrystal dislocations.[1)]

The problem has one spatial dimension which is the surface position in the direction of growth and can be analyzed within a simplified one-dimensional model. The cut-and-project method of generation of the atomic structure of quasicrystals[9] can be used to generate a 1D quasiperiodic sequence of the minima of pinning potential through the projection from a 2D square lattice. The ''physical space'' here is a straight line with a slope equal to the ''golden mean'' $\tau=(\sqrt{5}+1)/2$, and the node (p,q) is projected to the point

$$(p,q)_{||}=(p\tau+q)/\sqrt{\tau+2} \tag{4}$$

in the physical space if (p,q) falls within a parallel ''tube'' of width w:

$$|(p,q)_{\perp}|=\frac{|-p+q\tau|}{\sqrt{\tau+2}}<\frac{w}{2}=\frac{1}{2}\,\frac{\tau+1}{\sqrt{\tau+2}}. \tag{5}$$

The pinning potential at this point is defined in a manner similar to $\Delta\sigma(z)$, as $\mathcal{V}((p,q)_{||})=(p,q)_{\perp}^2$. It can be shown that for sufficiently small supercoolings this model is equivalent to the quasiperiodic pinning potential

$$\mathcal{V}(z)=-V_G(\cos(Gz)+\cos(Gz/\tau)), \tag{6}$$

used previously in a continuous model[8] and in a Monte Carlo simulation.[12]

The growth process can be fully characterized by a sequence of surface locations $(p,q)_{||}$ with the nucleus heights $h_{||}$ being the difference between two sequential positions. At any current point $(p,q)_{||}$ the next surface position is determined by the smallest $h_{||}$ satisfying the condition of positivity of the effective supercooling,

$$\Delta\mu_{\rm eff}(h)=\Delta\mu-\frac{((p,q)+\mathbf{h})_{\perp}^2-(p,q)_{\perp}^2}{h_{||}}>0. \tag{7}$$

Here $h_{||}$ corresponds to a unique 2D lattice vector $\mathbf{h}$ and the supercooling is measured in units such that the constant A in the expression (2) for $\Delta\mu_{\rm eff}$ disappears. Due to the irrational slope of the projection from the 2D square lattice there is a one-to-one correspondence between points of the ''physical'' and orthogonal space and, hence, the

growth process can be described by the surface locations in the ''perpendicular'' space. At every step the minimal jump length $h_{||}$ is selected from all lengths satisfying condition (7) that can be written as

$$h_{\perp}(p,q)_{\perp} < \frac{1}{2}(\Delta\mu\, h_{||} - h_{\perp}^2). \tag{8}$$

Since the nodes of the 2D square lattice form a dense set of points in the orthogonal space, the spectral weight of a particular $h_{||}$ is equal to the relative size occupied in this set by those $(p,q)_{\perp}$ at which the condition (8) leads to the selection of $h_{||}$.

The ratio of two sequential Fibonacci numbers f_{m+1}/f_m are known to give the best rational approximation to the ''golden mean'' τ. Then Eqs. (4) and (5) imply that a 2D square lattice vector of the kind $\mathbf{h}_m = (f_{m+1}, f_m)$ has the lowest ''orthogonal'' length $h_{\perp}$ from among all those with a comparable ''parallel'' component $h_{||}$, and the corresponding nucleus height is the lowest one satisfying the condition (8). Thus the nucleus height spectrum in this model of quasicrystal growth for sufficiently small supercoolings should include only heights $\mathbf{h}_m$ corresponding to the Fibonacci numbers. It has the form of a discrete set of peaks with spectral weights $\{x_m(\Delta\mu)\}$ determined by the supercooling $\Delta\mu$.

Using the definition of the Fibonacci sequence in recurrent form with $f_0 = 0$ and $f_1 = 1$, we can get from Eqs. (4) and (5)

$$h_{m_{||}} = \frac{\tau^{m+1}}{\sqrt{\tau+2}}, \quad h_{m_{\perp}} = (-1)^{m-1}\frac{\tau^{-m}}{\sqrt{\tau+2}}. \tag{9}$$

Introducing the following set of points in the ''perpendicular'' space

$$S_m = \frac{h_{m_{\perp}}}{2}(\Delta\mu\, \tau^{3m+1}\sqrt{\tau+2} - 1), \tag{10}$$

we can get the condition (8) in the form

$$(p,q)_{\perp} < S_m \quad \text{for} \quad h_{m_{\perp}} > 0 \tag{11a}$$

$$(p,q)_{\perp} > S_m \quad \text{for} \quad h_{m_{\perp}} < 0. \tag{11b}$$

At every location of the growing surface $(p,q)_{||}$ the nucleus height $h_{m_{||}}$ is selected according to the lowest m that satisfies condition (11).

Using (9), we can obtain from the definition (10) the following recurrent scaling law:

$$S_{m+1}(\tau^{-3}\Delta\mu) = -\tau^{-1} S_m(\Delta\mu). \tag{12}$$

As the jump lengths (9) satisfy similar recurrent relationships $h_{(m+1)_{\perp}} = -\tau^{-1} h_{m_{\perp}}$, this scaling holds for the set of points $(p,q)_{\perp}$ representing the surface position in perpendicular ''space'' satisfying (11). Since the appearance of a particular height in the spectrum is determined by the relative size of a subset of points $(p,q)_{\perp}$ satisfying Eq. (11) for particular m, such a scaling implies that the nucleus height spectrum has the following invariance:

$$x_{m+1}(\tau^{-3}\Delta\mu)=x_m(\Delta\mu). \tag{13}$$

Thus we need consider the supercooling only within the interval between $\Delta\mu^*\,\tau^{-3}$ and $\Delta\mu^*$ for some particular $\Delta\mu^*$. The spectrum for the all other $\Delta\mu$'s can be easily obtained through (13). Let us choose a value $\Delta\mu_m^*$ that corresponds to an equality $S_m = S_{m-1}$ for some odd m. Introducing the relative supercooling κ_m by $\Delta\mu=\kappa_m\,\Delta\mu_m^*$, we can obtain

$$S_{m+l}=\frac{h_{(m+l)_\perp}}{2}\left(\frac{\kappa_m\,\tau^{3\,(l+1)}}{\sqrt{5}}+1\right) \tag{14}$$

with

$$S_{m-1}+h_{(m-1)_\perp}<S_m<S_{m-1}<S_m+h_{m_\perp}. \tag{15}$$

Direct geometrical analysis of the condition (11) shows that regardless of the starting point, the perpendicular component of the surface position $(p,q)_\perp$ falls into the interval between $S_{m-1}+h_{(m-1)_\perp}$ and $S_m+h_{m_\perp}$ in a finite number of steps. For $(p,q)_\perp > S_m+h_{m_\perp}$ only jumps with negative $h_{(m+l)_\perp}$ are possible, and for $(p,q)_\perp<S_{m-1}+h_{(m-1)_\perp}$ only positive $h_{(m+l)_\perp}$ can occur. Once inside this interval, the point representing the surface remains confined and fills this interval closely on account of the irrational slope of the projection line. By comparing $\Delta\mu_{\rm eff}(h_{(m+l)_\parallel})$ for different l it is easy to see that for jumps of $h_{(m+l)_\perp}$ the surface position in perpendicular space $(p,q)_\perp$ should belong to the following intervals:

$$S_{m-1}<(p,q)_\perp<S_m+h_{m_\perp}, \quad l=-1, \tag{16a}$$

$$S_{m-1}+h_{(m-1)_\perp}<(p,q)_\perp<S_m, \quad l=0, \tag{16b}$$

$$S_m<(p,q)_\perp<S_{m-1}, \quad l=1, \tag{16c}$$

with only finite possible appearances of other $h_{(m+l)_\perp}$. The relative size of these intervals gives us the spectral weight of different peaks:

$$x_{m-1}(\kappa_m)=\frac{\kappa_m-\tau^{-3}}{\kappa_m+1}, \quad x_m(\kappa_m)=\frac{\kappa_m+\tau^{-3}}{\kappa_m+1}, \quad x_{m+1}(\kappa_m)=\frac{1-\kappa_m}{\kappa_m+1}. \tag{17}$$

All the other $h_{(m+l)_\perp}$ correspond to a finite number of points $(p,q)_\perp$. Such subsets have zero measure in the perpendicular space and thus do not contribute to the spectrum. The mean nucleus height in the spectrum (17) is given by the expression

$$h_{\rm mean}(\kappa_m)=2\,\tau^{(m-1)}\frac{\sqrt{3-\tau}}{\kappa_m-1}. \tag{18}$$

At the borders of the κ_m interval there are only two peaks:

$$x_{m-1}(\tau^{-3})=0, \quad x_m(\tau^{-3})=\frac{2\,\tau^{-3}}{1+\tau^{-3}}, \quad x_{m+1}(\tau^{-3})=\frac{1-\tau^{-3}}{1+\tau^{-3}}=\tau\,x_m(\tau^{-3}) \tag{19}$$

and

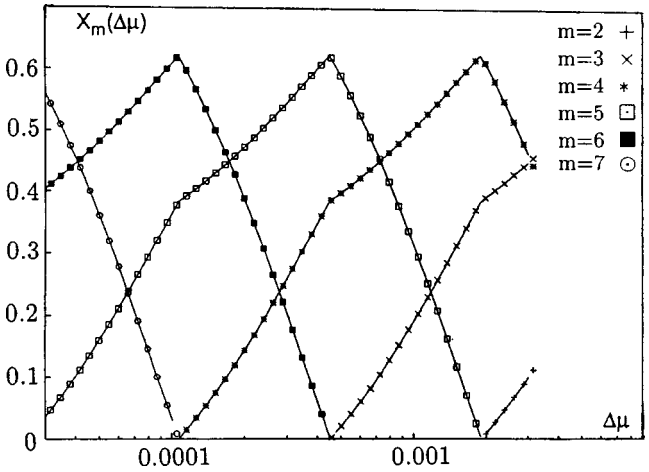

FIG. 1. The nucleus height spectrum calculated in the present model as a function of supercooling $\Delta\mu$ (full curves) in comparison with the results of a numerical simulation.

$$x_{m-1}(1)=\frac{1-\tau^{-3}}{2}, \quad x_m(1)=\frac{1+\tau^{-3}}{2}=\tau x_{m-1}(1), \quad x_{m+1}(1)=0. \tag{20}$$

For $\kappa_m>1$ a peak at $m-2$ appears, as does the $m+2$ peak for $\kappa_m<\tau^{-3}$.

The main features of this spectrum agree well with the results of a Monte Carlo simulation,[12] where a universal discrete spectrum corresponding to three subsequent Fibonacci numbers has been found for a quasiperiodic double-cosine pinning potential. The calculated spectrum is shown in Fig. 1 in a comparison with results of numerical calculations,[13] where a periodic dependence of the spectrum on the logarithm of $\Delta\mu$ was obtained with a period of $3\log\tau$. Figure 2 shows the periodic dependence of the mean

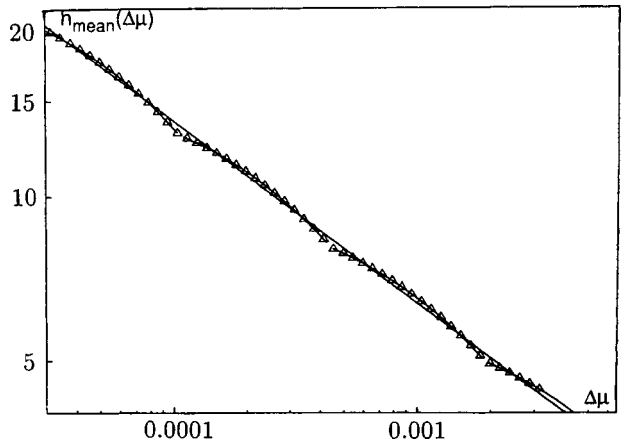

FIG. 2. Calculated dependence of the mean step height h_{mean} on $\Delta\mu$ in the present model (full curve) compared with numerical results (triangles). The straight line is a power-law dependence $h_{\text{mean}}\propto\Delta\mu^{-1/3}$.

nucleus height on the supercooling, with a small deviation from the power-law expression (3) obtained in a continuous model which appears to be a good average approximation for Eq. (18).

The discrete nature of the spectrum of nucleus heights leads to a steplike dependence of the growth rate on the supercooling.[12] Since the activation barriers for different $h_{m_{||}}$ differ by orders of magnitude,[7] the growth is controlled by the nucleation of the layer with maximal thickness. This means that when the supercooling $\Delta\mu$ varies in the interval between $\Delta\mu^*_{m+1}$ and $\Delta\mu^*_m$ the growth rate experiences small changes. However, when the supercooling passes through $\Delta\mu^*_m$, the highest peak corresponding to h_{m+2} disappears and the growth rate undergoes a drastic increase.

A similar pattern should appear in the case of quasicrystal dislocations, where the growth rate corresponds to the dislocation velocity. It should have small variations for stress values corresponding to the same peaks in the spectrum, with drastic changes around the critical stress at which new peaks appear in the spectrum. If the quasicrystal has a finite density of defects then the defects prevent the formation of kinks larger than some particular size. Hence, activation-driven movement of dislocations would not be possible at a stress level that implies the appearance of larger kinks in the spectrum of kink sizes.

Thus, unlike the case of the growth of quasicrystals, not only do the critical stress levels correspond to drastic changes in dislocation velocity, but the dislocations become frozen for a critical stress corresponding to some m. This permits an experimental test of the proposed model, since the stress level associated with drastic changes in the dislocation velocity should form a periodic pattern on a logarithmic scale, and the critical stress leading to the freezing of dislocations should belong to this pattern as well.

*On leave from Institute of Crystallography, Russian Academy of Sciences, 117333 Moscow, Russia.
e-mail: cu111@freenet.carleton.ca
[1)]R. Mikulla, private communication.

[1] S. T. Chu and J. D. Weeks, Phys. Rev. Lett. **40**, 733 (1978).
[2] P. Nosieres and F. Gallet, J. Phys. (France) **48**, 353 (1987).
[3] A. A. Chernov, *Modern Crystallography*, Vol. 3, Springer-Verlag, Berlin, 1981.
[4] A. Garg and D. Levine, Phys. Rev. Lett. **59**, 1683 (1987).
[5] R. Lipowsky and C. L. Henley, Phys. Rev. Lett. **60**, 2394 (1988).
[6] L. V. Mikheev, Phys. Lett. **132**, 137 (1988).
[7] M. A. Fradkin and A. A. Chernov, JETP Lett. **55**, 162 (1992).
[8] J. Toner, Phys. Rev. B **43**, 915 (1991).
[9] P. A. Kalugin, A. Yu. Kitaev, and L. S. Levitov, JETP Lett. **41**, 145 (1985).
[10] M. Kléman, in *Quasicrystalline Materials*, edited by Ch. Janot and J. M. Dubois, World Scientific, Singapore, 1988.
[11] L. D. Landau and E. M. Lifshitz, *Theory of Elasticity*, 3rd edition, Oxford, Pergamon, 1981.
[12] A. V. Artemyev and M. A. Fradkin, JETP Lett. **55**, 343 (1992).
[13] M. A. Fradkin, in *Proceedings of the International Conference on Aperiodic Crystals*, edited by G. Chapuis, World Scientific, Singapore, 1994.

Published in English in the original Russian journal. Edited by Steve Torstveit.

On the lower critical field and phase diagram of a thin cylindrical type-II superconductor

E. A. Shapoval*
All-Russia Scientific-Research Institute of the Metrological Service, 119361 Moscow, Russia

(Submitted 24 February 1999)
Pis'ma Zh. Éksp. Teor. Fiz. **69**, No. 8, 537–542 (25 April 1999)

The lower critical field $H_{c1}^{cyl}(T)$ of a superconducting cylinder with radius $r_0 \sim \xi(T) \ll \lambda(T)$ is found on the basis of the Ginzburg–Landau theory with various boundary conditions. These results together with the well-known results for the upper critical field are used to construct phase diagrams in terms of the field versus the reduced radius $r_0/\xi(T)$ variables. The jump in the average magnetization at $H_{c1}^{cyl}(T)$ is calculated as a function of the reduced radius. © *1999 American Institute of Physics.* [S0021-3640(99)00308-4]

PACS numbers: 74.60.Ec, 74.25.Dw

For the last few years a great deal of attention has been devoted to the experimental and theoretical investigation of mesoscopic objects. Specifically, the behavior of a superconducting disk in a magnetic field near the upper critical field, where the disk radius is of the order of the coherence length, is attracting great interest.[1–4] The upper critical field of continuous and hollow cylinders wtih various boundary conditions has been studied in Ref. 5, but the vortex structure of the superconducting cylinder or disk near the lower critical field thus far has been studied only in the London approximation, where the radius r_0 of the cylinder or disk is much greater than the coherence length $\xi(T)$.[6,7] Therefore the problem of calculating the lower critical field of a cylinder with $r_0 \sim \xi(T)$ remains open.

The present Letter is devoted to the calculation of the lower critical field, parallel to the axis of a continuous superconducting cylinder, and the jump in the average magnetization of the cylinder at this transition, where $r_0 \sim \xi(T) \ll \lambda(T)$ is the penetration depth, i.e. for $\kappa \gg 1$, on the basis of the Ginzburg–Landau (GL) theory. Two limiting cases of boundary conditions are considered: $(\nabla - 2ie\mathbf{A}) \cdot \Psi = 0$ and $\Psi = 0$. For the first boundary condition the results hold for a cylinder of arbitrary height, including a thin disk, and for the second condition they hold when the height of the cylinder is much greater than $\xi(T)$. Our results, together with the existing results for the upper critical field,[5] are used to construct phase diagrams in terms of the reduced external field versus the reduced cylinder radius.

Böbel[8] has found in the London approximation an expression for the lower critical field of a cylinder that is valid for cylinder radius $r_0 \gg \xi(T)$:

$$\frac{H_{c1}^{cyl}(T)}{\sqrt{2}H_c(T)}=\frac{1}{2\kappa}\left(\ln\kappa+C_1-\frac{K_0(r_0')}{I_0(r_0')}\right)\frac{I_0(r_0')}{I_0(r_0')-1}, \tag{1}$$

where, as usual in the GL theory, $r'=r/\lambda(T)$, i.e. length is measured in units of the penetration depth, K_0 and I_0 are modified Bessel functions, and the constant C_1 enters in the well-known Abrikosov expression for the lower critical field of a bulk type-II superconductor:[9]

$$\frac{H_{c1}(T)}{\sqrt{2}H_c(T)}=\frac{1}{2\kappa}(\ln\kappa+C_1). \tag{2}$$

There is still no concensus concerning the numerical value of this constant for $\kappa\gg 1$. Sometimes the value $C_1=0.081$, obtained in the original work Ref. 9, is used[8,10,11] though even Clem's simple variational method[12] gives $C_1\approx 0.52$, and the numerical solution of the nonlinear GL differential equation for an isolated vortex, undertaken by Hu,[13] gave $C_1=0.4968$. Our independent, i.e. even before we knew of Ref. 13, numerical solution of the GL differential equation using the Mathematica 2.2 program gave $C_1=0.496815$, and $C_0=-0.282276$, which appear in the expression for the field at the center of an isolated vortex:

$$\frac{H(T,0)}{\sqrt{2}H_c(T)}=\frac{1}{\kappa}(\ln\kappa+C_0). \tag{3}$$

Thus our results agree excellently with Ref. 13, where it was found that $C_0=-0.2823$.

Let us return to a cylindrical superconductor. Taking account of the behavior of the modified Bessel functions for small values of their arguments, we find from Eq. (1) that for $\kappa\gg 1$ and $\xi(T)\ll r_0\ll\lambda(T)$ the lower critical field

$$\frac{H_{c1}^{cyl}(T)}{H_{c2}(T)}\equiv h_{c1}^{cyl}=\frac{2}{\rho_0^2}(\ln\rho_0+0.380884),\quad 1\ll\rho\ll 1/\kappa. \tag{4}$$

Here we have introduced, and we shall employ below, the most convenient units of length and field intensity for our problem: $\rho=r/\xi(T)$ and $h=H/H_{c2}(T)$, where $H_{c2}(T)=\sqrt{2}\kappa H_c(T)=\phi_0/2\pi\xi^2(T)$ is the upper critical field of a bulk superconductor and ϕ_0 is the flux quantum. We call attention to the fact that in this region the lower field of a cylinder is independent of the penetration depth, increases with decreasing radius of the cylinder mainly as $1/r_0^2$, and approaches in order of magnitude the upper critical field as $r_0\to\xi(T)$.

To find the lower critical field of a cylinder with $r_0\sim\xi(T)$ we turn to the system of GL equations. Taking account of the symmetry of the problem we assume that the order parameter $\Psi(\rho,\varphi,z)=\Psi_0 f(\rho)e^{im\varphi}$. Then the GL free-energy functional in an external field h_0 is, to within a constant factor,

$$\mathcal{F}_H=\frac{2\pi}{\kappa^2}\int_0^{\rho_0}\left(f'^2+\left(A(\rho)-\frac{m}{\rho}\right)^2 f^2+\kappa^2 h(\rho)^2\right)\rho\,d\rho-2h_0\Phi, \tag{5}$$

where Φ is the flux of the field through the cross section of the cylinder

$$\Phi = 2\pi \int_0^{\rho_0} h(\rho)\rho\, d\rho. \tag{6}$$

Taking account of Maxwell's equations, the GL equations in our case have the form

$$\frac{1}{\rho}\frac{d}{d\rho}\left(\rho\frac{df}{d\rho}\right) - \left(A(\rho) - \frac{m}{\rho}\right)^2 f + f(1-f^2) = 0; \tag{7}$$

$$\frac{dh}{d\rho} = \frac{f^2}{\kappa^2}\left(A(\rho) - \frac{m}{\rho}\right); \quad h = \frac{d}{\rho d\rho}(\rho A(\rho)). \tag{8}$$

The boundary conditions for these equations are

$$f'(0) = 0 \quad \text{if } m = 0, \quad \text{or } f(0) = 0 \quad \text{if } m \neq 0, \quad h'(0) = 0, \tag{9}$$

$$f'(\rho_0) = 0 \text{ or } f(\rho_0) = 0, \quad h(\rho_0) = h_0.$$

As we have already stated, here we shall consider two limiting cases of boundary conditions at the surface of the cylinder: $f'(\rho_0) = 0$, which occurs on the boundary of an ordinary superconductor with a vacuum or dielectric, and $f(\rho_0) = 0$, which actually occurs at a boundary with a normal metal[14,15] or at the boundary of a *d* superconductor with diffuse reflection.[16]

It is evident from Eq. (8) that for large values of the parameter κ the additional field produced inside the cylinder by the Meissner and vortex currents is substantially weaker, of the order of $1/\kappa^2$ relative to the uniform external field h_0. This is entirely natural considering that the penetration depth is large compared to the radius of the cylinder. Therefore when $\kappa \gg 1$ this additional field can be neglected when solving the first GL equation (7), setting there $A(\rho) = h_0\rho/2$. This cannot be done when calculating the free energy (5) because of the third term in the integrand and the last term. However, integrating this expression by parts, using Eq. (7) and the boundary conditions (9) and calculating the additional field from Eq. (8), we obtain up to terms of second order in $1/\kappa$

$$\mathcal{F}_H = \pi \int_0^{\rho_0} (1 - f^4(\rho))\rho\, d\rho - \pi h_0^2 \rho_0^2. \tag{10}$$

From the condition that the free energies of the vortex-free and one-vortex states equal one another at the transition point it follows that for $H_0 = H_{c1}^{\text{cyl}}$

$$\int_0^{\rho_0} f_0^4 \rho\, d\rho = \int_0^{\rho_0} f_1^4 \rho\, d\rho, \tag{11}$$

where the index indicates the azimuthal number of the order parameter.

The computational results for the lower critical field as a function of the cylinder radius with the boundary condition $f'(\rho_0) = 0$ are shown in Fig. 1 (the bottom solid curve *1*), which shows the phase diagram including the normal (region *A*), vortex (region *B*), and vortex-free (region *C*) superconducting states. The bottom dashed curve *2* shows the asymptotic behavior of the lower critical field as $\rho_0 \to \infty$, described by the limiting expression of the London approximation (4).

The upper broken curve *3* in Fig. 1 represents the upper critical field, determined as the maximum field at which a nontrivial solution of the linearized first GL equation (7)

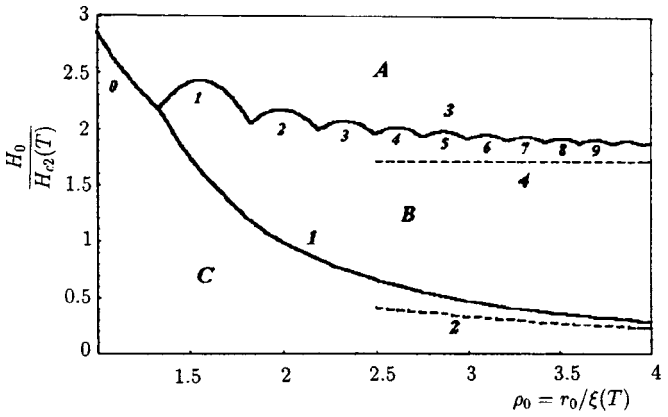

FIG. 1. Phase diagram of a cylinder under the condition $(\nabla - 2ie\mathbf{A})\cdot\Psi = 0$ at the surface of the cylinder. Region *A* — normal state, *B* — vortex state, *C* — vortex-free state. Lower solid curve *1* — reduced lower critical field $h_{c1}^{\rm cyl} = H_{c1}^{\rm cyl}(T)/H_{c2}(T)$ of the cylinder as a function of the reduced radius $\rho_0 = r_0/\xi(T)$ of the cylinder. Lower dashed curve *2* — asymptotic field, where $r_0 \gg \xi(T)$ (*4*). Upper broken curve *3* — reduced upper critical field $h_{c2}^{\rm cyl} = H_{c2}^{\rm cyl}(T)/H_{c2}(T)$ of the cylinder. The numbers below the sections of the curve indicate the azimuthal number, i.e. the multiplicity of the vortex. Upper dash curve *4* — asymptotic field, equal to the surface critical field of a bulk sample $h_{c3} = 1.695$.

first appears, when $f \to 0$, and $A(\rho) = h_0\rho/2$. The solution of this equation can be expressed in terms of a confluent hypergeometric function $\Phi(a,c;x)$ as[4,7]

$$f_m(\rho) = \rho^m \exp\left(-\frac{h_0\rho^2}{4}\right)\Phi\left(\frac{h_0-1}{2h_0}, m+1; \frac{h_0\rho^2}{2}\right). \tag{12}$$

Using the boundary condition $f'(\rho_0) = 0$ and the recurrence relations for the confluent hypergeometric function, a transcendental equation determining in an implicit form the dependence of the magnetic field on the cylinder radius and the azimuthal number m, determining the multiplicity of the central vortex, can be found as

$$(m+x)\Phi\left(\frac{h_0-1}{2h_0}, m+1, x\right) = 2m\Phi\left(\frac{h_0-1}{2h_0}, m, x\right), \tag{13}$$

where $x = h_0\rho_0^2/2$. Comparing for fixed ρ_0 the magnitude of the magnetic fields for various azimuthal numbers m, we choose the maximum value and thereby find the upper critical field of the cylinder as a function of the reduced radius of the cylinder. The numbers below the sections of the upper curve *3* in Fig. 1 indicate the corresponding azimuthal number m.

The oscillations of the upper critical field as a function of the cylinder radius resemble the Little–Parks oscillations for a hollow cylinder.[17] This is not surprising. The boundary condition $f'(\rho_0) = 0$ promote the appearance of surface superconductivity, the result of which is that the superconducting cylinder becomes in some way similar to a hollow cylinder. As one can see from the diagram in Fig. 1, the upper critical field of a continuous cylinder is higher than the surface field $H_{c3}(T)$ of a bulk sample, equal in our units to 1.695 and shown in Fig. 1 by the upper dashed line 4. It is also evident from this

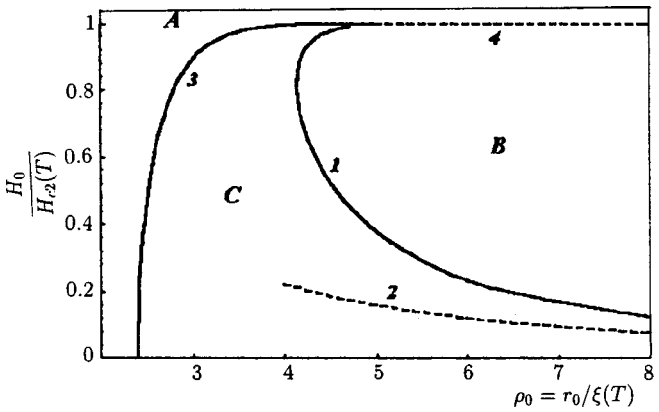

FIG. 2. Phase diagram of a cylinder under the boundary condition $\Psi=0$ at the surface. The notations are the same as in Fig. 1, except the upper dashed curve is the asymptotic upper critical field, equal here to the upper critical field of a bulk sample $h_{c2}=1$.

figure that for $\rho_0<1.333$ the cylinder passes from the normal state immediately into a vortex-free state, bypassing the mixed state where the field decreases.

The mixed state (region B) includes for $H_0>H_{c2}(T)$ phases with a gigantic vortex with different multiplicity m at the center of the cylinder. As the external field decreases, somewhere for $H_0<H_{c2}(T)$ such a gigantic vortex decoposes into single vortices, so that the cylinder passes into an Abrikosov phase.[3,18]

Figure 2 shows the phase diagram in the other limiting case of boundary conditions at the surface of the cylinder where $f(\rho_0)=0$. The notations in this diagram have the same meaning as above. An important difference is that here states with a gigantic vortex do not appear, and the upper critical field of the cylinder is less than the upper critical field $H_{c2}(T)$ of a bulk sample, in our units equal to $h=1$ and shown in the diagram by the upper dashed line 4. This is due to the suppression of superconductivity at the cylinder surface and a zero boundary condition. For the same reason the upper critical field vanishes when $\rho_0=r_0/\xi(T)=j_{01}=2.4048$ (the first zero of the zero-order Bessel function), which corresponds to the well-known decrease of the superconducting transition temperature in small samples with zero boundary conditions for the order parameter. If $\rho_0<4.14$, then as the external field decreases, the cylinder passes at $H=H_{c2}^{\rm cyl}(T)$ from the normal state immediately into a vortex-free superconducting state and remains in this state right down to zero field. However, if $\rho_0>4.14$, a thin cylinder first passes from the normal state into a superconducting vortex-free state (into the rapidly narrowing with increasing ρ_0 region C) and then at $H=H_{c1}^{\rm cyl}(T)$ (upper branch of curve *1*) it passes into the region of an Abrikosov state B and finally at $H=H_{c1}^{\rm cyl}(T)$ (bottom branch of curve *1*) once again into the vortex-free superconducting state C.

Thus one can judge, specifically, from the behavior of a cylinder in a magnetic field the boundary conditions at the cylinder surface and therefore the symmetry of the order parameter. It is obvious that the results obtained hold for a cylinder of arbitrary height if $(\nabla-2ie\mathbf{A})\cdot\Psi=0$ on the flat surfaces, while for $\Psi=0$ they are valid as long as the height of the cylinder is much greater than the coherence length.

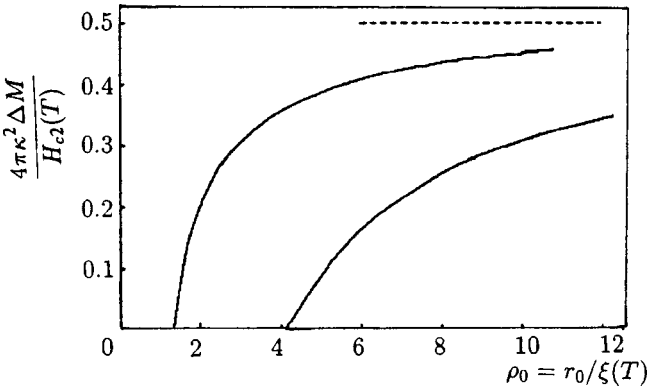

FIG. 3. Jump in the average reduced magnetization $4\pi\kappa^2\langle\Delta M\rangle/H_{c2}(T)$ as a function of the reduced radius. Curve *1* – under boundary condition $(\boldsymbol{\nabla}-2ie\mathbf{A})\cdot\boldsymbol{\Psi}=0$, curve *2* — boundary condition $\boldsymbol{\Psi}=0$. Dashed curve *3* — their asymptotic value (16) for large ρ.

To calculate the magnetization of a very thin cylinder, the case considered here, one can set once again $A(\rho)=h_0\rho/2$ on the right-hand side of the second GL equation (8) to accuracy $1/\kappa^2$. Then the average magnetization of the cylinder in the one-vortex state is

$$\frac{4\pi<M>}{H_{c2}(T)}=\frac{<B>-H_0}{H_{c2}(T)}=\frac{1}{2\kappa^2}\left(\frac{2}{\rho_0^2}\int_0^{\rho_0}f^2\rho\,d\rho-\frac{h_0}{\rho_0^2}\int_0^{\rho_0}f^2\rho^3\,d\rho\right). \tag{14}$$

The first term on the right-hand side determines the magnetic moment produced by the vortex currents and the second term determines the moment produced by the Meissner screening currents. Therefore the same expression but without the first term holds in the vortex-free state. Since $H_{c2}(T)\sim\kappa^2 H_{c1}(T)$, the average magnetization is of the order of the lower critical field in a bulk sample.

It follows from Eq. (14) that the jump in the average magnetization at a transition from a vortex-free into a one-vortex state is

$$4\pi\frac{<\Delta M>}{H_{c2}(T)}=\frac{<\Delta B>}{H_{c2}(T)}=\frac{1}{2\kappa^2}\left(\frac{2}{\rho_0^2}\int_0^{\rho_0}f_1^2\rho\,d\rho-\frac{h_{c2}^{cyl}}{\rho_0^2}\int_0^{\rho_0}(f_1^2-f_0^2)\rho^3\,d\rho\right). \tag{15}$$

For $\lambda(T)\gg r_0\gg\xi(T)$ (i.e. $\kappa\gg\rho_0\gg1$) we find from Eq. (15)

$$4\pi\frac{<\Delta M>}{H_{c2}(T)}=\frac{<\Delta B>}{H_{c2}(T)}=\frac{1}{2\kappa^2}, \tag{16}$$

where h_{c2}^{cyl} is determined by Eq. (14). This result is, of course, identical to that obtained in the London approximation.[8]

Figure 3 shows the jump in the average reduced magnetization as a function of the reduced radius under the boundary conditions $f'=0$ (upper solid curve *1*) and $f=0$ (lower solid curve *2*). The dashed curve *3* shows their asymptotic behavior (16) in the limit $\rho_0\to\infty$. We call attention to the fact that under the second boundary condition the magnetization jump (curve *2*) changes sign at $\rho_0=4.14$, which is shown in greater detail in Fig. 4. The lower branch of this curve corresponds to the upper branch of the lower

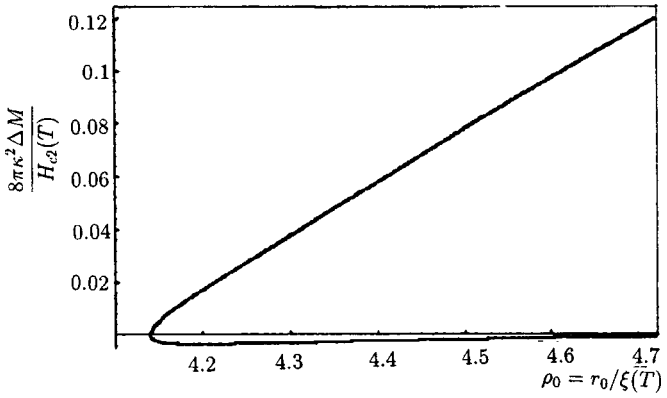

FIG. 4. Enlarged representation of the magnetization jump near $\rho = 4.14$ under the second boundary condition.

critical field (curve *1*) in Fig. 2. This effect can apparently be observed for a thin cylinder enclosed in a shell consisting of a normal metal, thereby providing the required boundary condition $\Psi = 0$.

Just as in the case of the field, the results obtained for the magnetization jump hold for a cylinder of arbitrary height with the restriction indicated above.

This work is supported by the Scientific Council on the Direction ''Superconductivity'' of the State Scientific and Technical Program ''Current Directions in Condensed-Media Physics'' as part of project No. 96024 and was performed at the P. N. Lebedev Center for Physical Studies.

*e-mail: shap@mics.msu.su

[1] A. K. Geim, I. V. Grigorieva, S. V. Dubonos *et al.*, Nature (London) **390**, 259 (1997).
[2] V. A. Schweigen and F. M. Peeters, Phys. Rev. B **57**, 13817 (1998).
[3] V. V. Moshchalkov, L. Gielen, C. Strunk *et al.*, Nature (London) **373**, 319 (1995).
[4] V. V. Moshchalkov, X. G. Qui, and V. Bruyndonex, Phys. Rev. B **55**, 11793 (1997).
[5] N. C. Constatinou, M. Masale, and D. R. Tilley, J. Phys.: Condens. Matter **4**, 4499, L293 (1992).
[6] A. S. Krasilnikov, L. G. Mamsurova, K. K. Puchov *et al.*, Physica C **235-240**, 2859 (1994); Supercond. Sci. Technol. **8**, 1 (1995).
[7] A. I. Buzdin and J. P. Brison, Phys. Lett. A **196**, 267 (1994).
[8] G. Böbel, Nuovo Cimento B **38**, 1740 (1965).
[9] A. A. Abrikosov, Zh. Éksp. Teor. Fiz. **46**, 1464 (1964) [Sov. Phys. JETP **19**, 988 (1964)].
[10] A. A. Abrikosov, *Foundations of the Theory of Metals* (North-Holland, Amsterdam, 1988) [Russian original, Nauka, Moscow, 1987].
[11] O. N. Shevtsova and S. V. Shiyanovskii, Phys. Stat. Sol. B **207**, 455 (1998).
[12] J. R. Clem, J. Low Temp. Phys. **18**, 427 (1975).
[13] Chia-Ren Hu, Phys. Rev. B **6**, 1756 (1972).
[14] P. G. de Gennes and J. Matricon, Rev. Mod. Phys. **36**, 45 (1964).
[15] R. O. Zaĭtsev, Zh. Éksp. Teor. Fiz. **48**, 664 (1965) [Sov. Phys. JETP **21**, 426 (1965)]; ibid., 1759 (1965) [ibid., 1178 (1965)].
[16] E. A. Shapoval, JETP Lett. **64**, 381 (1996).
[17] W. A. Little and R. D. Parks, Phys. Rev. Lett. **9**, 9 (1962).
[18] H. J. Fink and A. G. Presson, Phys. Rev. **151**, 219 (1962).

Translated by M. E. Alferieff

Intersubband collective excitations in quasi-two-dimensional systems in a strong magnetic field

V. E. Bisti*

Institute of Solid-State Physics, Russian Academy of Sciences, 142432 Chernogolovka, Moscow Region, Russia

(Submitted 25 February 1999)
Pis'ma Zh. Éksp. Teor. Fiz. **69**, No. 8, 543–547 (25 April 1999)

The spectrum of intersubband collective excitations of spin and charge density in a system of quasi-two-dimensional electrons is calculated in the strong magnetic field limit for filling factors $\nu \leqslant 4$. For $\nu \geqslant 2$ two new closely spaced modes of collective excitations are obtained. The modes obtained make it possible to give a new interpretation of the experimentally observed line, which is usually interpreted as being due to single-particle excitations. © *1999 American Institute of Physics.* [S0021-3640(99)00408-9]

PACS numbers: 73.20.Mf, 71.45.Lr

The properties of quasi-two-dimensional electrons in systems such as inversion layers, single quantum wells, and superlattices have been attracting a great deal of attention from investigators in the last few years. A characteristic feature of such systems, which is of interest to both theoreticians and experimenters, is the appearance of collective excitations of a special kind due to the presence of several size-quantization levels. The specific collective excitations associated with intersubband transitions are intersubband plasma oscillations or charge-density waves (CDE) and spin-density waves (SDE). This problem in the absence of a magnetic field has been investigated theoretically in Refs. 1–7. In the random-phase approximation (RPA), together with the standard two-dimensional plasmons, CDE (intersubband plasmons) were obtained.[1,2] Taking account of the exchange interaction of the electrons made it possible to obtain excitations of a second type — SDE.[3–7] The exchange interaction was taken into account in the local-density approximation (LDA)[3,4] as well as by direct methods.[5–7] Collective excitations in a magnetic field (intersubband and intrasubband magnetoplasmons) have been studied in the RPA and LDA.[8–10] Infrared absorption and resonance Raman scattering methods are used to study SDE and CDE experimentally.[11–16]

Lines due to scattering by collective excitations of the spin and charge densities as well as an intense line located between these excitations are observed in the intersubband Raman scattering spectra in a magnetic field.[13–16] This line is interpreted in most cases as being due to single-particle excitations (SPE).[13,14] However, it is indicated in Refs. 15 and 16 that the polarization and spectral characteristics of the SPE line are at variance with the standard interpretation of this line in terms of single-particle excitations, and its nature is not entirely clear.

In the present Letter the spectrum of intersubband collective excitations in a strong magnetic field is calculated by the direct method in the Hartree–Fock approximation. It is shown that the number of collective modes depends on the filling factor. Thus, for $\nu \leqslant 2$ two types of excitations — CDE and SDE — occur in the system. For $\nu > 2$ four types of excitations are obtained, two CDE and two SDE. Besides the ordinary CDE and SDE, two new, closely spaced modes of collective excitations appear. The appearance of these modes is associated with the filling of the second Landau level. This makes it possible to give a new explanation of the SPE line appearing in a magnetic field for[1)] $\nu > 2$. This is not a single unpolarized SPE line, but rather two almost coincident CDE and SDE lines.

The spectrum of intersubband collective excitations is sought as a function of the magnetic field H under the following conditions.

1. Two size-quantization subbands are present in the system. All other subbands can be neglected. The density n_s of two-dimensional electrons is such that the lower subband E_0 is filled and the next subband E_1 is empty. The energies E_0 and E_1 are calculated in the Hartree approximation.

2. A strong quantizing magnetic field H perpendicular to the two-dimensional layer is present. The region of strong magnetic fields, for which $0 < \nu \leqslant 4$, is studied.

3. Only processes without spin flip are taken into account. For simplicity the g factor of the electrons is assumed to be $g = 0$ ($\mu_0 g \ll T$, T is the temperature of the system), but the spin degeneracy is included in the calculation.

4. The long-wavelength limit $ka \ll 1$, $ka_H \ll 1$ (a — width of the quantum well, $a_H = (\hbar c/eH)^{1/2}$ — magnetic length) is considered.

5. The energy scales are such that $T \ll |E_{CD} - E_{10}|$, $|E_{SD} - E_{10}| \ll \hbar\omega_C$, E_{10} ($E_{10} = E_1 - E_0$, $\omega_c = eH/mc$ — cyclotron frequency).

6. The width of the Landau levels, which is due to the interaction with impurities, is small compared with temperature (this corresponds to the experimental situation, where the width of the lines due to Raman scattering by CDE and SDE is small compared with T).

The energies of the collective excitations are poles of the total polarization operator $\Pi(\mathbf{k}, \omega)$. Let us consider the intersubband polarization operator (in the long-wavelength limit the inter- and intrasubband excitations can be studied independently):

$$\Pi_{01}(\mathbf{k}, \omega) = \sum_{n,n',\sigma,} \Pi_{0n,1n',\sigma}(\mathbf{k}, \omega) = \sum_{n,n',\sigma} \sum_{m,m',\sigma'} \Pi^{0m,1m',\sigma'}_{0n,1n',\sigma}(\mathbf{k}, \omega), \tag{1}$$

where m, m', n, and n' are the numbers of the Landau levels.

For an integer filling factor all energy-degenerate Landau levels are filled with probability 1. Let us assume that even with an arbitrary filling factor the Landau levels are equally likely to be filled because their width is small compared with temperature (condition 6 holds). In waht follows we shall employ the Green's functions technique for $T = 0$. Comparing E_{CD} in the RPA approximation, calculated by the proposed method, with the result obtained in Ref. 10 using the temperature technique shows that them to be equivalent under the indicated assumptions.

The system of equations for $\Pi_{0n,1n',\sigma}$ includes summation of ladder and loop diagrams describing, respectively, the excitonic and depolarization effects. Exchange corrections to the self-energy part are included in the single-particle Green's functions. This set of diagrams, which corresponds to the Hartree–Fock approximation, was taken into account in Refs. 5–7, which are devoted to the calculation of intersubband collective excitations in the absence of a magnetic field and in the analysis of magnetoplasmon excitations in purely two-dimensional systems[17,18] and partially in Ref. 19 in an analysis of the Mott exciton in quasi-two-dimensional semiconductors in a strong magnetic field. In this approximation the single-particle Green's functions in a magnetic field depend only on frequency, and the interaction depends only on the momenta. Therefore the interaction can be averaged over the momenta and the system becomes algebraic.

The following two types of interactions are present:

$$\alpha_{0n,1n'\sigma}^{0m,1m',\sigma'}(k)=V_{01}^{01}(k)I_{nn'}(k,0)I^{*}_{m'm}(k,0)=\alpha_{nn'}^{mm'}(k),\quad \alpha_{nn'}^{mm'}(0)=V_{01}^{01}(0)\,\delta_{nn'}\delta_{mm'}, \tag{2}$$

which determines the depolarization shift, and

$$\beta_{0n,1n',\sigma}^{0m,1m',\sigma'}(k)=-\delta_{\sigma\sigma'}(2\pi)^{-1}\int V_{00}^{11}(q)J_{nm}(\mathbf{q})J^{*}_{n'm'}(\mathbf{q})e^{ia_H^2q_yk}d\mathbf{q}=\delta_{\sigma\sigma'}\beta_{nn'}^{mm'}(k), \tag{3}$$

$$\beta_{nn'}^{mm'}(0)=\beta_{nn'}^{mm'}\delta_{n-n',m-m'},\quad \beta_{nn}^{mm}=-(2\pi)^{-1}\int V_{00}^{11}(q)|I_{nm}(\mathbf{q})|^2d\mathbf{q},$$

which determines the excitonic corrections. Here

$$V_{ik}^{jl}(q)=\frac{2\pi e^2}{\varepsilon q}\int \exp(-q|z_1-z_2|)\psi_i(z_1)\psi_k(z_1)\psi_j(z_2)\psi_l(z_2)dz_1dz_2, \tag{4}$$

where i, j, k, and l are subband indices and $\psi_i(z)$ are electron wavefunctions in the direction of the quantization axis, and

$$\begin{aligned} &I_{nn'}(q_x,q_y)=\int \phi_n(y)\phi_{n'}(y+q_xa_H^2)\exp(-iq_yy)dy,\\ &\phi_n(y)=\pi^{-1/4}(a_H2^nn!)^{-1/2}\exp(-y^2/2a_H^2)H_n(y/a_H), \end{aligned} \tag{5}$$

where H_n are Hermite polynomials and the x axis is directed along $\mathbf{k}$.

For $k=0$ the transitions of interest to us between the corresponding Landau levels from different subbands ($m=m'$, $n=n'$) can be studied independently of transitions with a change in the Landau level. The conditions (4) and (5) make it possible to study them independently for $k\neq 0$ also. The system of equations for $\Pi_{0n,1n,\sigma}$ becomes finite ($[\nu]+1$ equations in all). To find the poles we equate to zero the determinant of this system

$$\begin{aligned} &\det|\Pi_{0n,1n,\sigma}^{0}V_{0n,1n,\sigma}^{0m,1m,\sigma'}-\delta_{n\sigma,m\sigma'}|=0,\\ &V_{0n,1n,\sigma}^{0m,1m,\sigma'}=\alpha_{nn}^{mm}+\beta_{nn}^{mm}\delta_{\sigma\sigma'}. \end{aligned} \tag{6}$$

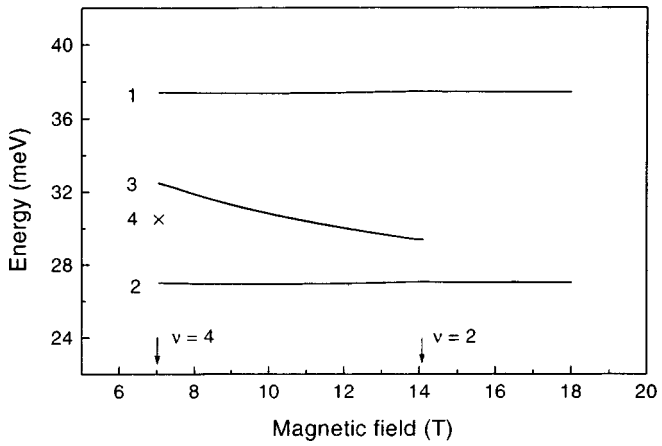

FIG. 1. Dependence of the energies of intersubband collective excitations of a system of two-dimensional electrons in a single 250 Å wide quantum well ($n_s = 6.8 \times 10^{11}$ cm^{-2}) versus the perpendicular magnetic field: *1* — CDE, *2* — SDE, *3* — CDE1 and SDE1, *4* — CDE2 and SDE2 (calculated for one value of the field $\nu = 4$).

The zeroth polarization operators, including exchange corrections, are

$$\Pi^0_{0n,1n,\sigma} = \frac{n_{n\sigma}}{\omega - E_{10} - \Sigma_{10,n\sigma}}; \quad \Sigma_{10,n\sigma} = \Sigma_{1n\sigma} - \Sigma_{0n\sigma}, \tag{7}$$

where $n_{n\sigma}$ is the density of electrons in the $(0,n,\sigma)$ level. For $g = 0$ $n_{m,1/2} = n_{m,-1/2}$.

The exchange corrections to the single-particle energies have the form

$$\Sigma_{in\sigma} = \sum_m \varepsilon^{0i}_{nm} n_{m\sigma}, \quad \varepsilon^{0i}_{nm} = -(2\pi)^{-1} \int V^{0i}_{0i}(q) |I_{nm}(\mathbf{q})|^2 d\mathbf{q} \quad (i = 0,1). \tag{8}$$

If only the spin sublevels of the zeroth Landau level are filled ($\nu \leqslant 2$, $n_{0,1/2} = n_{0,-1/2} = n_s/2$), we obtain that the existence of two types of particles in the system leads to the existence of two types of collective excitations — CDE and SDE with energies E_{CD} and E_{SD}. CDE are excitations with $S = 0$ and SDE are excitations with $S = 1$ and $S_z = 0$ (by virtue of the condition 3). They can also be interpreted as in-phase and antiphase intersubband transitions of particles with different spins.

For $2 < \nu \leqslant 4$ we obtain that, besides the basic CDE and SDE, two additional modes with close energies, CDE1 and SDE1, appear between SDE and CDE. These modes can be interpreted, though not completely correctly, as antiphase transitions of particles from different Landau levels. Therefore the appearance of the new types of particles leads to the appearance of new types of collective excitations.

Figure 1 shows as an example the spectrum of collective excitations for a rectangular GaAs/AlGaAs quantum well ($a = 250$ Å ; $n_s = 6.8 \cdot 10^{11}$ cm^{-2}) with $k = 0$ in the magnetic field range corresponding to $\nu \leqslant 4$. One can see that E_{CD} and E_{SD} are essentially independent of H, while E_{CD1} and E_{SD1}, starting not far from E_{SD}, have an appreciable slope, which qualitatively agrees with experiment.[16,17] It should be underscored that the modes CDE1 and SDE1, which coincide in the figure, are actually nondegenerate.

Similarly, the spectrum of collective excitations for any ν can be found from Eq. (6). New modes will arise every time for even values of ν. The modes will arise in pairs, CD and SD types, and lie approximately in the same location as CDE1 and SDE1. The point where the pairs of modes CDE2 and SDE2 with $\nu=4$ appear is shown in the figure. We note that the appearance of modes in pairs and the strict division of the excitations into CDE and SDE occurs only if the electronic system is spin-unpolarized. However, in any case the appearance of a particles of a new type in the system should be accompanied by the appearance of a new mode of collective excitations.

In summary, in the present Letter the spectrum of collective excitations in a strong magnetic field was calculated assuming that the energy-degenerate levels at low but finite temperature are filled with equal probability. The proposed method makes it possible to obtain the complete spectrum of intersubband collective excitations as a function of the magnetic field and to give a new interpretation of the line previously attributed to SPE. It is asserted that all observed modes are collective.

I thank S. V. Iordanskii for helpful discussions, I. V. Kukushkin for his unfailing attention to this work, and L. V. Kulik and O. V. Volkov for assistance in the numerical calculations.

This work was supported in part by the Russian Fund for Fundamental Research (Project 98-02-16659).

*e-Mail: bisti@issp.ac.ru

[1)]I. V. Kukushkin, private communication.

[1] Jainendra K. Jain and S. Das Sarma, Phys. Rev. B **36**, 5949 (1987).
[2] D. H. Ehlers, Phys. Rev. B **38**, 9706 (1988).
[3] S. Das Sarma and I. K. Marmorkos, Phys. Rev. B **47**, 16343 (1993).
[4] I. K. Marmorkos and S. Das Sarma, Phys. Rev. B **48**, 1544 (1993).
[5] S. L. Chuang, M. S. C. Luo, S. Schmitt-Rink *et al.*, Phys. Rev. B **46**, 1897 (1992).
[6] M. S.-C. Luo, S. L. Chuang, S. Schmitt-Rink *et al.*, Phys. Rev. B **48**, 11086 (1993).
[7] J. C. Ryan, Phys. Rev. B **43**, 12406 (1991).
[8] K. W. Chui and J. J. Quinn, Phys. Rev. B **9**, 4724 (1974).
[9] A. Tselis, J. J. Quinn, Surf. Sci. **113**, 362 (1982).
[10] L. Wendler and R. Pechstedt, J. Phys.: Condens. Matter **2**, 8881 (1990).
[11] D. Gammon, B. V. Shanabrook, J. C. Ryan *et al.*, Phys. Rev. B **41**, 12311 (1990).
[12] D. Gammon, B. V. Shanabrook, J. C. Ruan *et al.*, Phys. Rev. Lett. **68**, 1884 (1992).
[13] G. Brozak, B. V. Shanabrook, D. Gammon *et al.*, Superlattices Microstruct. **12**, 251 (1992).
[14] G. Brosak, B. V. Shanabrook, D. Gammon *et al.*, Phys. Rev. B **47**, 9981 (1993).
[15] V. E. Kirpichev, I. V. Kukushkin, K. von Klitzing, and K. Eberl, JETP Lett. **67**, 210 (1998).
[16] V. E. Kirpichev, L. V. Kulik, I. V. Kukushkin *et al.*, Phys. Rev. 1998, at press.
[17] Yu. A. Bychkov, S. V. Iordanskiĭ, and G. M. Eliashberg, JETP Lett. **33**, 143 (1981).
[18] C. Kallin and B. I. Halperin, Phys. Rev. B **30**, 5655 (1984).
[19] I. V. Lerner and Yu. E. Lozovik, Zh. Éksp. Teor. Fiz. **78**, 1167 (1978) [Sov. Phys. JETP **51**, 588 (1980)].

Translated by M. E. Alferieff

Two-dimensional incommensurate superlattices in precious-metals alloys: nature of formation

O. I. Velikokhatnyĭ and I. I. Naumov*
Institute of the Physics of Strength and Materials Science, Siberian Branch of the Russian Academy of Sciences, 634021 Tomsk, Russia

S. V. Eremeev and A. I. Potekaev
Siberian Physicotechnical Institute, 634050 Tomsk, Russia

(Submitted 4 March 1999)
Pis'ma Zh. Éksp. Teor. Fiz. **69**, No. 8, 548–554 (25 April 1999)

The nature of two-dimensional incommensurate superlattices Ll_2(MM) obtained in the precious-metals alloys Au_3Cu and Cu_3Pd is investigated on the basis of first-principles calculations of the electronic structure. It is shown that their stability can be explained by the opening of energy gaps on coinciding sections of the Fermi surface in two mutually perpendicular directions. It is important that this explanation holds only if the superlattice is treated as a superstructure with respect to ordinary superstructures (Ll_2): the electronic spectrum of the superstructure and not the disordered alloy (as in the existing electronic theory of one-dimensional long-period structures) should serve as the starting spectrum. Arguments supporting the fact that in a number of quasicrystalline substances the Ll_2(MM) phases fall between incommensurate systems and quasicrystals are presented. © *1999 American Institute of Physics.* [S0021-3640(99)00508-3]

PACS numbers: 73.20.Dx, 71.20.Gj, 61.44.Br

The heightened interest in the physics of nano- and low-dimensional structures is focusing attention on very exotic objects formed in the alloys Au_3Cu, Cu_3Pd, Cu_3Pt, Au_3Mn, and others — *two-dimensional incommensurate* superlattices with strongly different periods $2M_1$ and $2M_2$ in two mutually orthogonal directions.[1–3] The nature of the formation of such objects and their place among quasicrystalline media have remained unclear up to now.

The superlattices under discussion are often designated as Ll_2(MM),[1] having in mind the fact that they can be obtained from the ordinary short-period superstructure Ll_2 by introducing a corresponding sequence of discommensurations — domain walls or solitons, on passage of which the phase of the long-range order parameter changes by π (in this connection, such discommensurations structures are also said to be antiphase boundaries— APBs). Characteristically, the distance between the closest APBs is random but locally commensurate: Antiphase domains of different length are distributed randomly in the directions [010] and [001] of the base Ll_2 structure. As the composition or temperature varies, the average half-periods M_1 and M_2 over the random ensemble vary

continuously, also taking on irrational values (in Cu_3Pd, for example, $M_1=3.5-4.5$ and $M_2=5.5$;[1] according to other measurements[2] $M_1=4.1$ and $M_2=6.3$).

The existing electronic theory of long-period states in precious-metals alloys[1,4–9] attributes these states to the Peierls instability of the electronic spectrum $\epsilon(\mathbf{k})$ of the initial disordered state. The one-dimensional superlattices can be explained in a natural manner on the basis of this theory — their period $2M$ is determined by the vector $2\mathbf{k}_F$, parallel to the $\langle 110\rangle$ direction and separating the coinciding (''nesting'') sections of the Fermi surface (FS). If it is assumed that even two-dimensional structures are stabilized by a decrease of the electronic energy as a result of gaps opening on coinciding sections of the FS, then together with the known nesting there should exist another nesting on the FS in the same $\langle 100\rangle$ directions. However, all attempts to find the required nesting starting from the initial electronic spectrum $\epsilon(\mathbf{k})$ of the disordered alloy have been unsuccessful.

In the present Letter we wish to show for the alloys Au_3Cu and Cu_3Pd that two-dimensional superlattices can be derived only starting from the electronic spectrum of the short-period superstructure Ll_2 but not the initial disordered alloy. This is not surprising: Superlattices always coexist with a very high degree of ''short'' range order η, which on cooling arise as a result of sharp first-order transitions with a typical jump $|\eta|\sim 0.6-0.7$.[1] The strong and nontrivial influence of ''short'' range ordering on the ''long'' range ordering, as will be seen from what follows, is due to the fact that it leads to splitting and deformations of the electronic states that determine the nesting on the FS (and therefore the stability of the superlattices). In many cases there arises a unique ''multiplication'' of the initial flat section of the FS into two and more sections. These are the characteristic cases for alloys with two-dimensional superlattices.[10]

We used the full LMTO method[11] in the density approximation to calculate the electronic-energy spectrum $\epsilon_\lambda(\mathbf{k})$ of different sections of the FS and the polarizability $\chi(\mathbf{q})$ of noninteracting electrons. The Barth–Hedin form of the exchange-correlation potential was chosen;[12] the integration over occupied states was performed by the tetrahedron method,[13] using 296 reference points for the self-consistent calculation of the spectrum $\epsilon_\lambda(\mathbf{k})$ and 12341 points in the irreducible part of the Brillouin zone of the Ll_2 structure (the latter is identical to that of a simple cubic lattice) for calculating $\chi(\mathbf{q})$.

In going from the fcc solution to the Ll_2 structure the above-mentioned flattened sections of the FS along $\langle 110\rangle$ turn out to be close to the point M of the new Brillouin zone (BZ). Therefore we shall examine the electronic spectrum of the alloys near this point (Fig. 1). Figure 1 shows together with Au_3Cd and Cu_3Pd the alloy Cu_3Au and pure copper (the latter is of interest as a prototype of a disordered alloy Cu–Au). One can see that in pure copper (and disordered alloys) the electronic term is four-fold degenerate at the point M. Such a high degree of degeneracy is, of course, of formal origin and is due to the artificial representation of the electronic spectrum of fcc copper in the BZ of the Ll_2 structure. For true Ll_2 alloys this term splits, as should happen, into a doubly degenerate level M_5' and singlet levels M_1 and M_3. For what follows it is important that the relative arrangement of the split levels can be arbitrary. This is easy to show using the four-wave approximation of the pseudopotential method.[14] In this approximation the values of the terms M_5', M_1, and M_3 can be found explicitly. They are, respectively, $T-\Delta v_{110}$, $T+\Delta v_{110}+2\Delta v_{100}$, and $T+\Delta v_{110}$, where T is the kinetic energy in the ''empty'' lattice, and Δv_{110} and Δv_{100} are the differences of the pseudopotentials of the components at the superstructural sites of the reciprocal lattice $2\pi/a$ [110] and

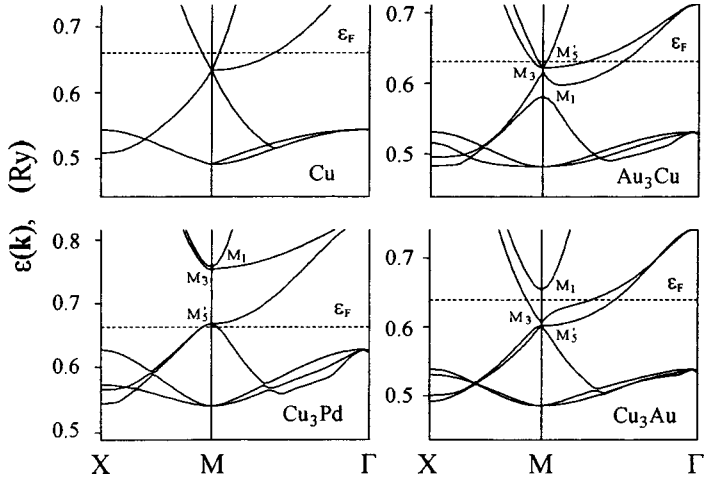

FIG. 1. Electron-energy spectrum $\epsilon_\lambda(\mathbf{k})$ near the point M in Cu, Au_3Cu, Cu_3Pd, and Cu_3Au.

$2\pi/a$ [100]. Since the signs and absolute values of the form factors Δv_{110} and Δv_{100} can be arbitrary, the relative arrangement of the levels is not completely determined. In Au_3Cu, for example, the M_5' level lies above the other two, while in Cu_3Pd and Cu_3Au M_5' lies below them.

As one can see from Fig. 1, in Au_3Cu two electronic sections of the FS (23rd and 24th bands), which are genetically related with the splitting of the M_5' level accompanying a transition into the **k** points of the general position, arise near the point M. In the section $z=0$ (Fig. 2a) they have the form of a star and a circle with a very small radius, respectively, and in the section $x=0.5$ they have the form of thin rectangular strips (Fig. 2b) strongly prolate along the line $T(M-R)$ and centered on it. The latter fact is partially due to the circumstance that the M_5' level does not split on the line T itself. On the whole, the electronic section of the 24th band is a thin cylindrical rod, which coincides with itself under a translation by the small vector $\mathbf{D}_2=0.0275(2\pi/a)$ [100] (Figs. 2a and 2b). The corresponding electronic polarizability (due to the transitions 24→24 only) demonstrates a characteristic kink at the point $\mathbf{q}=\mathbf{D}_2$ (see inset in Fig. 3). The rod under study also coincides well with the electronic section of the 23rd band under a translation by the vector $\mathbf{D}_1=0.065(2\pi/a)$ [100] (Figs. 2a and 2b). This fact is manifested as a kink in the total electronic polarizability $\chi(\mathbf{q})$ at $\mathbf{q}=\mathbf{D}_1$ (Fig. 3). It is evident from the figure that this kink is formed by contributions from the interband electronic transitions 23→24 and 24→23.

In the alloy Cu_3Pd, just in Cu_3Au, the term M_5' is closest to ϵ_F. Now, however, this term lies somewhat above ϵ_F and there are no occupied states in the immediate vicinity of the point M. This point serves as a center of a prolate hole pocket formed by the 21st band (in the remaining part of the BZ this band is virtually completely occupied). Moreover, the electronic pockets from the 22nd band, which are centered at the points X (Fig. 2c), approach very close to it. The hole pocket coincides with the electronic pocket under a translation by the vector $\mathbf{D}_2=0.082(2\pi/a)$ [100], leading to a sharp maximum of the total polarizability (Fig. 4). Moreover, the electronic pockets centered at neighboring X

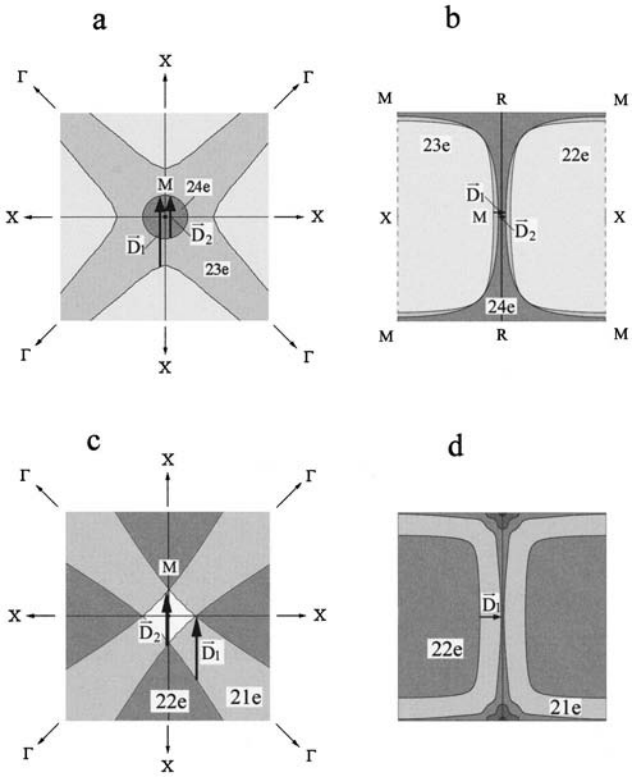

FIG. 2. Fragments of the cross sections of the Fermi surface: a, b) in Au_3Cu, d) Cu_3Pd. a, c — Fragments on an enlarged scale in the plane $z=0$; b — in the plane $x=0.5(2\pi/a)$; d — in the plane $x=0.45(2\pi/a)$.

points fit with one another, to a high degree of accuracy, under a translation of one of them by the vector $\mathbf{D}_1=0.105(2\pi/a)$ [100] — this is expressed as the appearance of a kink in the total $\chi(\mathbf{q})$ and a peak in the partial contribution of 22→22 (Fig. 4). It is interesting that, in contrast to all cases considered above, the nesting vector $\mathbf{D}_1$ lies not on the line MX itself but rather close to it, as is evident from the section $x=0.45(2\pi/a)$ (Fig. 2d).

We shall show that the coinciding sections of the FS which were determined above do indeed explain the formation of two-dimensional superlattices in Au_3Cu and Cu_3Pd. For Au_3Cu the calculations predict the following values for the given half-periods $M_1 \sim \pi/|\mathbf{D}_1|=7.7$ and $M_2 \sim \pi/|\mathbf{D}_2|=18$ (in units of the lattice parameter a); they agree well with the observed values $M_1=6.7\pm0.5$ and $M_2=17\pm19$.[1] For Cu_3Pd the calculations give $M_1=4.7$ and $M_2=6.1$, which are also close to the experimental values $M_1=3.5-4.5$ and $M_2=5.5-6.3$.[1,2] These correlations indicate the following simple mechanism leading to the formation of two-dimensional superlattices. Each of the two systems of coinciding sections of the FS induces the formation of a its superperiod in one of the two mutually orthogonal directions. If, say, the coinciding sections separated by the vector $\mathbf{D}_1$ induce a period along the [100], then the sections corresponding to the vector $\mathbf{D}_2$ induce a period along an orthogonal direction ([010] or [001]).

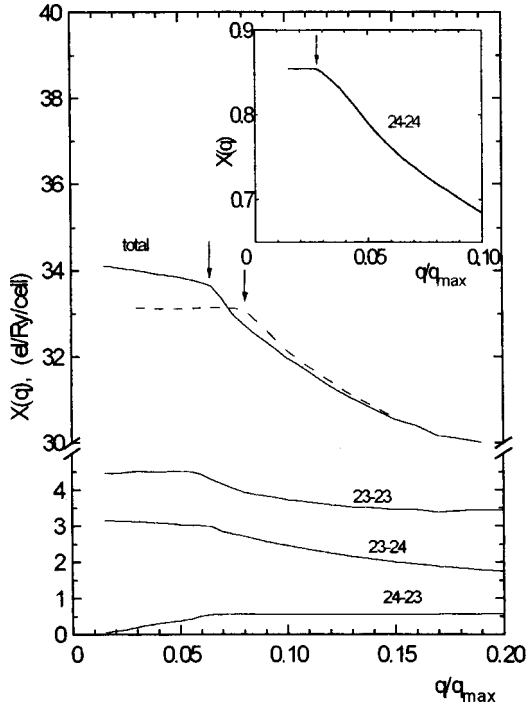

FIG. 3. Electronic polarizability $\chi(\mathbf{q})$ and its partial components, calculated for Au_3Cu in the $\langle 100 \rangle$ direction. The arrows mark the nesting vectors $\mathbf{D}_1$ and $\mathbf{D}_2$. The dashed curve corresponds to pure copper.

It should be underscored that the presence of sharp peaks in the electronic polarizability for vectors of the type $\mathbf{D}_1$ and $\mathbf{D}_2$ is not necessary for the formation of superlattices. Indeed, as Vul' and Krivoglaz showed analytically,[8] stabilization of the superperiod is possible not only in systems with flat and cylindrical sections of the FS but also with ellipsoidal sections, leading to a relatively weak (logarithmic) singularity in $\chi(\mathbf{q})$. In our cases the ''critical'' sections of the FS are still quite strongly flattened and are nearly cylindrical, as the above-indicated characteristic kinks in the polarizability attest.

There can arise the question of why, for example, only one-dimensional (but not two-dimensional) superlattices are observed in the system Cu_3Au, even though its electronic structure seems to be similar to that of Au_3Cu. The electronic spectrum of this system near the point M differs from the spectrum of Au_3Cu in that the singlet terms M_1 and M_3 are closest to the Fermi level, the term M_1 (24th band) lying above the Fermi level (Fig. 1). As a result of the latter circumstance, the additional electronic section of the FS near the point M does not arise (the flat sections do not split). The existing electronic section (23rd band) coincides with itself under a translation by the vector $2\mathbf{k}_F$ such that $M \sim \pi/|2\mathbf{k}_F| \sim 8.3$. At relatively low temperatures the observed half-period of the one-dimensional superlattice in Cu_3Au is $M \sim 8.4$ (Ref. 1).

Switching from disordered alloys to Ll_2 superstructures the ''quality'' of the nesting decreases because of the above-examined splitting and deformation of the ''critical'' electronic states. It is evident from Fig. 3 that in pure copper the polarizability has a

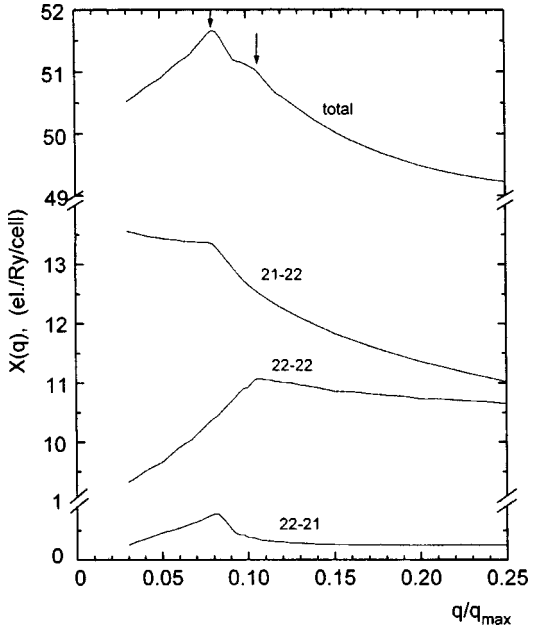

FIG. 4. Electronic polarizability $\chi(\mathbf{q})$ and its partial components, calculated for Cu_3Pd in the $\langle 100 \rangle$ direction. The arrows mark the nesting vectors $\mathbf{D}_1$ and $\mathbf{D}_2$.

sharper feature than in Au_3Cu — a step at $q=0.08(2\pi/a)$. Hence follows the very unexpected result that as temperature decreases, at a certain stage short-period ordering can start to destabilize the superlattice. This circumstance is important for explaining why in the alloys Cu–Au (and in certain other alloys) superlattices exist only in a narrow temperature range and at sufficiently low temperatures become energetically unfavorable compared with the usual superstructures Ll_2 (or Ll_0).

In closing, we shall discuss the question of the place of incommensurate superlattices (one- and two-dimensional) among other quasicrystalline materials. In some respects they are undoubtedly similar to ordinary incommensurate crystals (systems with charge-density waves, helicoidal magnetic structures, and so on). Thus, as the concentration varies they can undergo a transition into commensurate superlattices, whose average period can be expressed in the form of a rational fraction m/n (m and n are integers). In the system Cu–Pd, for example, such a *lock-in* transition occurs with increasing Pd concentration (at the point 21.3 at.% Pd).[2] As the composition changes above this point the values of m/n start to change discretely[2] — a ''devil's staircase'' of commensurate transitions arises.

Despite the similarity, the behavior of the superlattices still does not fit well with the conventional ideas about the behavior of ordinary incommensurate crystals.[15–17] In the first place, as we have already mentioned, they are formed as a result of sharp first-order transitions, immediately acquiring a domain (soliton) character and bypassing the initial stage, corresponding to their modulation by a single plane wave. As temperature decreases, the density of domain walls changes very little, usually increasing slightly. On further cooling the superlattices undergo a sharp first-order transition to the Lifshitz

superstructures Ll_0 or Ll_2.[18] In ordinary incommensurate systems, however, as is well known,[15,17] the evolution of the soliton lattice is different: The soliton density rapidly decreases with temperature and vanishes at the *lock-in* transition (second-order or nearly so) point.

The fundamental difference of incommensurate superlattices from ordinary incommensurate systems lies in the fact that in them the average domain size $2M$ cannot assume arbitrary values, but rather it is determined by the diameters $2\mathbf{k}_F$ of the initial FS. But this circumstance makes them similar to quasicrystals, whose stability is based essentially on the same factors — the ''interaction'' of the FS with Bragg planes.[19] It is well known[20] that quasicrystals can be represented in the form of a quasiperiodic packing of two (or more) unit cells of different forms. This packing is organized in a manner so that the FS is in contact with a pseudo-BZ, due to the icosahedral symmetry of the quasicrystal.[19] It is easy to see that valleys of different length in superlattices and different unit cells in quasicrystals essentially play the same role — by their specific alternation they give the quasiperiod $M \sim \pi/|2\mathbf{k}_F|$ required to lower the electronic energy. Therefore the superlattices considered occupy a unique place among quasicrystallines materials — between commensurate systems and quasicrystals.

We thank É. V. Kozlov for helpful discussions and consultations. This work was supported by the Federal Science Program ''Surface Atomic Structures'' (Grant 3.8.99).

*e-mail: naumov@ispms.tsc.ru

[1] N. M. Matveeva and É. V. Kozlov, *Ordered Phases in Metallic Systems* (Nauka, Moscow, 1989).
[2] D. Broddin, G. Van Tendeloo, J. Van Layduyt *et al.*, Philos. Mag. **54**, 395 (1986).
[3] D. Watanabe and O. Terasaki, in *Phase Transformations in Solids Symposium*, Maleme-Chania, Crete, June-July, 1983, N. Y. (1984), p. 231.
[4] M. Tachiki and K. Teramoto, J. Phys. Chem. Solids **28**, 375 (1966).
[5] V. M. Dement'ev and É. V. Kozlov, Izv. Vyssh. Uchebn. Zaved. Fiz. **6**, 21 (1973).
[6] V. M. Dement'ev and É. V. Kozlov, Izv. Vyssh. Uchebn. Zaved. Fiz. **6**, 30 (1974).
[7] D. A. Vul' and M. A. Krivoglaz, Fiz. Met. Metalloved. **51**, 231 (1981).
[8] D. A. Vul' and M. A. Krivoglaz, Fiz. Met. Metalloved. **55**, 869 (1983).
[9] M. A. Krivoglaz, *Diffuse Scattering of X-Rays and Neutrons by Fluctuation Nonuniformities in Nonideal Crystals* (Naukova dumka, Kiev, 1984).
[10] O. I. Velikokhatnyĭ, S. V. Eremeev, I. I. Naumov *et al.*, Izv. Vyssh. Uchebn. Zaved. Fiz., Tomsk (1999); VINITI, February 18, 1999, No. 217.
[11] S. Yu. Savrasov and D. Yu. Savrasov, Phys. Rev. B **46**, 12181 (1992).
[12] U. Barth and L. Hedin, J. Phys. C **5**, 1629 (1972).
[13] J. Rath and A. J. Freeman, Phys. Rev. B **11**, 2109 (1975).
[14] W. Heine, M. Cohen, and D. Weaire, in *Solid State Physics*, Vol. 24, edited by H. Ehrenreich, F. Seitz, and D. Turnbull (Academic Press, New York, 1970; Mir, Moscow, 1973).
[15] W. L. McMillan, Phys. Rev. B **14**, 1496 (1976).
[16] W. L. McMillan, Phys. Rev. B **16**, 4655 (1977).
[17] L. N. Bulaevskiĭ and D. I. Khomskiĭ, Zh. Éksp. Teor. Fiz. **74**, 1863 (1978) [Sov. Phys. JETP **47**, 971 (1978)].
[18] A. I. Potekaev, Izv. Vyssh. Uchebn. Zaved. Fiz. **6**, 3 (1995); A. I. Potekaev, Izv. Vyssh. Uchebn. Zaved. Fiz. **6**, 22 (1996).
[19] J. Friedel and F. Denoyer, C. R. Acad. Sci., Paris II **305**, 171 (1987).
[20] J. E. S. Sokolar, T. C. Lubensky, and P. J. Steinhardt, Phys. Rev. B **34**, 3345 (1986).

Translated by M. E. Alferieff

Thermally activated transformation of magnetization-reversal modes in ultrathin nanoparticles

A. F. Popkov
F. V. Lukin State Scientific-Research Institute of Physical Problems, 103460 Moscow, Russia

L. L. Savchenko
M. V. Lomonosov Moscow State University, 119899 Moscow, Russia

N. V. Vorotnikova
Physicotechnical Institute, Russian Academy of Sciences, 117218 Moscow, Russia

(Submitted 17 March 1999)
Pis'ma Zh. Éksp. Teor. Fiz. **69**, No. 8, 555–560 (25 April 1999)

The influence of thermal fluctuations on magnetization-reversal processes in ultrathin magnetic particles is investigated on the basis of a numerical solution of the Landau–Lifshitz–Gilbert equations taking account the thermal-activation fluctuation field. It is shown that for nanoparticles there exists a region of magnetic and geometric parameters where a strong jump-like instability of the critical field for magnetization reversal arises. This instability is due to the thermally activated transformation of magnetization configurations far from the switching threshold. The thermal-instability mechanism described is important for particles of much larger sizes than for the single-mode Néel–Brown instability. © *1999 American Institute of Physics.* [S0021-3640(99)00608-8]

PACS numbers: 75.50.Kj, 75.50.Tt, 61.46.+w, 75.60.Nt

The question of the thermal instability of the magnetization of small magnetic particles is a fundamental problem of micromagnetism.[1,2] It is especially important for magnetic microelectronics in connection with miniaturization. For example, the Néel–Brown thermal instability[2] of flat nanoparticles limits the maximum information density of longitudinal storage on a magnetic disk and makes vertical storage preferable.[3,4] The critical particle sizes for the single-mode Néel–Brown instability are determined by the ratio of the thermal energy k_BT to the energy density u determining the magnetization-reversal energy barrier: $V \sim k_BT/u$. However, a multimode switching instability, associated with the existence of alternative magnetic configurations due to the influence of the film edges, as described in, for example, Ref. 5, can be expected to arise long before the critical volume is reached in a thin particle. Each magnetization-reversal mode is characterized by its own switching threshold. We shall show that thermal fluctuations can lead to a random transformation of magnetic configurations during switching as well as far from the magnetization-reversal threshold — in the region where the energy barrier separating different mode states is small. In consequence this leads to a very strong

variance of the switching fields long before Néel–Brown superparamagnetism arises. The indicated instability mechanism could be important, specifically, in nanosize magnetoresistance memory elements which are under development.

To study magnetization reversal processes in ultrathin nanoparticles the Landau–Lifshitz equations written in Gilbert's form were solved numerically:

$$\frac{\partial \mathbf{M}}{\partial t} = \gamma[\mathbf{M}\times\mathbf{H}^{\mathbf{eff}}] - \frac{\alpha\gamma}{M}[\mathbf{M}\times[\mathbf{M}\times\mathbf{H}^{\mathrm{eff}}]], \tag{1}$$

where $\mathbf{M}$ is the magnetization vector; M, γ, and α are the saturation magnetization, gyromagnetic ratio, and the Gilbert damping parameter, respectively; $\mathbf{H}^{\mathrm{eff}}$ is the effective magnetic field given by a sum of fields

$$\mathbf{H}^{\mathrm{eff}} = \mathbf{H} + \mathbf{H}^{m} + \mathbf{H}^{\mathrm{anis}} + \mathbf{H}^{\mathrm{exch}} + \mathbf{H}^{\mathrm{fl}}, \tag{2}$$

where $\mathbf{H}$ is the external magnetic field;

$$\mathbf{H}^{m}(\mathbf{r}) = -\int_{V} \operatorname{div}\mathbf{M}(\mathbf{r})\,\frac{\mathbf{r}-\mathbf{r}'}{|\mathbf{r}-\mathbf{r}'|^{3}}\,d\mathbf{r}' + \int_{S}(\mathbf{M}(\mathbf{r}')\cdot\mathbf{n}_{s})\,\frac{\mathbf{r}-\mathbf{r}'}{|\mathbf{r}-\mathbf{r}'|^{3}}\,dS$$

is the magnetostatic field, $\mathbf{r}$ is the radius vector of a point in the layer, V and S are, respectively, the volume and surface area of a particle, $\mathbf{n}_{s}$ is the vector normal to the particle boundary, $\mathbf{H}^{\mathrm{anis}} = (2K/M^{2})\,(\mathbf{M}\cdot\mathbf{n})\mathbf{n}$ is the uniaxial anisotropy field, K is the anisotropy constant, $\mathbf{n}$ is a unit vector along the easy magnetization axis, $\mathbf{H}^{\mathrm{exch}} = (2A/M^{2})\,\Delta\mathbf{M}$ is the nonuniform exchange field; A is the in-layer exchange constant, Δ is the two-dimensional Laplacian, and $\mathbf{H}^{\mathrm{fl}}$ is the random magnetic field giving rise to thermal fluctuations of the spins. We assume that the thickness of the flat magnetic-film particle is much less than the exchange length, $d \ll l_{\mathrm{exch}} = \sqrt{A/2\pi/M^{2}}$, and therefore magnetization is uniform over the thickness. Assuming the spins on the surface to be free, we employ a boundary condition of the form

$$\left.\frac{\partial \mathbf{M}}{\partial n_{s}}\right|_{S} = 0. \tag{3}$$

Methods for numerical integration of the Landau–Lifshitz equations are described in detail in the literature[1] and have been well tested (see, for example, Refs. 6–10). Similarly to Ref. 6, which employs a dynamic approach to describing the thermodynamic fluctuations on the basis of the fluctuation-dissipation theorem,[11] we shall assume that after a magnetic particle is divided into a grid of unit cells, a uniform random field $\mathbf{H}^{\mathrm{fl}}(t)$ (t is the time) corresponding to white noise with the correlation function $\langle \mathbf{H}^{\mathrm{fl}}(t)\cdot\mathbf{H}^{\mathrm{fl}}(t')\rangle = \sigma^{2}\delta_{ij}\delta_{tt'}$, where $\sigma^{2} = 2k_{B}T\alpha/\gamma v M\,\delta t$, v is the unit cell volume, and δt is the integration time interval, is generated in each (ith) cell.

In the absence of fluctuations ($\mathbf{H}^{\mathrm{fl}}(t) = 0$) a thin rectangular particle has two different configurations of the magnetic distribution in the remanent state — C and S types, characterized by parallel or antiparallel magnetizations near the opposite short edges (Fig. 1). The calculations show that the energy of the remanent states varies with the geometric parameters of the particle and the bias magnetic field in the transverse direction, so that for small form factors and strong bias fields the S configuration is preferred. There exists a line of first-order phase transitions (Fig. 2) on which the energies of the C and S states

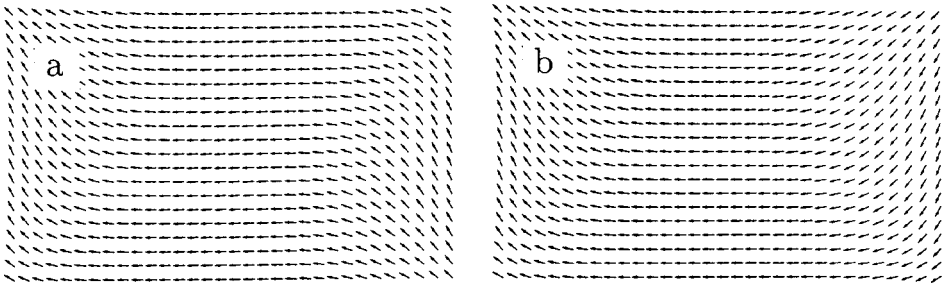

FIG. 1. Remanent-magnetization configurations corresponding to the main magnetization modes of a $400\times250\times4$ nm ultrathin, rectangular, permalloy particle with magnetization $M=800$ G and longitudinal uniaxial anisotropy $K=1000$ ergs/cm^3: a — *S* state, b — *C* state.

are equal. To each remanent state there corresponds a unique magnetization reversal mode and a hysteresis loop. The critical magnetization reversal field (coercivity) can differ very strongly, as shown in Fig. 3. It is obvious that when thermal fluctuations are switched on ($\mathbf{H}^{\mathrm{fl}}(t)\neq0$) intertransformation of the switching modes can be expected to occur in the range of parameters corresponding to the phase-transition line, if the height of the separating energy barrier is comparable to the thermal energy $\delta E \approx k_B T\ln(\omega\tau/\ln P^{-1})$, where ω is the resonance frequency, τ is the characteristic thermal-activation time of the intermode interaction, and P is the expected intermode transformation probability. It should be noted that the energy barrier decreases with increasing saturation field (see the computational example in Fig. 4) right down to zero at the point of instability of one of the configuration modes, and the probability of thermally-activated change of the *C* and *S* modes increases with advancement into the saturation

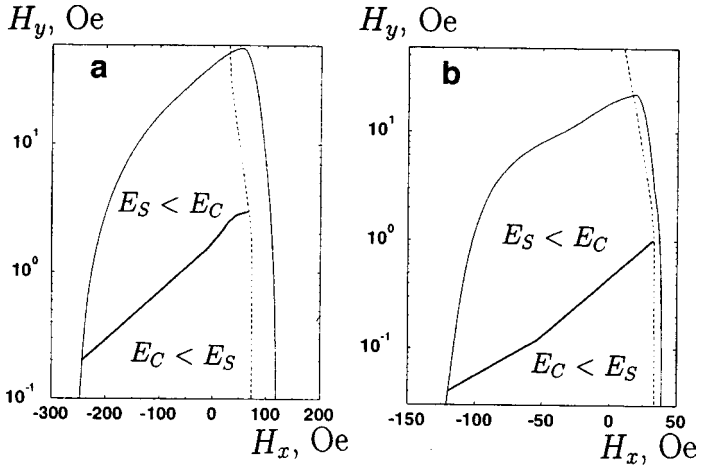

FIG. 2. Energy diagram of the modal magnetization states of two rectangular permalloy particles with dimensions a — $400\times250\times4$ nm and b — $800\times400\times2$ nm in longitudinal, H_x, and transverse, H_y, magnetic fields. Thick line — the line of first-order phase transitions that separates the region of stability of the *S*- and *C*-mode states. Thin line — the line of instability of the *C* state; dashed line — the line of instability of the *S* state.

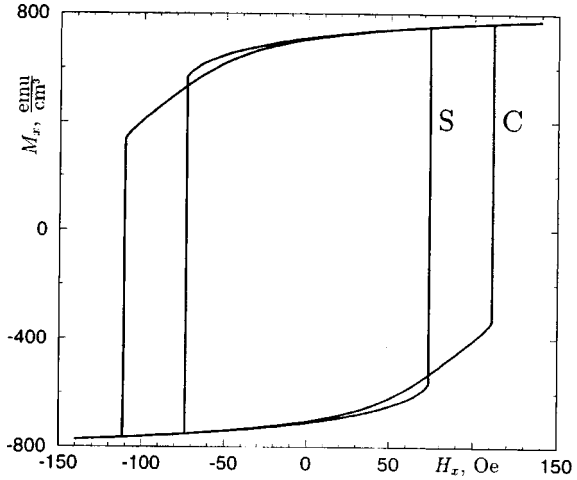

FIG. 3. Magnetic hysteresis loops of the main magnetization-reversal modes of a 400×250×4 nm permalloy rectangle for the *S* and *C* modes.

region. Therefore it should be expected that near the line of degeneracy of the mode states a thermally activated change of the states in the region of saturation fields is always possible in thin films.

Figure 5a shows the results of numerical simulation of hysteresis switching of a 400×250×4 nm flat permalloy particle at room temperature in an ac magnetic field $\mathbf{H}=\mathbf{H}_0\cos(2\pi t/t_\Omega)$ with cycling periodicity along the loop $t_\Omega=1$ μs and a constant bias field of 1.5 Oe in the transverse direction. Figure 5b shows the time variation of the transverse magnetization components at the opposite poles of the particle subject to

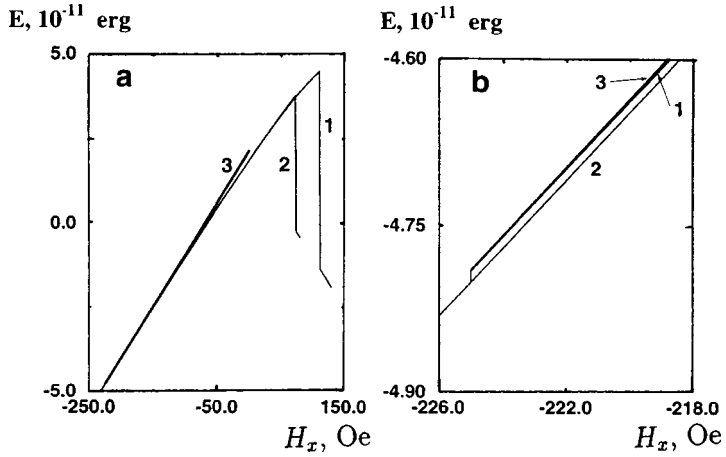

FIG. 4. Energy of the main modal configurations and energy barrier separating the modal states of a 400 ×250×4 nm rectangle as a function of the longitudinal magnetization field: a — general view; b — enlarged fragment of the dependence in the region shown by the square in Fig. 4a near the line of instability of the *C* mode: 1 — energy of the *C* mode, 2 — energy of the *S* mode, 3 — energy barrier.

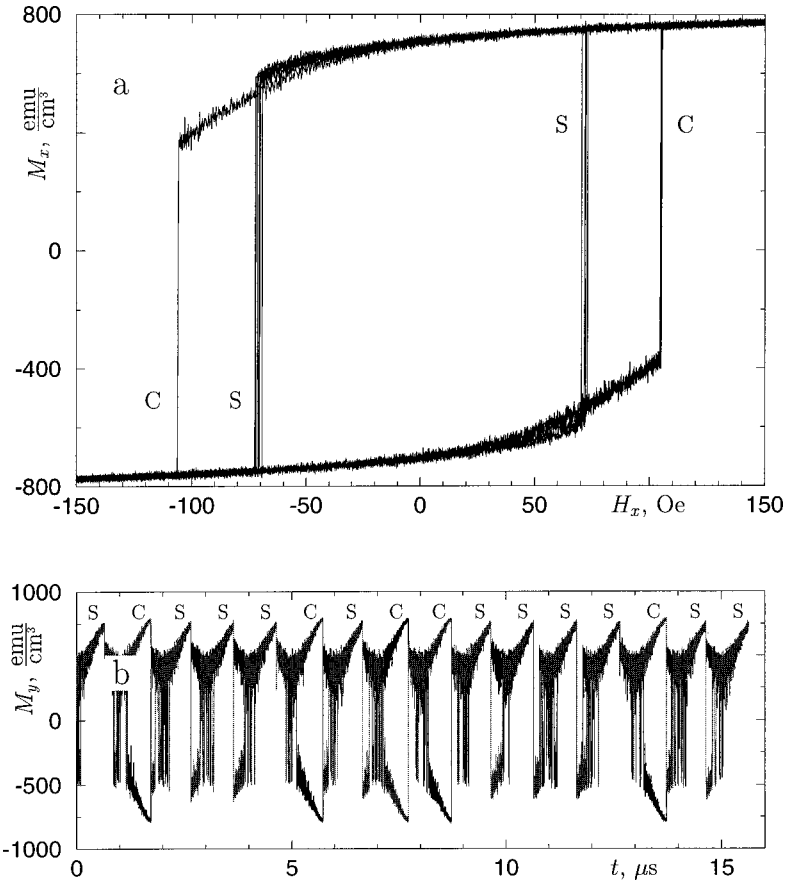

FIG. 5. a) Magnetic hysteresis cycles of a $400\times250\times4$ nm permalloy particle taking account of thermal fluctuations. b) Time scan of the values of the transverse magnetization components at the opposite poles of a magnetic particle. The transverse component of the magnetization at the origin $M_y(x=0)$ is shown in black. The time dependence of the average transverse magnetization at the opposite edge $M_y(x=400$ nm) is shown in gray.

magnetization reversal. In the case shown, the coercivity of magnetization reversal of a nanoparticle changed abruptly by 30%. In the process, the decrease of coercivity due to the single-mode thermally activated Néel–Brown instability[6] did not exceed 10%. The random changing of the magnetization-reversal modes, as shown in Fig. 5b, can be described by the kinetic equations $d\mathbf{P}/dt=\mathbf{GP}$ for the mode-state vector $\mathbf{P}=(P_S^{\uparrow},\ P_C^{\uparrow},\ P_S^{\downarrow},\ P_C^{\downarrow})$, determined by the probabilities for realization of the corresponding modes, where an arrow distinguishes the state of longitudinal magnetization and corresponds to the upper or lower hysteresis branch. The state vector corresponds to at least four modes in a zero base field and at most eight modes in the presence of a transverse bias field. The transition-rate matrix $\mathbf{G}=\mathbf{G}(t)$ varies in time because the energy barriers vary together with the cycling field along the hysteresis loop.

We shall consider a simplified example of single passage of a magnetized state far from the magnetization-reversal threshold, where only two mode states, corresponding to

one of the hysteresis loops (for example, the upper one), are important, so that $\mathbf{P}=(P_S,\ P_C)$. We approximate the decrease in the energy barrier by a linear function $\delta E_{S,C}=U_{S,C}+\kappa|t|$, where $U_{S,C}$ are, respectively, the minimum achievable barrier for the S or C mode, $\kappa=|dU/dt|$ is the rate of passage through the minimum. The decay rates of each mode will contain an exponential time dependence, and the kinetic equation becomes

$$\frac{d\mathbf{P}}{dt}=-\begin{bmatrix} G_S^0 & -G_C^0 \\ -G_S^0 & G_C^0 \end{bmatrix}\exp\left(-\frac{\kappa|t|}{k_BT}\right)\mathbf{P}, \tag{4}$$

where $G_{S,C}^0=\omega_{S,C}\exp(-U_{S,C}/k_BT)$ and $\omega_{S,C}$ are the characteristic frequencies of the modal oscillations. Since $P_C=1-P_S$, integrating the system (4) we find the change in the probability with a single passage through the minimum barrier

$$P_S(t=\infty)=P_S^0+(P_S(-\infty)-P_S^0)\exp\left(-\frac{2k_BT}{\kappa}(G_S^0+G_C^0)\right), \tag{5}$$

where $P_S^0=G_C^0/(G_S^0+G_C^0)$ is the probability of being in the S state after an unlimited number of passage cycles along the hysteresis loop. It is evident from the last equation that the characteristic thermally activated interaction time is $\tau=2k_BT/\kappa$. The number N of passage cycles along the loop for which the probability of a given magnetization-reversal mode being realized approaches a stationary value can be estimated using the approximate condition $(P_S(N)-P_S^0)/P_S^0<0.1$. It follows from this condition, iterating Eq. (5), that

$$N>\frac{\ln(10(1-P_S^0)/P_S^0)}{\tau(G_S^0+G_C^0)}=\frac{\ln(10G_S^0/G_C^0)}{\tau(G_S^0+G_C^0)}. \tag{6}$$

In our case, according to an estimate using Eq. (6) taking account of the energy dependences presented in Fig. 4 for the S and C states with a characteristic half-period for passage $\tau\sim 1$ μs and the characteristic frequency of magnetization oscillations $\omega\sim 1$ GHz, for the maximum amplitude $H_0=160$ Oe of the magnetization-reversing field two cycles are sufficient to establish a thermodynamically equilibrium probability of being in the S state, and for $H_0=120$ Oe 850 magnetization-reversal cycles are required.

In summary, the closeness of the energies of the configuration modes of the magnetization and a low separating barrier are important for the mechanism of multimode thermally activated instability in nanoparticles. To suppress this effect in practical applications the magnetic and geometric parameters of an element must be chosen to be far from the line of energy degeneracy of alternative magnetization states, using, for example, a magnetic or an exchange bias field in the hard direction. We note that a multimode switching instability with energy degeneracy of the mode states of a magnetic particle is also possible, in principle, at ultralow temperatures on account of the macroscopic quantum fluctuations of the magnetization. Together with the conventional magnetic-relaxation methods this can be used to observe such fluctuations.

We thank the Russian Fund for Fundamental Research for financial support (Grant No. 98-02-16469).

[1] H. N. Bertram and J. G. Zhu, Solid State Phys. **46**, 271 (1992).

[2] L. Néel, Ann. Geophys. **5**, 99 (1949); W. F. Brown, Phys. Rev. **130**, 1677 (1963).
[3] P.-L. Lu and S. H. Charap, IEEE Trans. Magn. **31**, 2767 (1995).
[4] S. Charap, P. Lu, and Y. He, IEEE Trans. Magn. **33**, 978 (1997).
[5] Y. Zheng and J.-G. Zhu, J. Appl. Phys. **81**, 5471 (1997).
[6] E. D. Boerner and H. N. Bertram, IEEE Trans. Magn. **33**, 3052 (1997).
[7] Y. Nakatani, Y. Uesaka, and N. Haiashi, Jpn. J. Appl. Phys., Part 1 **28**, 2485 (1989).
[8] S. G. Osipov and M. M. Khapaev, Zh. Eksp. Teor. Fiz. **90**, 1354 (1990) [Sov. Phys. JETP **71**, 756 (1990)].
[9] N. A. Usov and S. E. Peschany, JMMM **130**, 275 (1994).
[10] S. G. Filippov and L. G. Korzunin, Fiz. Tverd. Tela (St. Petersburg) **38**, 2442 (1996) [Phys. Solid State **38**, 1343 (1990)].
[11] L. D. Landau and E. M. Lifshitz, *Statistical Physics* (Pergamon Press, New York) [Russian original, Nauka, Moscow, 1964].

Translated by M. E. Alferieff

Lateral tunneling through the controlled barrier between edge channels in a two-dimensional electron system

A. A. Shashkin, V. T. Dolgopolov, and E. V. Deviatov
Institute of Solid State Physics, Russian Academy of Sciences, 142432 Chernogolovka, Moscow Region, Russia

B. Irmer, A. G. C. Haubrich, and J. P. Kotthaus
Ludwig-Maximilians-Universität, D-80539 München, Germany

M. Bichler and W. Wegscheider
Walter Schottky Institut, Technische Universität München, D-85748 Garching, Germany

(Submitted 18 March 1999)
Pis'ma Zh. Éksp. Teor. Fiz. **69**, No. 8, 561–566 (25 April 1999)

A study is made of the lateral tunneling between edge channels at the depletion-induced edges of a gated two-dimensional electron system, through a gate-voltage-controlled barrier arising when the donor layer of the heterostructure is partly removed along a fine strip by means of an atomic force microscope. For a sufficiently high barrier the typical current–voltage characteristic is found to be strongly asymmetric, having, in addition to the positive tunneling branch, a negative branch that corresponds to the current overflowing the barrier. It is established that the barrier height depends linearly on both the gate voltage and the magnetic field, and the data are described in terms of electron tunneling between the outermost edge channels. © *1999 American Institute of Physics.* [S0021-3640(99)00708-2]

PACS numbers: 73.40.Gk, 73.40.Hm

Recently there has arisen much interest in lateral tunneling to the edge of a two-dimensional electron system (2DES), which is related not only to the problem of integer and fractional edge states in the 2DES but also to that of resonant tunneling and Coulomb blockade.[1–7] The tunneling regime was identified by the presence of exponential dependences of the measured current on either source–drain voltage[1–4] or magnetic field.[5] For producing a tunnel barrier a number of methods were used: (i) gate voltage depletion of a narrow region inside the 2DES;[1–4,7] (ii) focused-ion-beam insulation writing;[6] (iii) cleaved-edge overgrowth technique.[5] Insofar as the tunnel barrier parameters are not well-controllable values, it is important for using the first method that one can tune the barrier on the same sample. In contrast to vertical tunneling into the bulk of the 2DES in a quantizing magnetic field, when the 2DES spectrum is manifested,[8,9] in lateral tunneling the electrons can always tunnel to Landau levels that bend up at the edge to form edge channels where they intersect the Fermi level, i.e., the spectrum gaps are not seen directly in lateral tunneling. Instead, it reflects the edge channel structure and density of states. For both the integer and fractional quantum Hall effect, a power-law behavior of

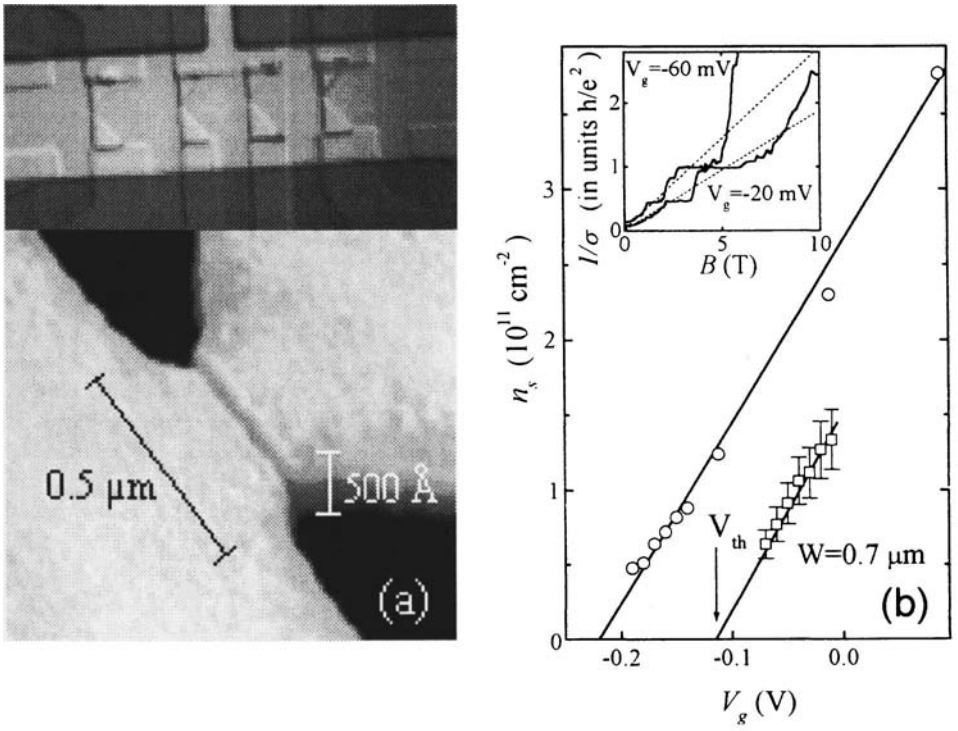

FIG. 1. (a) Top view on the sample (top), and a blowup of one of the constrictions after etching of the oxidized part of the mesa as performed solely for visualization purposes (bottom). (b) Gate voltage dependences of the electron density in the oxidized (squares) and unoxidized (circles) regions of the 2DES. An example of the magnetoconductance in the barrier region is shown in the inset. The value of n_s is extracted from the slope of the dashed lines with 10% uncertainty.

the density of states at the 2DES edge is expected. Since this can interfere with the barrier distortion at electric fields in the nonlinear response regime, the results of lateral tunneling experiments obtained from measurements of the current–voltage curves[5] should be treated with care.

Here we investigate the lateral tunneling in narrow constrictions in which, along a thin strip across, the donor layer of a GaAs/AlGaAs heterostructure is partly removed using an atomic force microscope (AFM). A controlled tunnel barrier is created by gate depletion of the whole of the sample. The well-developed tunneling regime is indicated by strongly asymmetric diodelike current–voltage characteristics of the constriction, which are sensitive to both the gate voltage V_g and the normal magnetic field B. The behavior of the tunneling part of the current–voltage curves points to electron tunneling between the outermost edge channels.

The samples are triangular constrictions of a 2D electron layer with different widths $W=0.7$, 0.4, 0.3, and 0.2 μm of the thinnest part; see Fig. 1a. These are made using standard optical and electron beam lithography from a wafer of GaAs/AlGaAs heterostructure with a low-temperature mobility $\mu=1.6\times10^6$ cm^2/Vs and a carrier density $n_s=4\times10^{11}$ cm^{-2}. Within each constriction the donor layer is removed along a fine line

by locally oxidizing the heterostructure using AFM induced oxidation.[10] This technique allows one to define 140 Å wide oxide lines of sufficient depth and oxide quality so as to partly remove the donor layer and, therefore, locally decrease the original electron density. The whole structure is covered with a metallic gate, which enables us to tune the carrier density everywhere in the sample. As the 2D layer is depleted, the oxidized regions get depopulated first, resulting in the creation of tunnel barriers. Potential probes are made to the sample to permit transport measurements.

For the measurements we apply a dc voltage, V_{sd}, between the source (grounded) and drain contacts of one of the constrictions, modulated with small ac voltage with amplitude $V_{ac}=40$ μV and frequency $f=20$ Hz. A gate voltage is applied between the source and the gate. We measure the real part of the ac current, which is proportional to the differential conductance dI/dV, as a function of bias voltage V_{sd} ($I-V$ characteristics) using a home-made $I-V$ converter and a standard lock-in technique. The behavior of the $I-V$ characteristics is investigated as a function of both the gate voltage and magnetic field. The measurements are performed at a temperature of about 30 mK in magnetic fields of up to 14 T. The results obtained on different constrictions are qualitatively similar.

To characterize the sample we extract the gate-voltage dependence of the electron density from the behavior of magnetoconductance plateaus in the barrier region and in the rest of the 2DES (Fig. 1b). The analysis is made at high fields, where the size-quantization-caused effect of conductance plateaus in narrow constrictions is dominated by magnetic field quantization effects.[11] As is seen from Fig. 1b, if the barrier region is depopulated ($V_g<V_{th}$), the electron density in the surrounding areas is still high enough to provide good conduction. The slopes of the curves $n_s(V_g)$ in the oxidized region and in the rest of the 2DES turn out to be equal within our accuracy. The distance between the gate and the 2DES is determined to be $d\approx 570$ Å; as the corresponding growth parameter is about 400 Å, the 2D layer thickness contributes appreciably to the distance d. We have found that even in the unoxidized region the electron density at $V_g=0$ can be different after different coolings of the sample on account of slight threshold shifts: it falls within the range 2.5×10^{11} to 4×10^{11} cm^{-2} and is always higher than in the barrier region.

The typical $I-V$ characteristic of the constriction in the well-developed tunneling regime is strongly asymmetric and includes an overflowing branch at $V_{sd}<0$ and the tunneling branch at $V_{sd}>0$; see Fig. 2a. The tunneling branch is much smaller and saturates rapidly in zero B with increasing bias voltage. The onset voltages V_O and V_T for these branches are defined in a standard way as shown in the figure. The tunneling regime can be attained both by decreasing the gate voltage and by increasing the magnetic field, as is evident from Fig. 2a. We have checked that the shape of $I-V$ characteristics is not influenced by interchanging the source and drain contacts. Hence, the tunnel barrier is symmetric, and the asymmetry observed is not related to the constriction geometry.

To understand the origin of the asymmetry, let us consider a gated 2DES containing a potential barrier of approximately rectangular shape, with width $L\gg d$, in zero magnetic field. The 2D band bottom in the barrier region coincides with the Fermi level E_F of the 2DES at V_g equal to the threshold voltage V_{th}. Since in the barrier region for $V_g<V_{th}$ an incremental electric field is not screened, the 2D band bottom follows the gate potential, so that the barrier height is equal to $-e\Delta V_g=e(V_{th}-V_g)$, where $-e$ is the charge of an electron (Fig. 2b). Applying a bias voltage V_{sd} shifts the Fermi level in the drain contact

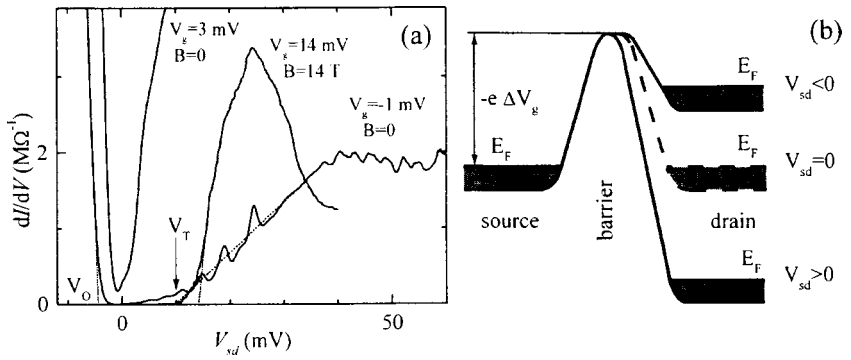

FIG. 2. (a) I–V curves at different gate voltages and magnetic fields. The cases $B=0$ and $B\neq 0$ correspond to two coolings of the sample as compared in Fig. 3a. $W=0.4$ μm. (b) A sketch of the 2D band bottom in the barrier region for different source–drain biases $V_{\rm sd}$.

by $-eV_{\rm sd}$. Because of gate screening the voltage $V_{\rm sd}$ drops over a distance scale of the order of d near the boundary between the barrier and drain, and so the barrier height on the source side remains practically unchanged; see Fig. 2b. If $V_{\rm sd}$ reaches the onset voltage $V_O=\Delta V_{\rm g}$, the barrier on the drain side vanishes, and electrons start to overflow from the drain to the source. In contrast, for $V_{\rm sd}>0$ only the electron tunneling through the barrier from the source to the drain is possible. As $V_{\rm sd}$ increases above $-\Delta V_{\rm g}$, the tunneling distance diminishes and the barrier shape becomes close to triangular. Within the triangular barrier approximation, in the quasiclassical limit of small tunneling probabilities, it is easy to deduce that the derivative of the tunneling current with respect to the bias voltage is expressed by the relation

$$\frac{{\rm d}I}{{\rm d}V}=\sigma_0\exp\left(-\frac{4(2m)^{1/2}(-e\Delta V_{\rm g})^{3/2}L}{3\hbar eV_{\rm sd}}\right)\ll\sigma_0, \tag{1}$$

where $\sigma_0\approx-(e^2/h)\Delta V_{\rm g}W/V_{\rm sd}\lambda_F$, $m=0.067m_0$ (m_0 is the free electron mass), and λ_F is the Fermi wavelength in the source. Obviously, the tunneling current is dominated by electrons in the vicinity of the Fermi level, and the tunneling distance $L_T=-\Delta V_{\rm g}L/V_{\rm sd}$ should satisfy the inequality $d\ll L_T<L$. In accordance with Eq. (1), the expected dependence of the tunneling onset voltage V_T on gate voltage is given by $V_T\propto(-\Delta V_{\rm g})^{3/2}$.

As is seen from Fig. 3a, the expected behavior of both V_O and V_T with changing $V_{\rm g}$ does indeed occur. The dependences $V_O(V_{\rm g})$ and $V_T^{2/3}(V_{\rm g})$ are both linear; the slope of the former is very close to one. Extensions of these straight lines intercept the $V_{\rm g}$ axis at slightly different voltages, which points out that the triangular barrier approximation is good. The threshold voltage $V_{\rm th}$ for the generation of a 2DES in the barrier region, which is defined as a point of vanishing V_O (Fig. 3a), is coincident, within experimental uncertainty, with the value of $V_{\rm th}$ determined from the analysis of magnetoconductance plateaus (Fig. 1b).

A fitting of the set of I–V characteristics at different $V_{\rm g}$ by Eq. (1) with parameters L, $V_{\rm th}$, and σ_0 is depicted in Fig. 3b. The dependence of σ_0 on $\Delta V_{\rm g}$ and $V_{\rm sd}$ is ignored against the background of the strong exponential dependence of dI/dV. Although three

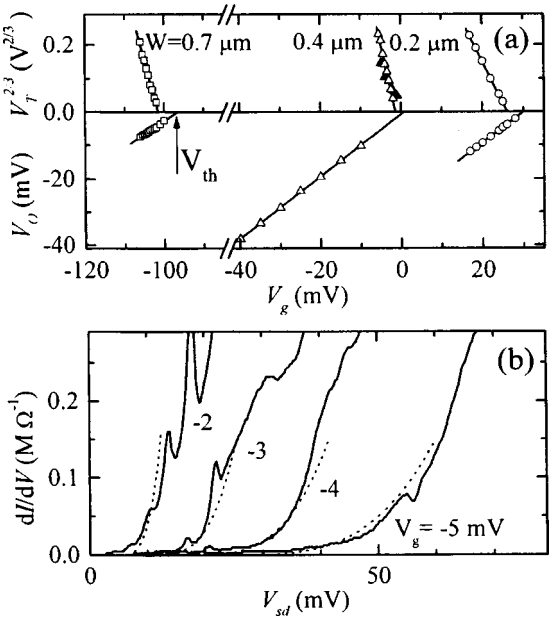

FIG. 3. (a) Change of the onset voltages V_O and V_T as defined in Fig. 2a with V_g at $B=0$; and (b) the fit (dashed lines) of the $I-V$ curves (solid lines) by Eq. (1) with the parameters $L=0.6$ μm, $\sigma_0=38$ $M\Omega^{-1}$, $V_{th}=-0.4$ mV; $W=0.4$ μm. In case (a), the data marked by filled triangles are obtained for the same cooling of the sample as the data at $B=0$ in Fig. 2a and in case (b), whereas the open triangles correspond to the $B\neq 0$ data of Figs. 2a and 4 as measured for the other cooling.

parameters are varied, the fit is very sensitive, except for σ_0, to their variation because of the exponential behavior of the $I-V$ characteristics. One can see from Fig. 3b that the above model describes well the experiment at zero magnetic field. As expected, the determined parameter $L=0.6$ μm is much larger than d, i.e., the barrier shape at $V_{sd}=0$ is approximately rectangular, and the value of V_{th} is close to the point where V_O (and V_T) tends to zero (Fig. 3a). Similar results are obtained at the other two constrictions. In addition, we find that the coefficient σ_0 for different constrictions does not scale with the constriction width W. This probably implies that the tunnel barriers, even with submicron lengths, are still inhomogeneous, which, however, does not seem crucial for the case of exponential $I-V$ dependences.

Having tested that we are dealing with a controlled tunnel barrier, we investigate the tunneling in a normal magnetic field that gives rise to an emerging tunnel barrier in a manner similar to gate depletion (Fig. 2a). At a constant $V_g > V_{th}$, where there is no tunnel barrier in zero B, the magnetoconductance σ obeys a $1/B$ law at weak fields and drops exponentially with B in the high-field limit, signaling the tunneling regime. Figure 4a presents the magnetic field dependence of the onset voltage V_O, which determines the barrier height. It is seen from the figure that the change of the barrier height $-eV_O$ with B is very close to $\hbar\omega_c/2$, which points to a shift of the 2D band bottom by one-half of the cyclotron energy.

For describing the tunneling branch of the $I-V$ characteristics we calculate the

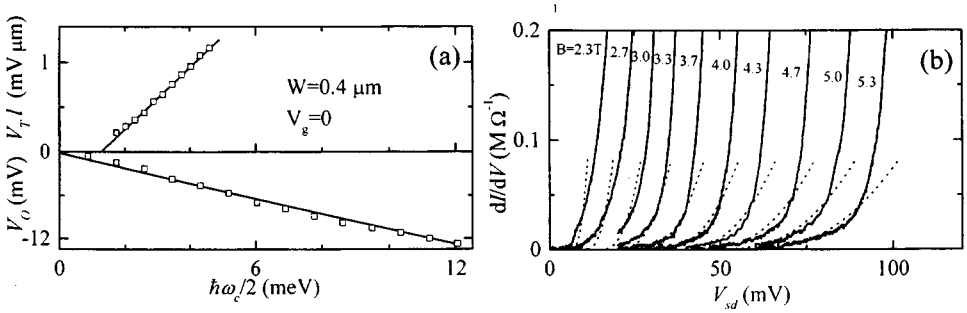

FIG. 4. (a) Behavior of the onset voltages V_O and V_T with magnetic field; and (b) the fit (dashed lines) of the $I-V$ curves (solid lines) by Eq. (4) with the parameters $L=0.6$ μm, $\sigma_0=1.3\,\mathrm{M\Omega}^{-1}$, and $V_{\mathrm{th}}=-1.4$ mV; $W=0.4$ μm, $V_{\mathrm{g}}=0$.

tunneling probability in the presence of a magnetic field. This is not so trivial as at $B=0$ because electrons tunnel through the magnetic parabola between edge channels at the induced edges of the 2DES. In the triangular barrier approximation one has to solve the Schrödinger equation with the barrier potential

$$U(x)=\frac{\hbar\omega_{\mathrm{c}}}{2l^2}(x-x_0)^2-eV_{\mathrm{sd}}\frac{x}{L}-e\Delta V_{\mathrm{g}},\quad 0<x<L, \tag{2}$$

where ω_{c} is the cyclotron frequency, l is the magnetic length, and eV_{sd} is larger than the barrier height in the magnetic field. An electron at the Fermi level in the source tunnels through $U(x)$ from the origin to a state with orbit center x_0 such that $0<x_0<L$. If the barrier potential is dominated by the magnetic parabola (i.e., the magnetic length is the shortest), the problem reduces to the known problem of finding the energy levels in the shifted parabolic potential as caused by the linear term in Eq. (2). The value of x_0 is determined from the condition of coincidence of a Landau level in the potential $U(x)$ with the Fermi level in the source. If only the lowest Landau level is taken into consideration and the spin splitting is ignored, we get the minimum tunneling distance to the outermost edge channel in the drain:

$$x_0=L_T=\frac{l}{2}\left(\frac{\hbar\omega_{\mathrm{c}}L}{eV_{\mathrm{sd}}l}-\frac{2\Delta V_{\mathrm{g}}L}{V_{\mathrm{sd}}l}-\frac{eV_{\mathrm{sd}}l}{\hbar\omega_{\mathrm{c}}L}\right)\gg d. \tag{3}$$

The first term in brackets in Eq. (3), which is dominant, is large compared to unity. Knowing the wave function of the lowest Landau level in the potential $U(x)$ and neglecting the last term in Eq. (3), we obtain for the shape of the $I-V$ characteristics near the onset, where the tunneling probability is small,

$$\frac{\mathrm{d}I}{\mathrm{d}V}=\sigma_B\exp\left(-\frac{(\hbar\omega_{\mathrm{c}}/2-e\Delta V_{\mathrm{g}})^2L^2}{e^2V_{\mathrm{sd}}^2l^2}\right)\ll\sigma_B. \tag{4}$$

Here σ_B is a prefactor which can be tentatively expected to be of the same order of magnitude as σ_0. From Eq. (4) it follows that at sufficiently strong magnetic fields the tunneling onset voltage V_T is related to the barrier height as $V_T l\propto\hbar\omega_{\mathrm{c}}/2-e\Delta V_{\mathrm{g}}$, which is consistent with the experiment (Fig. 4a). The solution (4) includes the case $e\Delta V_{\mathrm{g}}>0$,

when a tunnel barrier is absent at zero magnetic field but arises with increasing B. This occurs apparently because of depopulation of the barrier region in the extreme quantum limit of magnetic field.

Figure 4b displays the fit of the $I-V$ characteristics at different magnetic fields by Eq. (4) with the parameters L, $V_{\rm th}$, and σ_B. The optimum values of $L=0.6$ μm and $V_{\rm th}=-1.5$ mV are found to be very close to the ones for the $B=0$ case as determined for the same range of barrier heights; see Fig. 3b. Although this fact supports our considerations, they are not rigorous enough to permit discussing the considerable discrepancy between the preexponential factors with and without magnetic field.

The observed behavior of the $I-V$ characteristics with magnetic field in the transient region where their asymmetry is not yet strong (Fig. 2a) is similar to that of Refs. 4 and 5. Over this region, which is next to the region of exponential $I-V$ dependences at higher magnetic-field-induced tunnel barriers, our $I-V$ curves are close to power-law dependences, as was discussed in Ref. 5. There is little doubt that it is very difficult to analyze and interpret such $I-V$ curves without solving the tunneling problem rigorously. We note that the peak structures on the tunneling branch of the $I-V$ characteristics (see Figs. 2a and 3b) persist at relatively low magnetic fields and are very similar to those studied in Ref. 4. These may be hint at resonant tunneling through impurity states below the 2D band bottom.

This work was supported in part by the Russian Fund for Fundamental Research under Grants 97-02-16829 and 98-02-16632, the Program ''Nanostructures'' from the Russian Ministry of Sciences under Grant 97-1024, and the Volkswagen-Stiftung under Grant I/68769.

[1] A. Palevski, M. Heiblum, C. P. Umbach *et al.*, Phys. Rev. Lett. **62**, 1776 (1989).
[2] K. Ismail, D. A. Antoniadis, and H. I. Smith, Appl. Phys. Lett. **55**, 589 (1989).
[3] S. J. Manion, L. D. Bell, W. J. Kaiser *et al.*, Appl. Phys. Lett. **59**, 213 (1991).
[4] A. J. Peck, S. J. Bending, J. Weis *et al.*, Phys. Rev. B **51**, 4711 (1995).
[5] A. M. Chang, L. N. Pfeiffer, and K. W. West, Phys. Rev. Lett. **77**, 2538 (1996); M. Grayson, D. C. Tsui, L. N. Pfeiffer *et al.*, Phys. Rev. Lett. **80**, 1062 (1998).
[6] T. Bever, A. D. Wieck, K. von Klitzing, and K. Ploog, Phys. Rev. B **44**, 3424 (1991); T. Bever, A. D. Wieck, K. von Klitzing *et al.*, Phys. Rev. B **44**, 6507 (1991).
[7] T. Heinzel, D. A. Wharam, J. P. Kotthaus *et al.*, Phys. Rev. B **50**, 15113 (1994).
[8] J. P. Eisenstein, L. N. Pfeiffer, and K. W. West, Phys. Rev. B **50**, 1760 (1994).
[9] V. T. Dolgopolov, A. A. Shashkin, A. V. Aristov *et al.*, Phys. Rev. Lett. **79**, 729 (1997).
[10] B. Irmer, M. Kehrle, H. Lorenz, and J. P. Kotthaus, Appl. Phys. Lett. **71**, 1733 (1997).
[11] B. J. van Wees, L. P. Kouwenhoven, H. van Houten *et al.*, Phys. Rev. B **38**, 3625 (1988).

Published in English in the original Russian journal. Edited by Steve Torstveit.

Anomalies of the electronic spin-lattice relaxation of Gd^{3+} in $YBa_2Cu_4O_8$ and $YBa_2Cu_3O_{6+x}$ near 200 K

V. A. Atsarkin,* G. A. Vasneva, and V. V. Demidov
Institute of Radio Engineering and Electronics, Russian Academy of Sciences, 103907 Moscow, Russia

M. Gutmann
Laboratory for Neutron Scattering, ETH Zürich and Paul Scherer Institute, 5232 Villigen PSI, Switzerland

G. Böttger
Laboratory for Crystallography, ETH Zentrum, 8092 Zürich, Switzerland

(Submitted 22 March 1999)
Pis'ma Zh. Éksp. Teor. Fiz. **69**, No. 8, 567–572 (25 April 1999)

A sharp kink in the temperature dependence of the electronic spin-lattice relaxation rate near 200 K was found in the high-temperature superconductors $YBa_2Cu_4O_8$ and $YBa_2Cu_3O_{6+x}$. The effect is correlated with opening of a spin gap and microscopic phase separation. [S0021-3640(99)00808-7]

PACS numbers: 74.72.Bk, 76.60.Es

In the physics of high-temperature superconductors (HTSCs) the nature of the so-called spin gap, which opens in the energy spectrum of ''underdoped'' oxide HTSCs at temperatures $T^* \approx 150-200$ K (i.e. much higher than the superconducting transition temperature T_c) and is manifested, specifically, as an exponential decrease of the nuclear spin-lattice relaxation rate and Knight shift on cooling (see, for example, Ref. 1), remains an enigma. To understand the nature of this phenomenon it is extremely important to find some anomalies in the behavior of HTSC materials near T^*. In the last few years such features have been intensively sought. For example, in Ref. 2 the system $YBa_2Cu_4O_8$ (1248), containing an additional, compared with the widely used material $YBa_2Cu_3O_{6+x}$ (123), layer of CuO and distinguished by high stability and definiteness in the oxygen distribution over the lattice sites, was chosen as the object of investigation. The authors were able to find some anomalies near 180–200 K for a number of spectral and relaxation characteristics of ^{87}Y, ^{63}Cu, and ^{17}O NMR and NQR. This was taken as evidence of ''electronic crossover'' associated with the opening of a spin gap and possibly the appearance of charge-density waves.[3] However, these features (small jumps and changes in slope of the temperature dependences) are all only negligibly above the experimental error, so that the search for new effects of this kind remains urgent. In the present Letter we report a new anomaly which we observed near 200 K in the temperature dependence of the electronic spin-lattice relaxation rate of Gd^{3+} ions introduced as a spin probe into the lattice of the 1248 and 123 oxide HTSCs.

The measurements were performed on $Y_{0.99}Gd_{0.01}Ba_2Cu_4O_8$ and $Y_{0.99}Gd_{0.01}Ba_2Cu_3O_{6+x}$ samples. The 123 samples were prepared at the Institute of

Single Crystals (Khar'kov, Ukraine) by the standard method of solid-phase synthesis. Their characteristics were $x=0.59$ and 0.95 and $T_c=90$ K and 56 K, respectively. The 1248 sample ($T_c=84$ K) was prepared at ETH (Zürich) using the following technology.[4] The oxides Gd_2O_3, Y_2O_3, CuO, and the nitrate $Ba(NO_3)_2$, taken in the stoichiometric ratio and heated up to 900 °C, were dissolved in concentrated (65%) HNO_3 and then polymerized by adding ethylene glycol and citric acid. The gel formed after the liquid was evaporated was dried at 120°C and annealed at 700°C. To obtain a single-phase sample with the required composition the initial powder obtained was sintered in an oxygen flow at 820°C for 60 h. X-Ray investigation confirmed all 123 and 1248 samples to be single-phase.

The experimental samples in the form of pulverized powder were set in epoxy resin and oriented along the *c* axis in a 2 T magnetic field. The ESR spectra were recorded on a standard Bruker ER-200 spectrometer near 3.2 cm. The powder particle sizes (of the order of 10 μm) were much smaller than the depth of the skin layer. This ensured the absence of Dyson distortions of the line shape.

The main method of investigation in this work was to measure the electronic spin-lattice relaxation time T_1 of Gd^{3+} ions. Small values of T_1 ($10^{-7}-10^{-9}$ s), together with a large ESR linewidth (hundreds of G) preclude using standard methods for measuring the relaxation time in the investigation of HTSC materials. For this reason, in the present work we used a novel modulation method in which the longitudinal (with respect to the external magnetic field **B**) spin magnetization of the sample

$$M_z(t)=U\cos(\Omega t)+V\sin(\Omega t) \tag{1}$$

was recorded. Here U and V are the in-phase and quadrature components of the longitudinal relaxational response with respect to amplitude modulation of the microwave power, performed at the frequency Ω. This method, which makes it possible to measure times T_1 down to 10^{-10} s, has been successfully used to investigate HTSCs and fullerides.[5–7]

The values of U and V in the simplest case are determined by the equations

$$U=AM_0\omega_1^2 g(\omega)\Omega T_1/[1+(\Omega T_1)^2], \tag{2a}$$

$$V=AM_0\omega_1^2 g(\omega)(\Omega T_1)^2/[1+(\Omega T_1)^2], \tag{2b}$$

where A is the instrumental proportionality coefficient, M_0 is the static spin magnetization, ω_1 is the amplitude of the microwave field (in frequency units), and $g(\omega)$ is the form factor of the ESR line. In this work we used mainly the phase variant of this technique, in which the longitudinal (spin-lattice) relaxation time is given by

$$\Omega T_1=V/U. \tag{3}$$

The amplitudes U and V were measured using synchronous detection of the signal M_z recorded by a longitudinal inductance coil. The modulation frequency in these experiments was $\Omega=10^7$ s^{-1}. The details are described in Ref. 5.

The 123 system. In the $Y_{0.99}Gd_{0.01}Ba_2Cu_3O_{6+x}$ samples with field orientation $\mathbf{B}\|c$ and sufficiently low temperatures, the standard for spin $S=7/2$ fine structure of the ESR spectrum with parameters in agreement with the published data was observed.[8] As the temperature increases above 100 K, the spectra gradually merge into a single, approxi-

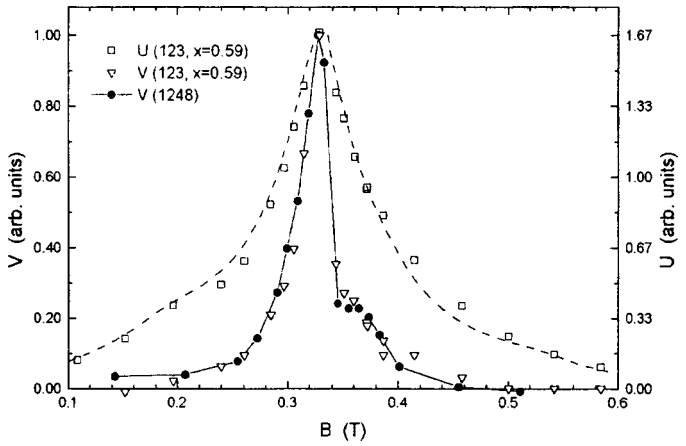

FIG. 1. Relaxation longitudinal responses V (left-hand scale) and U (right-hand scale) in Y-Ba-Cu-O:Gd^{3+} versus the external magnetic field at $T=78$ K. The data for the 1248 sample are normalized to the value of V for the 123 sample. Dashed curve — form of the ESR absorption. The solid curve is drawn through the experimental points.

mately Lorentzian, central line. As is well known,[9] this is explained by the exchange coupling with the spin system of delocalized charge carriers. We note that the method used in the present work to record the longitudinal magnetization does not depend on the details of this merging, and in any case it gives the relaxation time of the total z component of the electronic spins.[7]

The magnetic field dependence of the signals U and V near resonance at $T=78$ K is shown in Fig. 1. It is clearly seen that the forms of the relaxation spectra for the in-phase and quadrature components of the magnetization are different. The U signal is essentially identical to the standard ESR absorption spectrum, whereas the field dependence of the V signal is a much narrower asymmetric line near $g=2$. This means that two types of paramagnetic centers with substantially different spin-lattice interaction efficiency are present in the sample. Centers of one type have such a short relaxation time that $\Omega T_1 \ll 1$. Therefore, in accordance with Eqs. (2) and (3), only the in-phase component U is observed from them. The fact that its field dependence matches the ESR absorption lines shows that these rapidly relaxing centers make the main contribution to the observed ESR spectrum. Conversely, centers of the second type are characterized by relatively slow spin-lattice relaxation. At 78 K $\Omega T_1 \gg 1$ for them, so that only the V component is observed. The fact that the corresponding narrow line is virtually absent in the observed ESR spectrum indicates that the density of the slowly relaxing centers is relatively low; they are manifested in the relaxation spectrum only because of the large value of T_1 (see Eq. (2)). The contribution of the slowly relaxing centers to the observed ESR absorption is estimated to be about 1% in these samples.

The results of the investigation of the rapidly relaxing part of the spectrum, which we attribute to Gd^{3+} ions in an ordinary metallic phase, are described in Ref. 7 and will not be examined in detail below. In the present Letter we shall concentrate on the slowly relaxing centers, which will be the subject of the discussion below.

The narrow line shown in Fig. 1 begins to appear in the signal U as the temperature

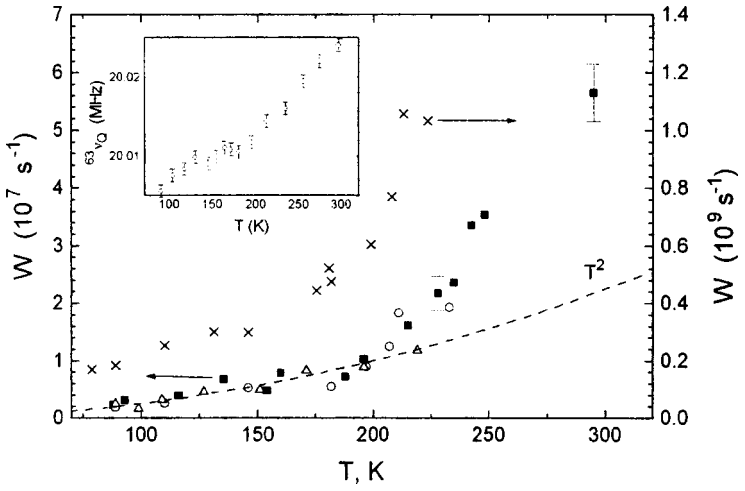

FIG. 2. Temperature dependence of the spin-lattice relaxation rate for the ''slow'' centers in Y-Ba-Cu-O:Gd^{3+} (left-hand scale): ○ — 123, $x=0.59$; Δ — 123, $x=0.95$; ■ — 1248; dashed curve — quadratic dependence; + — data of Ref. 7 for ''fast'' centers in 123, $x=0.59$ (right-hand scale). Inset: Temperature dependence of the NQR frequency of ^{63}Cu(1) in 1248.[2]

rises above 78 K. There are no special difficulties in distinguishing the signals due to the two types of centers, since the form of the rapidly relaxing component is known from ESR. Performing this separation and using Eq. (3), we obtained the temperature dependences of the spin-lattice relaxation rate $W=1/T_1$, which are shown in Fig. 2. One can see that at low temperatures the results for both samples are described quite well by the law $W\propto T^2$, but near 200 K the dependence changes, and at higher temperatures the experimental points (for $x=0.59$) lie appreciably higher. We note that at the same time a similar kink also occurs in the temperature dependence of the time T_1 for the ''fast'' centers; the corresponding data[7] are also shown in Fig. 2. At higher temperatures the method was too insensitive for reliable measurements because of the low density of ''slow'' centers. Much more definite results of this kind were obtained for the system 1248, which we discuss below.

The 1248 system. The central part of the ESR spectrum obtained on a magnetically oriented sample $Y_{0.99}Gd_{0.01}Ba_2Cu_4O_8$ for $\mathbf{B}\parallel c$ and $T=30$ K is shown in Fig. 3. The spectrum is unusual and does not correspond to the typical fine structure of a Gd^{3+} ion. Analysis showed that this is explained by the large ($\sim 50\%$) contribution from additional paramagnetic centers whose spectrum is virtually identical to the slowly relaxing component observed in the 123 samples. This is confirmed by the fact that the field dependences of the relaxation signals of type *V* for 1248 and 123 systems match (Fig. 1). Differentiating this dependence with the magnetic field we obtained the derivative of the corresponding ESR absorption signal. Then we subtracted this derivative from the observed spectrum. As one can see from Fig. 3, this procedure (with the proper fit of the amplitude) gives the ESR spectrum in a form characteristic for the fine structure of Gd^{3+} in the 1248 system.[10]

Thus the slowly relaxing centers which we observed earlier in 123 samples have

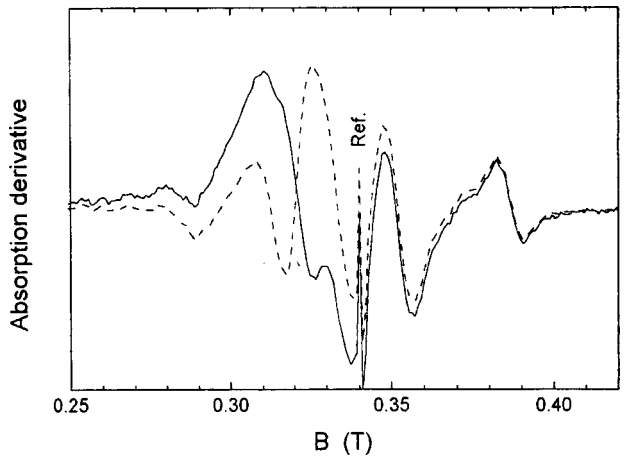

FIG. 3. Central part of the ESR spectrum of $Y_{0.99}Gd_{0.01}Ba_2Cu_4O_8$ with $\mathbf{B} \| c$, $T = 30$ K. Solid line — before processing; dashed curve — after subtraction of the signal from the ''slow'' centers.

also been found, with a much higher density, in the 1248 system. The latter circumstance made it difficult to investigate the relaxation of ''fast'' centers in the normal 1248 phase (the results for the superconducting phase will be published separately), but on the other hand more accurate measurements of T_1 could be performed for the ''slow'' centers right up to room temperature (filled squares in Fig. 2). One can see that right up to 180–200 K the experimental points lie on the curve $W \propto T^2$, and above 200 K they move sharply upward, more than two times above the previous dependence. We note that the data obtained on both materials (123 and 1248) match within the limits of the measurement error.

The main result of this work is the observation of a distinct feature — a sharp change in the slope of the temperature dependence T_1 near 190–200 K in $YBa_2Cu_4O_8$: 1%Gd^{3+} samples and, evidently, in the 123 system (at least for $x = 0.59$). The main question arising in this connection concerns the nature of the slowly relaxing centers demonstrating the anomaly indicated. Judging from the relatively large values of T_1 ($10^{-6} - 10^{-7}$ s) and from the typical for dielectrics quadratic temperature dependence in the range 80–200 K, most likely we are dealing with a nonconducting phase (in the metallic 123 phase the time T_1 is two orders of magnitude shorter, and its temperature dependence varies from a linear Koringa law to an exponential, due to the spin gap[5,7,11,12]). Thus the question posed above reduces to the following: Is the observed nonconducting phase macroscopic, i.e. parasitic and not associated with the experimental system, or have we encountered manifestations of a microscopic phase separation, which in the opinion of many authors is a fundamental characteristic of the lattices of oxide HTSCs?[13,14]

It is impossible to answer this question definitively on the basis of the present work. Of course, the simplest and most ''economical'' conclusion would be a macroscopic parasitic phase arising during synthesis. However, this assumption is difficult to reconcile with the existence of a similar jump in the temperature variation of T_1 of rapidly relaxing Gd^{3+} centers,[7] which unquestionably belong to the metallic phase. Even more convinc-

ing is the fact that the anomalies in the temperature dependences of the Knight shift, nuclear relaxation rates, and NQR frequencies, described by Suter *et al.*,[2] match in position and character. For comparison, one of these results is displayed in the inset in Fig. 2. It is difficult to imagine that the kink observed here at 180–200 K in the temperature variation of the quadrupole splitting of $^{63}\nu_Q$ could be due to an extraneous phase, macroscopically separated from the main lattice. Finally, it is impossible to ignore the unquestionable matching of the temperature at which these anomalies are observed with temperature T^* corresponding to the appearance of a spin gap.[1] These data can all be correlated by the hypothesis of microscopic phase separation in which the micro- or mesoscopic layers inside the HTSC material have different conducting and magnetic properties. Such electronic separation has been reliably observed in the La–Sr–Cu–O family of HTSCs and is being actively discussed in the literature (see, for example, Refs. 13 and 14). Evidently, it is also confirmed by recent experiments on electronic relaxation of Gd^{3+} in the 123 system.[7] In this case, the feature observed in the present work near 200 K could be explained by a phase transition in dielectric interlayers or chains separated from the metallic phase only microscopically and therefore inevitably having some influence on the nuclear and electronic relaxation in that phase. It is clear that the magnitude of the anomalies in the dielectric phase undergoing a phase transition should be much greater than in metallic layers which feel it only indirectly because of the proximity effect. This is what is observed experimentally.

The nature of the transition discussed is still unclear. For example, it can be correlated with antiferromagnetic ordering in CuO, occurring near 220 K,[15] or with hypothetical charge-density waves, whose appearance in the same temperature range is predicted theoretically in Ref. 3. It is obvious that further investigations are required to solve this problem.

We thank A. V. Duglav, A. V. Savinkov, and V. A. Ivan'shin for assisting in the preparation and inspection of the samples. This work was supported by the Russian Fund for Fundamental Research (Grants 96-02-19719 and 99-02-16024) and INTAS (Grant 96-0393).

*e-mail: atsarkin@mail.cplire.ru

[1] D. Brinkmann and M. Mali, NMR Basic Principles and Progress **31**, 171 (1994).
[2] A. Suter, M. Mali, J. Roos *et al.*, Phys. Rev. B **56**, 5542 (1997).
[3] I. Eremin, M. Eremin, S. Varlamov *et al.*, Phys. Rev. B **56**, 11305 (1997).
[4] P. Berastegui, M. Kakihana, M. Yoshimura *et al.*, J. Appl. Phys. **73**, 2424 (1993).
[5] V. A. Atsarkin, V. V. Demidov, and G. A. Vasneva, Phys. Rev. B **52**, 1290 (1995).
[6] V. A. Atsarkin, V. V. Demidov, and G. A. Vasneva, Phys. Rev. B **56**, 9448 (1997).
[7] V. A. Atsarkin, V. V. Demidov, and G. A. Vasneva, Appl. Magn. Reson. **15**, 323 (1998).
[8] S. Pekker, A. Jánossy, and A. Rockenbauer, Physica C **181**, 11 (1991).
[9] S. E. Barnes, Adv. Phys. **30**, 801 (1981).
[10] A. Jánossy, T. Feher, G. Oszlányi, and G. V. M. Williams, Phys. Rev. Lett. **79**, 2726 (1997).
[11] A. Jánossy, J. R. Cooper, L.-C. Brunel, and A. Carrington, Phys. Rev. B **50**, 3442 (1994).
[12] D. Shaltiel, C. Noble, J. Pilbrow *et al.*, Phys. Rev. B **53**, 12430 (1996).
[13] J. M. Tranquada, Physica C **282-287**, 166 (1997).
[14] O. N. Bakharev, M. V. Eremin, and M. A. Teplov, JETP Lett. **61**, 515 (1995).
[15] F. Mehran, S. E. Barnes, G. V. Chandrashekhar *et al.*, Solid State Commun. **67**, 1187 (1988).

Translated by M. E. Alferieff

Superfluidity of ''dirty'' excitons

Yu. E. Lozovik,* O. L. Berman, and A. M. Ruvinskiĭ
Institute of Spectroscopy, Russian Academy of Sciences, 142092 Troitsk, Moscow Region, Russia

(Submitted 22 March 1999)
Pis'ma Zh. Éksp. Teor. Fiz. **69**, No. 8, 573–578 (25 April 1999)

The effect of a random field due to impurities, boundary irregularities, and so on, on the superfluidity of a three-dimensional system of excitons and a quasi-two-dimensional system of direct or spatially indirect excitons is studied. The influence of a random field on the density of the superfluid component in the indicated excitonic systems at low temperatures T is investigated. The interaction between excitons is taken into account in the ladder approximation. For quasi-two-dimensional excitonic systems in a random field the Kosterlitz–Thouless temperature in the superfluid state is calculated. © *1999 American Institute of Physics.* [S0021-3640(99)00908-1]

PACS numbers: 71.35.Lk, 73.20.Dx

A system of spatially indirect excitons in coupled quantum wells[1–4] is of interest in connection with the superfluidity previously predicted for this system[5] and manifested as persistent electric currents, quasi-Josephson phenomena,[5] and unusual properties in strong magnetic fields.[6–8] Phase transitions occurring in systems with spatially separated electrons and holes were studied in Ref. 9. In these works the collective properties of indirect excitons in idealized *pure* systems neglecting the random field due to the presence of impurities and boundary irregularities of the quantum wells were studied.

However, in experiments a random field operates on a weakly-nonideal exciton gas. The transport properties of direct and indirect excitons and magnetoexcitons in random fields have been studied in Ref. 10, the influence of various random fields on excitonic and magnetoexcitonic absorption of light has been studied in Refs. 11 and 12, and Anderson localization of excitons has been studied in Ref. 13.

The effect of a random field on the superfluidity and the collective properties of excitons is of interest and has not been studied thus far. The effect of a random field on the properties of an excitonic system can be very substantial. Indeed, if the random field is sufficiently strong, it can induce a transition of the superfluid phase into a Bose-glass phase. We shall confine our attention to the effect of a weak random field on the collective properties and superfluidity of excitons in nonuniform systems.

In the present Letter we examine a rarefied system of three-dimensional excitons and two-dimensional excitons in a single quantum well and indirect excitons in coupled quantum wells in a random field. In two-dimensional systems the excitonic interaction in the Bogolyubov approximation operates only in an unphysically narrow range of the

system parameters because of the divergence of the two-dimensional scattering amplitude in the Born approximation. For this reason, the ladder approximation must be used to take account of the interaction between two-dimensional excitons. The random field was taken into account by perturbation theory. It is predicted here that a random field decreases the density n_s of the superfluid component in the indicated systems at low temperatures T and it also decreases the temperature of the superconducting transition induced by the random field.

Our analysis is also applicable to other physical realizations of nonuniform Bose systems, for example, liquid helium in random porous media[14] and so on.

We shall use perturbation theory up to second order in the interaction of excitons with the random field at finite temperatures T (see Fig. 1) to take account of the effect of the random field on the density of the superfluid component. In what follows we set $\hbar = k_B = 1$.

The Green's function $D^{(0)}(\mathbf{p}, i\omega_k)$ for the Bose condensate neglecting the random field is

$$D^{(0)}(\mathbf{p}, i\omega_k) = \frac{-(2\pi)^d n_0 \delta(\mathbf{p})}{\omega_k}, \quad \delta \to 0, \tag{1}$$

where $\omega_k = 2\pi kT$ (k is an integer), d is the dimension of the system, and n_0 is the density of the Bose condensate in the system of excitons in the absence of a random field.

The Green's function $D(\mathbf{p}, i\omega_k)$ of the Bose condensate taking account of the random field (Fig. 1) is

$$D(\mathbf{p}, i\omega_k) = D^{(0)}(\mathbf{p}, i\omega_k) + S_d^2 \int \frac{d\mathbf{p}}{(2\pi)^d} D^{(0)}(\mathbf{p_1}, i\omega_k) D^{(0)}(\mathbf{p_2}, i\omega_k)(G^{(0)}(\mathbf{p}, i\omega_k)$$
$$+ F^{(0)}(\mathbf{p}, i\omega_k) + G^{+(0)}(\mathbf{p}, i\omega_k) + F^{+(0)}(\mathbf{p}, i\omega_k) \langle\langle V^*_{\mathbf{pp_1}} V_{\mathbf{pp_2}} \rangle\rangle, \tag{2}$$

where $\langle\langle \ldots \rangle\rangle$ denotes averaging over various configurations of the random field, $S_{2(3)}$ is the area (volume) of the system, and $G^{(0)}(\mathbf{p}, i\omega_k)$ and $F^{(0)}(\mathbf{p}, i\omega_k)$ are the normal and anomalous Green's functions of the rarefied system of supercondensate particles[15] taking account of the weak repulsive interaction between excitons:

$$G^{(0)}(\mathbf{p}, i\omega_k) = -\frac{i\omega_k + \varepsilon_0(p) + \mu}{\omega_k^2 + \varepsilon^2(p)} \quad \text{and} \quad F^{(0)}(\mathbf{p}, i\omega_k) = -\frac{\mu}{\omega_k^2 + \varepsilon^2(p)}, \tag{3}$$

where $\varepsilon_0(p) = p^2/2M$ is the spectrum of noninteracting excitons, the spectrum of interacting excitons (in the absence of a random field) has the form $\varepsilon(p)$

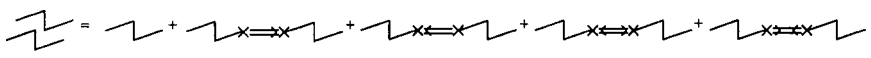

FIG. 1. Perturbation-theory diagrams for taking account of the effect of a random field on the Green's function of the condensate. A double straight line represents supercondensate particles, crosses represent the interaction with the random field, and broken lines represent the condensate.

$=\sqrt{(p^2/2M+\mu)^2-\mu^2}$, and for small momenta the excitation spectrum is acoustic $\varepsilon(p)=c_s p$, where $\mu=Mc_s^2$ is the chemical potential, M is the exciton mass, and c_s is the velocity of sound.

In the approximation employed (similarly to Ref. 14) only transitions of particles into and out of the condensate under the action of the random field are taken into account, and the scattering of supercondensate particles by the random field is neglected (but scattering of excitons by one another is taken into account in the ladder approximation — see above). The Green's function $D(x,x')$ is not a function only of the coordinate difference. In the momentum representation it can be considered to be only a function of the momentum $D(\mathbf{p},i\omega_k)$ only after averaging over different configurations of the random field.[15] The approximation used is valid provided that in the random field almost all particles at $T=0$ are in the condensate $(N-N_0)/N\ll 1$, if the correlation function of the random field is small with respect to the parameter: $\langle\langle V^*_{\mathbf{p}}V_{\mathbf{p}}\rangle\rangle/\mu^2\ll 1$. The fourth term in the perturbation theory (see Fig. 1) with four crosses contributes to the condensate density an amount less than the second term with respect to the same small parameter $(N-N_0)/N\ll 1$. The odd terms in the perturbation theory vanish for any Gaussian random field.

The density of the normal component, which is dissipated at the walls and impurities, can be calculated using the Kubo formula as the response of the total momentum to an external velocity:[16]

$$n_n=-\lim_{\omega\to 0}\left[\frac{Im(\pi(\omega))}{\omega}\right], \tag{4}$$

where $\pi(i\omega)$ is the polarization operator with zero transferred momentum

$$\pi(i\omega)=\frac{1}{dM}\sum_{\mathbf{p}} p^2 T\sum_{\omega_k'}\mathcal{F}(\mathbf{p},i\omega_k'+i\omega)\mathcal{F}(\mathbf{p},i\omega_k'), \tag{5}$$

where $\omega_k=2\pi kT$; $\mathcal{F}(\mathbf{p},i\omega_k')$ is the total single-particle Matsubara Green's function of an indirect exciton

$$\mathcal{F}(\mathbf{p},i\omega_k')=D(\mathbf{p},i\omega_k')+G(\mathbf{p},i\omega_k'). \tag{6}$$

The renormalization of the vertex by the interaction is neglected in the polarization operator (5). When the interaction is taken into account in the ladder approximation, a term which is small with respect to the parameter $M\Gamma\ll 1$ appears (Γ is the vertex in the ladder approximation). For a two-dimensional rarefied system of indirect excitons this parameter has the form $4\pi/\ln(1/8\pi n_{ex}M^2e^4D^4)\ll 1$ (n_{ex} and D are, respectively, the surface density of excitons and the distance between quantum wells, respectively).

We now substitute the Green's functions of the condensate (2) and supercondensate (3) particles into Eq. (6). Next, substituting the expression (6) into Eqs. (5) and (4) we have

$$n_n=n_n^0+\frac{N^2}{dM}\int\frac{d\mathbf{p}}{(2\pi)^d}p^2\langle\langle V^*_{\mathbf{p}}V_{\mathbf{p}}\rangle\rangle\frac{\varepsilon_0(p)}{\varepsilon^4(p)}. \tag{7}$$

Here N is the total number of particles, and n_n^0 is the density of the normal component in a pure system with no impurities,

$$n_n^0 = -\frac{1}{dM}\int \frac{d\mathbf{p}}{(2\pi)^d} p^2 \frac{\partial n(p)}{\partial \varepsilon}, \tag{8}$$

where $n_0(p) = (e^{\varepsilon(p)/T} - 1)^{-1}$ is the distribution of an ideal Bose gas of temperature excitations (compare with Ref. 14).

The first term in Eq. (7) corresponds to the contribution due to scattering of quasiparticles with an acoustic spectrum in an ordered system at $T \neq 0$ to the normal component. In a two-dimensional system $n_n^0 = 3\zeta(3)T^3/2\pi c_s^4 M$. The second term corresponds to the contribution of the interaction of the particles (excitons) with the random field to the normal component. The density of the superfluid component is $n_s = n - n_n$ (where n is the total density). In the approximation employed the random field does not affect the spectrum of collective excitations in the system. Therefore the random field decreases the density of the superfluid component.

For weakly interacting three- and two-dimensional direct excitons the sound velocity is, respectively,[9,17] $c_{s(3D)} = \sqrt{\mu/M} = \sqrt{13\pi n_{ex} a_{ex}/3M^2}$ (a_{ex} is the effective Bohr radius) and $c_{s(2D)} = \sqrt{\mu/M} = \sqrt{4.17 n_{ex}/M^2}$.

The theory of a weakly nonideal two-dimensional Bose gas can be used to take account of scattering of an indirect exciton by an indirect exciton.[18] The sound velocity for a two-dimensional system of particles interacting via a dipole-dipole repulsive interaction $U(R) = e^2D^2/R^3$ is in the ladder approximation

$$c_s = \sqrt{8\pi n_{ex}/2M^2 \ln(1/8\pi n_{ex} M^2 e^4 D^4)}.$$

In Eq. (7) $\varepsilon(p)$ is the collective spectrum, renormalized by the interaction between excitons, which for a rarefied system can be taken into account in the ladder approximation, making it possible to study the influence of a random field on two-dimensional systems of direct and indirect excitons, to describe which the Bogolyubov approximation works only in an unphysically narrow range of parameters of the system because of the divergence of the two-dimensional scattering amplitude in the Born approximation. However, two-dimensional systems are of interest in connection with experimental searches for superfluidity of a two-dimensional system of indirect excitons in coupled quantum wells.[1–3]

In a two-dimensional system superfluidity appears below the Kosterlitz–Thouless transition temperature $T_c = \pi n_s/2M$,[19] where only coupled vortices are present. Using the expression (7) for the density n_s of the superfluid component we obtain an equation for the Kosterlitz–Thouless transition temperature T_c. Its solution is

$$T_c = \left[\left(1 + \sqrt{\frac{16}{(6\cdot 0.45)^3 \pi^4} \left(\frac{MT_c^0}{n'} \right)^3 + 1} \right)^{1/3} + \left(1 - \sqrt{\frac{16}{(6\cdot 0.45)^3 \pi^4} \left(\frac{MT_c^0}{n'} \right)^3 + 1} \right)^{1/3} \right] \frac{T_c^0}{(4\pi)^{1/3}}. \tag{9}$$

Here T_c^0 is an auxiliary quantity, equal to the temperature at which the superfluid density vanishes in the mean-field approximation $n_s(T_c^0)=0$,

$$T_c^0=\left(\frac{2\pi n' c_s^4 M}{3\zeta(3)}\right)^{1/3}=\left(\frac{32}{3\zeta(3)\ln^2(1/8\pi n M^2 D^4)}\right)^{1/3}\frac{\pi n'}{M}. \tag{10}$$

In Eqs. (9) and (10) n' is

$$n'=n-\frac{N^2}{dM}\int\frac{d\mathbf{p}}{(2\pi)^d}p^2\langle\langle V_{\mathbf{p}}^* V_{\mathbf{p}}\rangle\rangle\frac{\varepsilon_0(p)}{\varepsilon^4(p)}. \tag{11}$$

Thus a random field decreases the Kosterlitz–Thouless transition temperature.

An interesting realization of a two-dimensional system of weakly interacting bosons is a system of indirect excitons in coupled quantum wells. Fluctuations of the thickness of a quantum well (QW), which arise during the fabrication process, lead to the appearance of a random field. The interaction of an indirect exciton and such a random field has the form

$$V(\mathbf{r}_e,\mathbf{r}_h)=V_e(\mathbf{r}_e)+V_h(\mathbf{r}_h), \tag{12}$$

where $\mathbf{r}_e$ and $\mathbf{r}_h$ are the electron and hole coordinates;

$$V_{e(h)}(\mathbf{r})=\alpha_{e(h)}(\xi_{1(3)}(\mathbf{r})-\xi_{2(4)}(\mathbf{r})), \tag{13}$$

where $\alpha_{e,h}=\partial E_{e,h}^{(0)}/\partial d_{e,h}$, $E_{e,h}^{(0)}$ are the lower energy levels of the electron and hole in the valence and conduction bands, d is the thickness of the wells, and $\xi_{1,2(3,4)}$ are fluctuations of the thickness on the top and bottom surfaces of the quantum well of an electron (hole). Next, we assume that fluctuations on different surfaces are statically independent, while on the ame surface they are described by a Gaussian correlation function of the white noise type

$$\langle\langle\xi_i(\mathbf{r}_1)\xi_j(\mathbf{r}_2)\rangle\rangle=g_i\delta_{ij}\delta(\mathbf{r}_2-r_1), \tag{14}$$

where g_i is proportional to the squared amplitude of the fluctuations of the ith surface.

Substituting the matrix element (12) of the transition from the state $\langle\mathbf{p}_1|$ into the state $\langle\mathbf{p}_2|$ for the excitonic wave functions in Eq. (11), we find the Kosterlitz–Thouless transition temperature, and the quantity

$$n'=n-\frac{n^2}{8c_s^2}[\alpha_e^2(g_1+g_2)+\alpha_h^2(g_3+g_4)]$$
$$\times\left(1+\frac{11}{8}M^2c_s^2a^2+\frac{3}{4}M^2c_s^2a^2\ln\left(\frac{1}{4}M^2c_s^2a^2\right)\right) \tag{15}$$

must be substituted into Eq. (9), where a is the effective Bohr radius of an indirect exciton, which depends on the distance between the e and h quantum wells, $a\approx a_{2D}=\epsilon/4m^*e^2$ for $D\ll a$, $a\sim a_{2D}^{1/4}D^{3/4}$ for $D\gg a$ ($m^*=m_em_h/(m_e+m_h)$, and m_e and m_h are the electron and hole masses, respectively).

The interaction of an exciton with the random field due to composition fluctuations of the solid substitution solution has the form[12]

$$V(\mathbf{r}_e,\mathbf{r}_h)=V(\mathbf{r}_e)+V(\mathbf{r}_h), \tag{16}$$

where

$$(\mathbf{r}_{e(h)})=\alpha_{e(h)}\xi(\mathbf{r}_{e(h)}), \tag{17}$$

$\alpha_{e,h}=(\partial E_{e,h}/\partial x)/N$, $\xi(\mathbf{r})$ is the fluctuation-induced change in the concentration of A sites, whose average fraction is x, and $\tilde{N}$ is the density of sites where atoms of both kinds can be found. The Gaussian random function $\xi(\mathbf{r})$ satisfies

$$\langle\langle \xi_i(\mathbf{r_1})\xi_j(r_2)\rangle\rangle = Nx(1-x)\,\delta(r_2-r_1). \tag{18}$$

Substituting the matrix element of the transition from the state $\langle \mathbf{p}_1|$ into the state $|\mathbf{p}_2\rangle$ (16) into Eq. (7) we find the density of the superfluid component

$$n_s=n_{\rm ex}-n_n^0-\frac{n^2 g(\alpha_e-\alpha_h)^2}{12\pi c_s}\left(1-\frac{35}{16}Mc_s a\right), \tag{19}$$

where $g=Nx(1-x)$ and $m_1=m_2=M/2$.

In summary, in the present Letter the effect of a random field on the density n_s of the superfluid component in a system of indirect excitons at low temperatures T and on the Kosterlitz–Thouless transition temperature in the superfluid state was analyzed. It was shown that the random field decreases the density of the superfluid component and the Kosterlitz–Thouless transition temperature.

This work was supported by grants from the Russian Fund for Fundamental Research, INTAS, and the International Scientific and Technical Program ''Solid-State Nanostructures.'' O. L. B. was supported by the program ''Soros Post-Graduate Students'' of the G. Soros Fund ISSEP and by the program ICFPM (International Center for Fundamental Physics in Moscow) (96-0457). A. M. R. was supported by the program ''Soros Graduate Students'' of the George Soros ISSEP Fund.

*e-mail: lozovik@isan.troitsk.ru

[1] T. Fukuzawa, E. E. Mendez, and J. M. Hong, Phys. Rev. Lett. **64**, 3066 (1990); J. A. Kash, M. Zachav, E. E. Mendez *et al.*, ibid. **66**, 2247 (1991).
[2] U. Sivan, P. M. Solomon, and H. Strikman, Phys. Rev. Lett. **68**, 1196 (1992).
[3] L. V. Butov, A. Zrenner, G. Abstreiter *et al.*, Phys. Rev. Lett. **73**, 304 (1994).
[4] M. Bayer, V. B. Timofeev, F. Faller *et al.*, Phys. Rev. B **54**, 8799 (1996).
[5] Yu. E. Lozovik and Yu. E. Yudson, JETP Lett. **22**, 274 (1975); Zh. Éksp. Teor. Fiz. **71**, 738 (1976) [Sov. Phys. JETP **44**, 389 (1976)]; Yu. E. Lozovik and V. I. Yudson, Solid State Commun. **19**, 391 (1976); A. V. Klyuchnik and Yu. E. Lozovik, Zh. Éksp. Teor. Fiz. **76**, 670 (1979) [Sov. Phys. JETP **49**, 335 (1979)].
[6] I. V. Lerner and Yu. E. Lozovik, Zh. Éksp. Teor. Fiz. **78**, 1167 (1980) [Sov. Phys. JETP **51**, 588 (1980)]; ibid. **80**, 1488 (1981) [Sov. Phys. JETP **53**, 763 (1981)]; ibid. **82**, 1188 (1982) [Sov. Phys. JETP **55**, 691 (1982)].
[7] A. B. Dzyubenko and Yu. E. Lozovik, Fiz. Tverd. Tela (Leningrad) **25**, 1519 (1983) [Sov. Phys. Solid State **25**, 874 (1983)]; ibid. **26**, 1540 (1984) [Sov. Phys. Solid State **26**, 938 (1984)]; A. B. Dzyubenko and Yu. E. Lozovik, J. Phys. A **24**, 415 (1991).
[8] Yu. E. Lozovik, O. L. Berman, and V. G. Tsvetus, JETP Lett. **66**, 355 (1997); Phys. Rev. B **59**, 5627 (1999).
[9] Yu. E. Lozovik and O. L. Berman, JETP Lett. **64**, 573 (1996); Zh. Éksp. Teor. Fiz. **111**, 1879 (1997) [JETP **84**, 1027 (1997)]; Fiz. Tverd. Tela (St. Petersburg) **39**, 1654 (1997) [Phys. Solid State **39**, 1476 (1997)]; A. V. Klyuchkov and Yu. E. Lozovik, Fiz. Tverd. Tela (Leningrad) **20**, 625 (1978) [Sov. Phys. Solid State **20**, 364 (1978)].
[10] Yu. E. Lozovik and A. M. Ruvinsky, Physica Scripta **58**, 90 (1998).
[11] Yu. E. Lozovik and A. V. Ruvinskiĭ, Zh. Éksp. Teor. Fiz. **114**, 1451 (1998) [JETP **87**, 788 (1998)].

[12] N. N. Ablyazov, M. É. Raĭkh, and A. L. Éfros, Fiz. Tverd. Tela (Leningrad) **25**, 353 (1983) [Sov. Phys. Solid State **25**, 199 (1983)].
[13] Zh. S. Gevorkyan and Yu. E. Lozovik, Fiz. Tverd. Tela (Leningrad) **29**, 1094 (1987) [Sov. Phys. Solid State **29**, 626 (1987)].
[14] K. Huang and H. F. Meng, Phys. Rev. Lett. **69**, 644 (1992); H. F. Meng, Phys. Rev. B **49**, 1205 (1994).
[15] A. A. Abrikosov, L. P. Gor'kov, and I. E. Dzyaloshinskiĭ, *Method of Quantum Field Theory in Statistical Physics* (Prentice-Hall, Englewood Cliffs, New Jersey, 1963) [Russian original, Fizmatgiz, Moscow, 1962].
[16] G. D. Mahan, *Many-Particle Physics* (Plenum Press, New York, 1990).
[17] L. V. Keldysh and A. N. Kozlov, Zh. Éksp. Teor. Fiz. **54**, 978 (1968) [Sov. Phys. JETP **27**, 521 (1968)].
[18] Yu. E. Lozovik and V. I. Yudson, Physica A **93**, 493 (1978).
[19] J. M. Kosterlitz and D. J. Thouless, J. Phys.: Condens. Matter **6**, 1181 (1973); D. R. Nelson and J. M. Kosterlitz, Phys. Rev. Lett. **39**, 1201 (1977).

Translated by M. E. Alferieff

Tunneling magnetoresistance and Hall effect of granular ferromagnetic metals

E. Z. Meĭlikhov

Institute of Molecular Physics, Russian Science Center ''Kurchatov Institute,'' 123182 Moscow, Russia

(Submitted 4 March 1999; resubmitted 22 March 1999)
Pis'ma Zh. Éksp. Teor. Fiz. **69**, No. 8, 579–584 (25 April 1999)

It is shown that two circumstances must be taken into account in order to describe the tunneling magnetoresistance and Hall effect in granular ferromagnetic metals: 1) the size variance of the metallic granules and 2) the percolation character of the tunneling conductivity of the system, determining the optimal (temperature-dependent) size of the granules through which current transport occurs. This complicates the dependences of the magnetoresistance and Hall resistance of the system on its magnetization and temperature. © *1999 American Institute of Physics.* [S0021-3640(99)01008-7]

PACS numbers: 75.50.Cc, 75.50.Kj, 73.50.Jt

Granular metals (metal-insulator nanocomposites) — a collection of small (size $a = 1-100$ nm) metallic inclusions in a dielectric matrix — possess a number of unique properties that depend on the volume content x of the conducting phase.[1–3] There exists a critical value x_c such that for $x>x_c$ the material possesses metallic properties and for $x<x_c$ it is a dielectric with a thermally activated conductivity. It has been established that it is due to the tunneling transitions of charge carriers between granules, and in this respect its mechanism is close to the well-known mechanism of hopping conductivity along impurities in doped semiconductors.[2] If the granule material is a ferromagnetic metal, such tunneling conductivity depends strongly on the magnetic field. The physical reason for this strong dependence is as follows. The probability of electronic tunneling through the insulator interlayer between two ferromagnetic metals (FM/I/FM transition) is determined by the relative orientation of the magnetic moments of the metallic electrodes. The tunneling conductance of an FM/I/FM junction is $G \propto (1+P^2\cos\theta)e^{-\xi}$, where $e^{-\xi}$ is the standard tunneling exponential, θ is the angle between the directions of the magnetic moments in the ''edges'' of the junction and depends on the external magnetic field, and $P=(D_\uparrow - D_\downarrow)/(D_\uparrow + D_\downarrow)$ is the magnetic-field-independent spin polarization of the conduction electrons in the ferromagnet ($D_\uparrow$ and $D_\downarrow$) are the densities of states at the Fermi level for electrons with $\uparrow$ and $\downarrow$ spins). The factor $\cos\theta$ arises because of the spinor transformation of the wave function of the electron, whose spin changes direction at a transition from one ferromagnet into the other.[4]

A magnetic field influences only the preexponential factor in the expression for the conductance of the tunneling junction. This means that the percolation model of conduc-

tivity, ordinarily employed to describe the properties of nonmagnetic nanocomposites, can also be used in the present case. Specifically, it is necessary to take account of the fact that when the size variance of the granules in the nanocomposite is large only a negligible fraction of the granules participates effectively in the conductivity, specifically, granules of so-called optimal size $a_{\rm opt}$, which decreases with increasing temperature.[5] The orientation of the magnetic moment of ferromagnetic granules in a magnetic field is determined by the magnitude of this moment, which is directly related with the granule size. For this reason, in contrast to the magnetization of the system, which is determined by *all* magnetic granules in it, the conductivity of a nanocomposite is determined only by granules with the ''optimal'' magnetic moment $\mu_{\rm opt}$, which is strongly temperature dependent. This circumstance is ignored in works devoted to the investigation and description of the properties of ferromagnetic granular metals with tunneling conductivity. Our objective in the present Letter is to show that the properties of magnetic nanocomposites can be described adequately only if the indicated circumstances are taken into account.

Since ferromagnetic granules are small, they are single-domain and are in a superparamagnetic state. The latter means that with respect to the action of an external magnetic field **H** and temperature T the collection of granules under study behaves similarly to a paramagnetic gas of atoms. The only difference is that in a gas the orientation of the atoms themselves changes together with their magnetic moments, whereas in stationary single-domain granules only the magnetic moment of the granules rotates.[6] As a result, the average relative orientation of the magnetic moments of neighboring granules, characterized by the quantity $\langle\cos\theta\rangle$, and hence also the average intergranular conductance $\langle G\rangle$ depend on the external magnetic field. In this model the calculation of the conductivity of the nanocomposite

$$\sigma(H,T)\propto\langle G\rangle\propto 1+P^2\langle\cos\theta\rangle \tag{1}$$

reduces to establishing the correct method of averaging $\langle\cos\theta\rangle$.

In what follows we shall consider only the situation where the interaction and hence the correlation of the directions of the magnetic moments of neighboring granules are negligible. Taking account of such a correlation (for example, using the simple scheme described in Ref. 7) shows that all conclusions derived below remain qualitatively unchanged. Let the moments of two neighboring granules 1 and 2 make the angles $\alpha_{1,2}$, $\beta_{1,2}$, and $\gamma_{1,2}$ with the coordinate axes x, y, and z, respectively. Then $\cos\theta=\cos\alpha_1\cos\alpha_2+\cos\beta_1\cos\beta_2+\cos\gamma_1\cos\gamma_2$. If an external magnetic field is directed along the z axis, then the angles $\alpha_{1,2}$ and $\beta_{1,2}$ (relative to the x and y axes) assume all values in the interval $[0,2\pi]$ with equal probability. Therefore $\langle\cos\alpha_1\cos\alpha_2\rangle=\langle\cos\beta_1\cos\beta_2\rangle=0$ and after averaging we obtain $\langle\cos\theta\rangle=\langle\cos\gamma_1\cos\gamma_2\rangle$, where now γ_1 and γ_2 are the angles between the magnetic moments of the granules and the external magnetic field. In the absence of a correlation between the directions of the magnetic moments of neighboring granules, the angles γ_1 and γ_2 are independent of one another, and therefore $\langle\cos\theta\rangle=\langle\cos\gamma\rangle^2$.

Having determined the relative magnetoresistance of the system as $\mathrm{MR}(H,T)=[\sigma(0,T)-\sigma(H,T)]/\sigma(0,T)$, taking account of Eq. (1) we obtain

$$\mathrm{MR}(H,T)=-P^2\langle\cos\gamma\rangle^2. \tag{2}$$

Thus the problem reduces to averaging over the angles γ between the external magnetic field and the magnetic moments of the granules that actually contribute to the conductivity of the system.

The simplest case is averaging over *all granules*[8] Then, assuming that the granules are all spheres with the same radius a_0 and therefore possess *identical magnetic moments* $\mu_0=(4\pi/3)a_0^3 I_s$ (I_s is the saturation magnetization of the granule material), the well-known Langevin formula can be used for the total magnetic moment of the system:

$$M(H,T)=N\mu_0\langle\cos\gamma\rangle=N\mu_0 L(m_0 H/kT), \quad L(x)=\coth(x)-1/x \tag{3}$$

(N is the total number of granules). Then

$$\mathrm{MR}(H,T)=-P^2L^2(\mu_0 H/kT)=-P^2[M(H,T)/M_s]^2, \tag{4}$$

where $M_s=N\mu_0$ is the saturation magnetic moment.

However, the size variance of the granules and hence their magnetic moments are virtually always quite large. If granules are once again assumed to be spherical, then this variance can be described by the distribution function $f(a)$ of their radii a. In this case the granules possess *different magnetic moments* $\mu=(4\pi/s)a^3 I_s$, whose variance is characterized by the distribution function $\varphi(\mu)=f[a(\mu)](\partial a/\partial\mu)=(36\pi I_s)^{-1/3}\times\mu^{-2/3}f[a(\mu)]$. In this case the total magnetic moment of the system

$$M(H,T)=N\int_0^\infty \mu L(\mu H/kT)\varphi(\mu)d\mu \tag{5}$$

once again is determined by averaging over *all* granules. However, to calculate the conductivity (and magnetoresistance) of the system only the granules which actually contribute to the conductivity need be taken into account. As shown in Ref. 5, from this standpoint only granules with sizes close to the ''optimal'' size are important: $a\approx a_{\mathrm{opt}}\propto T^{-1/2}$. Then we obtain from Eq. (2)

$$\mathrm{MR}(H,T)=-P^2L^2[\mu_{\mathrm{opt}}(T)H/kT], \tag{6}$$

where $\mu_{\mathrm{opt}}(T)=(4\pi/3)a_{\mathrm{opt}}^3(T)I_s$. The direct proportionality $\mathrm{MR}(H,T)\propto[M(H,T)]^2$, characteristic for a system where all granules have the same size, naturally, does not hold.

The model used in Ref. 5 is completely applicable to systems far from the percolation threshold. For this reason, the theoretical dependence (6) must be compared with experiments for systems with $(x_c-x)\gtrsim 0.1$. Such a comparison, moreover, requires knowledge of $\mu_{\mathrm{opt}}(T)$ at least for one temperature, for example, at room temperature $T=300$ K. If $\mu_{\mathrm{opt}}\equiv\mu_{300}$ is known, then $\mu_{\mathrm{opt}}(T)=\mu_{300}(300/T)^{3/2}$. Therefore μ_{300} can be used as an adjustable parameter.

The magnetoresistance of the systems $\mathrm{Fe}_x(\mathrm{SiO}_2)_{1-x}$ with $x<0.45$ was investigated in Ref. 9. Figure 1 shows the experimental temperature dependence $\mathrm{MR}(T)$ for a system with $x=0.26$. The theoretical dependence (6) shown in the same figure agrees well with experiment if it is assumed[1)] that $\mu_{300}=1450\mu_B$ and $P=0.2$. We should mention the following concerning the adjustable parameter μ_{300} found above. Since μ_{opt} decreases with increasing temperature, it should be expected that $\mu_{\mathrm{opt}}<\langle\mu\rangle=M_s/N$, since granules with large values of μ, which are ineffective from the standpoint of tunneling conductivity (because they are separated by large distances), make a large contribution to $\langle\mu\rangle$.[5] Approximating the magnetic-field dependence of the magnetization of the system

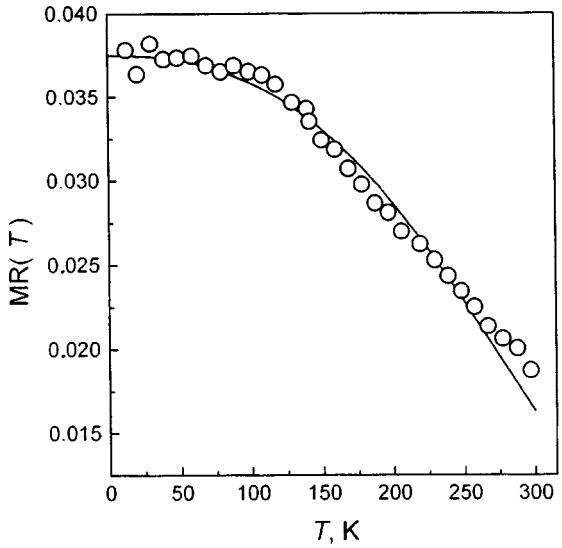

FIG. 1. Temperature dependences of the relative magnetoresistance MR(T,H=9 kOe) for the system $Fe_x(SiO_2)_{1-x}$ with $x=0.26$. Circles — experiment of Ref. 8. Curve — calculation using Eq. (6) with the parameters $P=0.2$ and $\mu_{300}=1450\mu_B$.

$Fe_x(SiO_2)_{1-x}$ with $x=0.26$ by a sum of two Langevin functions, the authors of Ref. 9 show that the system contains two types of Fe granules: large granules with magnetic moment $\mu_L=12500\mu_B$ and small granules with magnetic moment $\mu_S=2620\mu_B$, the concentration of the small granules being an order of magnitude higher than that of the large granules. Setting aside for the time being the question of the correctness of such an analysis (see below), we conclude that the adjustable quantity μ_{300} is indeed less than the values presented for μ_L and μ_S.

Taking account of the temperature dependence of the granule size changes (compared with a system of identical granules) the temperature dependence of the magnetoresistance, which is especially strong for weak magnetic fields. In the latter case, it follows from Eqs. (4) and (6) (since $\mu_{\rm opt}\propto T^{-3/2}$) that

$$\mathrm{MR}(H\to 0)\propto\begin{cases} T^{-2}, & \text{same size granules,} \\ T^{-5}, & \text{large granule-size variance.} \end{cases} \tag{7}$$

Figure 2 shows MR(T) in various magnetic fields.

We shall now discuss the correctness of the often used (see, for example, Refs. 7, 9, and 11) procedure for reconstructing the distribution function $\varphi(\mu)$ from the experimentally measured dependence $M(H,T)$. Mathematically, the problem reduces to solving the integral equation (5) and is a so-called ill-posed problem.[12] This means that in the absence of *a priori* information about the form of the function $\varphi(\mu)$ (and such information is almost always lacking) and in view of the approximate character of the experimental data many approximate solutions with radically different properties can be found for this equation. In approximating the function $M(H)$ by a sum of several Langevin functions

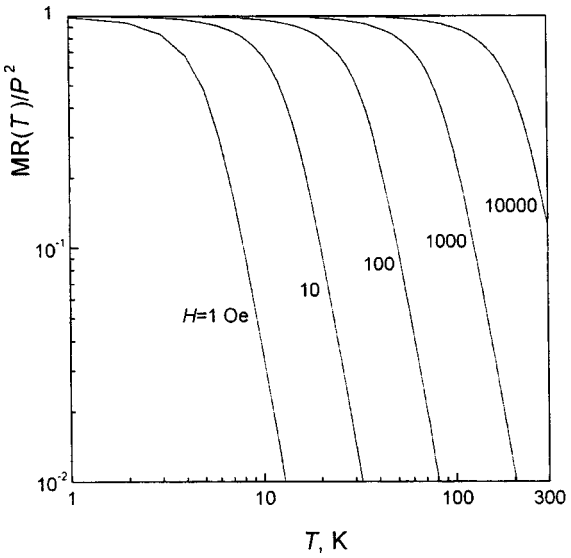

FIG. 2. Temperature dependences of the normalized relative magnetoresistance $\mathrm{MR}(T)/P^2$ in various magnetic fields. The curves were calculated using Eq. (6) for $\mu_{300}=1450\mu_B$.

the authors proceed from the unfounded assumption that the system consists of two[9,11] or four[7] sharply defined fractions and is not described by a wide and continuous distribution function $\varphi(\mu)$. The fact that this is doubtful is seen at least by comparing the results of a similar approximation and the TEM photographs of the experimental systems. Thus the procedure of approximation used in Ref. 9 ''shows'' that the system supposedly consists of granules with two sizes — 15 and 25 Å, while the particles with irregular shapes and arbitrary sizes, less than approximately 50 Å, can be seen in the photographs.

To illustrate how questionable the results obtained using this procedure are, we used Eq. (5) to calculate the magnetic-field dependence of the magnetization for the distribution function used in Ref. 11:

$$\varphi(\mu)=[1/\sqrt{2\pi}\sigma\mu]\exp[-\ln^2(\mu/\mu_0)/2\sigma^2]. \tag{8}$$

In Fig. 3 this function is shown by bars whose length represents the measurement error, equal to 3%. The figure also shows curves which were obtained by the described approximation for several sets of granule parameters. One can see that within the limits of accuracy of the ''experiment'' these sets are all indistinguishable (despite the large difference between them). This attests to the incorrectness of this procedure and many conclusions based on it.

We shall now consider the Hall effect in the system under study. It is known that in bulk ferromagnets two components contribute to the Hall field:[13]

$$\mathbf{E}^{(H)}=[R_0\mathbf{B}+4\pi R_s\mathbf{I}]\times\mathbf{j}. \tag{9}$$

One component corresponds to the normal Hall effect, which is associated with the Lorentz force and is proportional to the magnetic induction B (R_0 is the normal Hall coefficient). The other component, corresponding to the so-called anomalous Hall effect,

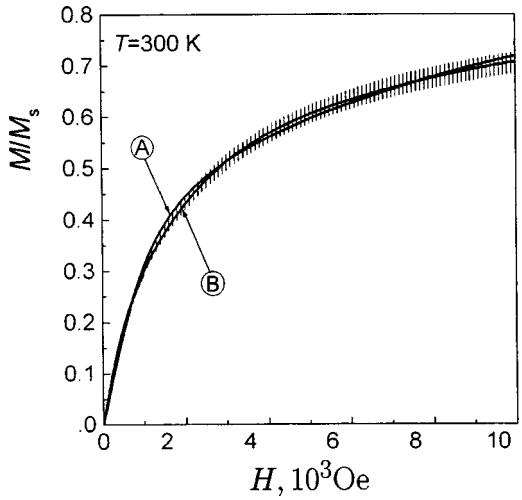

FIG. 3. Magnetic field dependence of the magnetization, calculated using Eq. (5), for a system of granules whose magnetic moments are distributed according to the law (8) with the parameters $\mu_{300}=250\mu_B$ and $\sigma=1.16$ at $T=300$ K. The length of the vertical bars represent a relative error of 3%. The curves were obtained by fitting the results of the numerical experiment with a sum of two (*A*) and three and four (*B*) weighted Langevin functions: $M/M_s=\Sigma_i \eta_i L(\mu_i H/kT)$, where $\eta_i=n_i\mu_i/\Sigma_i n_i\mu_i$ and n_i are, respectively, the relative fraction and concentration of granules of the *i*th kind. The adjustable sets of parameters (for the dominant fractions consisting of the smallest granules) are: *A* — $\mu_1=170\mu_B$, $\eta_1=0.92$, $\mu_2=2400\mu_B$, $\eta_2=0.08$ (system of two fractions); *B* — $\mu_1=100\mu_B$, $\eta_1=0.87$, $\mu_2=1000\mu_B$, $\eta_2\approx 0.13$ (system of three fractions); $\mu_1=65\mu_B$, $\eta_1=0.85$, $\mu_2=610\mu_B$, $\eta_2\approx 0.13$ (system of four fractions — first variant); $\mu_1=33\mu_B$, $\eta_1=0.78$, $\mu_2=330\mu_B$, $\eta_2\approx 0.22$ (system of four fractions — second variant).

is proportional to the magnetization I of the ferromagnet (R_s is the anomalous Hall coefficient). It is related with the spin-orbit interaction of conduction electrons with scatterers (phonons, magnetic inhomogeneities), which leads to their ''asymmetric scattering'' (skew scattering) or ''lateral displacement'' (side-jump).[14]

The tunneling current flows through granules of optimal size $a_{\rm opt}$, separated from one another by an average distance ℓ. Let this current be parallel to the x axis, and let the external magnetic field once again be directed along the z axis. Since ordinarily $R_s \gg R_0$, the Hall electric field arising in a granule is $\mathbf{e}\sim 4\pi R_s \mathbf{I}\times(\mathbf{i}/a_{\rm opt}^2)$, where $|\mathbf{i}|\sim|\mathbf{j}|\ell^2$ is the current in an individual granule and $|j|$ is the average current density. The Hall field $E^{(H)}$, directed along the y axis, in a sample is related by the simple relation $\mathbf{E}^{(H)}\sim\langle \mathbf{e}(a_{\rm opt}/\ell)\rangle$ with the Hall fields $\mathbf{e}$ in individual granules (here averaging is performed over all granules of optimal size). Therefore

$$\mathbf{E}^{(H)}\sim(4\pi R_s/\ell a_{\rm opt})\langle \mathbf{I}\times\mathbf{i}\rangle, \tag{10}$$

which after averaging gives $E_y^{(H)}\sim(4\pi R_s/\ell a_{\rm opt})\langle I_z\rangle\langle i_x\rangle = 4\pi R_s I_s\langle\cos\gamma\rangle(\ell/a_{\rm opt})j$. Here we have assumed all particles to be single-domain and hence $|I|=I_s$, and in addition we took account of the fact that $\langle i_x\rangle = j\ell^2$. In the absence of an interaction between granules we obtain hence for the Hall resistivity

$$\rho_H(H,T)\equiv E_y^{(H)}/j_x = 4\pi R_s I_s L[\mu_{\rm opt}(T)H/kT](\ell/a_{\rm opt}). \tag{11}$$

From the relations (6) and (11) for the relative magnetoresistance and Hall resistivity follows

$$|\mathrm{MR}| = \rho_H^2[(P/4\pi R_s I_s)(a_{\mathrm{opt}}/\ell)]^2. \tag{12}$$

At constant temperature (and in a varying magnetic field) the expression on the right-hand side of Eq. (12) remains constant, so that (if the model under study is correct) experiment should give the simple dependence $|\mathrm{MR}| \propto \rho_H^2$, making it possible to find the anomalous Hall effect. The experiments of Ref. 15 on measurement of the magnetoresistance and Hall effect in the systems $\mathrm{Fe}_x(\mathrm{SiO}_2)_{1-x}$ confirm this conclusion.

This work was supported by the Russian Fund for Fundamental Research (Grants 99-02-16955-a and 98-02-17412-a) and the program PICS–RFFI (Grant 98-02-22037).

[1)]The value of P presented can be compared with the known value $P \approx 0.3$ for Co.[8,10]

[1] Thematic issue, Philos. Mag. **65** (1992).
[2] C. J. Adkins, in *Metal-Insulator Transitions Revisited*, edited by P. P. Edwards and C. N. R. Rao (Taylor and Francis, 1995); J. Phys.: Condens. Matter **1**, 1253 (1989).
[3] P. Sheng, Philos. Mag. B **65**, 357 (1992).
[4] J. C. Slonczewski, Phys. Rev. B **39**, 6995 (1989).
[5] E. Z. Meĭlikhov, Zh. Eksp. Teor. Fiz. **115**, 624 (1999) [*sic*].
[6] S. V. Vonsovskiĭ, *Magnetism*, Vols. 1 and 2 (Wiley, New York, 1974) [Russian original, Nauka, Moscow, 1971].
[7] P. Allia, M. Knobel, P. Tiberto, and F. Vinai, Phys. Rev. B **52**, 15398 (1995).
[8] J. Inoue and S. Maekawa, Phys. Rev. B **53**, R11927 (1996).
[9] S. Honda, T. Okada, M. Nawate, and M. Tokumoto, Phys. Rev. B **56**, 14566 (1997).
[10] C. H. Shang, J. Nowak, R. Jansen, and J. S. Moodera, Phys. Rev. B **58**, R2917 (1998).
[11] E. F. Ferrari, F. C. S. da Silva, and M. Knobel, Phys. Rev. B **56**, 6086 (1997).
[12] A. N. Tikhonov and V. Ya. Arsenin, *Solutions of Ill-Posed Problems* (Halsted Press, New York, 1977, translation of the 1st Russian edition) [Russian original, 2nd edition, Nauka, Moscow, 1979].
[13] A. V. Vedyaev, A. B. Granovskiĭ, and O. A. Kotel'nikova, *Kinetic Phenomena in Disordered Ferromagnetic Alloys* (Moscow State University Press, Moscow, 1992).
[14] J. M. Luttinger, Phys. Rev. **112**, 739 (1958).
[15] V. V. Ryl'kov and D. Yu. Kovalev, private communication.

Translated by M. E. Alferieff

Stochastic resonance between limit cycles. Spring pendulum in a thermostat

Yu. N. Gornostyrev, D. I. Zhdakhin, and M. I. Katsnel'son
Institute of Metal Physics, Ural Branch of the Russian Academy of Sciences, 620219 Ekaterinburg, Russia

A. V. Trefilov
Russian Science Center ''Kurchatov Institute,'' 123182 Moscow, Russia

(Submitted 18 March 1999)
Pis'ma Zh. Éksp. Teor. Fiz. **69**, No. 8, 585–589 (25 April 1999)

The effect of white noise on phase synchronization is studied numerically for a classical model of a spring pendulum with a multiple ratio of the frequencies of small oscillations (Vitt–Gorelik model). It is shown that in the model investigated a Fermi resonance regime occurs for a system in a thermostat. A new type of nonlinear dynamics is found — stochastic resonance between limit cycles. © *1999 American Institute of Physics.* [S0021-3640(99)01108-1]

PACS numbers: 46.40.Ff, 05.40.Ca, 05.45.−a

The problem of the effect of noise (for example, thermal fluctuations) on the dynamical behavior of complicated nonlinear systems has been investigated traditionally in connection with the study of various scenarios leading to the appearance of turbulence.[1] In so doing it was assumed that the phenomena associated with the appearance of chaos in deterministic systems play the main role, while fluctuations do not lead to any qualitative changes in the behavior of these systems. In the last few years investigators have turned their attention to phenomena associated with stochastic resonance (SR)[2,3] which are observed in the most diverse processes (from chemical reactions to the evolution of the earth's climate) and in which noise plays a ''constructive'' role. Stochastic resonance appears as a more or less periodic behavior of a system with several positions of equilibrium under the action of random forces, in the simplest case — white noise. It is natural to ask about the possibility of SR-related phenomena in systems with attractors of a more complicated nature than a position of equilibrium (focus), for example, with limit cycles.[4] Although related problems have already been discussed (dynamic intermittency and deterministic SR in systems with chaotic behavior[3]), noise-induced transitions between limit cycles have not yet been considered. Limit cycles describe self-excited oscillations as well as phase synchronization in systems with several degrees of freedom. We shall be interested in the latter case. In the present Letter, in studying the Fermi resonance phenomenon well known in the physics of molecules[5] and crystals,[6] we demonstrate an analog of SR between limit cycles.

The clearest model describing Fermi resonance is the model of a spring pendulum with the frequencies of small oscillations in the ratio 1:2 (the Vitt–Gorelik model[7]). In

the absence of noise and dissipation it is described by the Lagrangian

$$L = 1/2(\dot{x}^2 + \dot{y}^2) - V(x,y), \tag{1}$$

$$V = \frac{k}{2}(r-l)^2 + gr(1-\cos\phi)$$

$$= 1/2\left\{ \omega_0^2[x^2+(y+1)^2] + 2(\Omega_0^2-\omega_0^2)\sqrt{x^2+(y+1)^2} - 2\Omega_0^2(y+1) + \frac{(\Omega_0^2-\omega_0^2)}{\omega_0^2} \right\},$$

where $\omega_0 = \sqrt{k}$ and $\Omega_0 = \sqrt{g/l}$ are the frequencies of small oscillations of the load on the spring and of the pendulum, respectively; k is the stiffness of the spring (the mass of the load is 1); g is the acceleration of gravity; r is the length of the spring; l is the equilibrium length of the spring; ϕ is the polar angle; and, x and y are Cartesian coordinates in units of l (the coordinate origin is located at the suspension point). The values of the parameters for which the frequencies are nearly in a multiple ratio $\omega_0 = 2\Omega_0 + \Delta$, $\Delta \ll \Omega_0$, are studied. This model describes the classical Fermi resonance regime, for example, for C–H bonds in organic molecules.[5] True, the classical limit $T \gg \hbar\omega_0$ cannot be literally achieved in this case, since $\hbar\omega_0 \geqslant 10^3$ K. However, as shown in Ref. 6, the model (1) for small x and y also describes phenomena related with the Fermi resonance for phonons at a definite point of the Brillouin zone of the bcc phase of alkali and alkaline-earth metals, where the classical case is of the main interest. When phonon damping (dissipation) and interaction with the thermostat are taken into account, synchronization is possible in the system.[6] As a result, a certain combination of the phases of the two oscillations is no longer random and for sufficiently small Δ the true ratio of the oscillation frequencies becomes precisely 1:2 (phase-locking). From the standpoint of the general theory of dynamical systems, synchronization corresponds to bifurcation of a torus into a limit cycle.[4] A numerical solution of the corresponding equations of motion for this system showed that for small amplitudes of the oscillations[8] the system possesses two synchronization regimes, i.e. *two* limits cycles. Together with the clarity of the initial mechanical system, this makes the Vitt–Gorelik model a suitable object for solving our problem.

The effect of noise and dissipation on the dynamics of the system was investigated by solving the numerically Langevin equations

$$\ddot{x} + 2\gamma\dot{x} + \frac{\partial V}{\partial x} = f_x(t),$$

$$\ddot{y} + 2\Gamma\dot{y} + \frac{\partial V}{\partial y} = f_y(t), \tag{2}$$

where γ and Γ are the damping constants (of the order of $10^{-2}\omega_0$) and f_i are Gaussian random forces of the white-noise type with correlation functions

$$\langle f_x(t) f_x(t') \rangle = 4T\gamma\delta(t-t'),$$

$$\langle f_y(t) f_y(t') \rangle = 4T\Gamma\delta(t-t'),$$

$$\langle f_x(t) f_y(t') \rangle = 0. \tag{3}$$

This choice of correlation functions guarantees that a Gibbs distribution with temperature T will be achieved in the state of thermodynamic equilibrium ($t \to \infty$).[9] To solve the

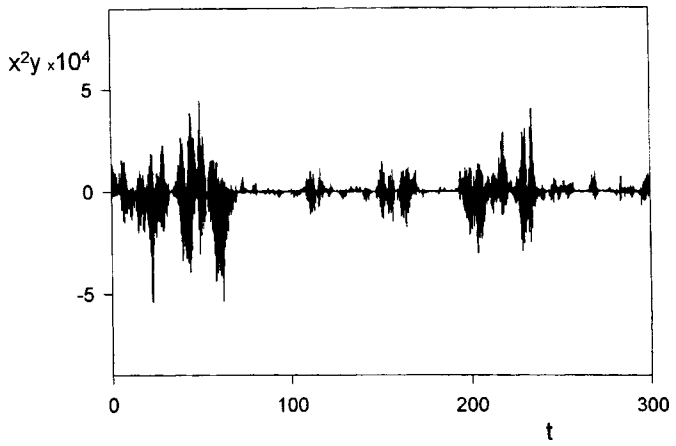

FIG. 1. Typical dependence $x^2(t)y(t)$ in the stationary state with $\Delta=0$, $T=0.025$, $\gamma=0.005$, and $\Gamma=0.005$.

system of stochastic differential equations (2) numerically we used one of the ''strong'' (rms) methods proposed in Ref. 10. Methods of this type guarantee convergence not only for quantities averaged over the realizations of the random force but also for individual trajectories (see Ref. 11 and the literature there for a more detailed discussion). The ''weak'' methods which we used in a previous work[8] did not make it possible to draw definite conclusions about the character of the dynamical behavior of the system under study, except to establish the fact of synchronization itself.

The initial quantities for analysis are the trajectories $x(t)$ and $y(t)$ in the stationary state, which was monitored according to the matching (to within 0.1%) of the distribution functions of the velocities $\dot{x}$ and $\dot{y}$ to the Maxwellian distribution. It is convenient to investigate intermode energy transfer by following the quantity $x^2(t)y(t)$. The typical form of this quantity for $\Delta=0$ and not too high temperatures $T\ll\omega_0^2 l^2$ is shown in Fig. 1. The latter inequality guarantees small oscillation amplitudes (for values of the parameters corresponding to Fig. 1 $|x|\leqslant 0.1$ and $|y|\leqslant 0.05$). Then, as follows from Eq. (1), the product x^2y is proportional to the intermode interaction energy.

One can see from Fig. 1 that the dynamics of intermode energy transfer is very complicated with sections of strong coupling alternating with sections of weak coupling. Figure 2 shows the results for the ''filtered'' variable

$$s(t)=\Omega_0\int_{t-n\pi/\Omega_0}^{t+n\pi/\Omega_0} x^2(t')y(t')\cos(4\Omega_0 t')\,dt' \tag{4}$$

(in Fig. 2 $n=2$). The variable $s(t)$ makes it possible to follow directly the appearance or disappearance of the phase-synchronization regime, since it is proportional to $\cos\Phi$, where $\Phi=2\phi_x+\phi_y$ and ϕ_x and ϕ_y are the phases of the variables x and y. As shown in Ref. 8, the values $\Phi\approx 0$ and $\Phi\approx\pi$ correspond to two limit cycles, so that $s(t)$ remaining positive for a sufficiently long period of time corresponds to motion according to the first limit cycle and negative $s(t)$ corresponds to the second limit cycle.

As one can see from Fig. 2, the synchronization regions (I) alternate with regions of chaotic motion, where $s\approx 0$. Moreover, fast transitions from one limit cycle to the other

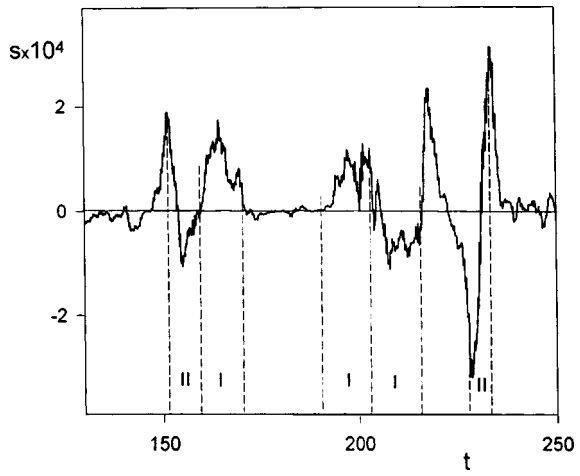

FIG. 2. $s(t)$ (see the expression (4)) for the same parameters as in Fig. 1. The sections corresponding to phase synchronization (limit cycles) are designated by I, and the sections corresponding to fast transitions between limit cycles are designated by II.

(II), to some extent similar to the ''transit'' trajectories in a bistable system,[11] are observed. The spectral density of $s(t)$ has a distinct maximum (Fig. 3), so that alternation of the time intervals during which phase synchronization occurs is of an approximately periodic character. The observed low-frequency dynamics is similar in this sense to SR, which occurs in this system despite the absence of several positions of equilibrium. Their role is played by limit cycles (regions of the type I in Fig. 2).

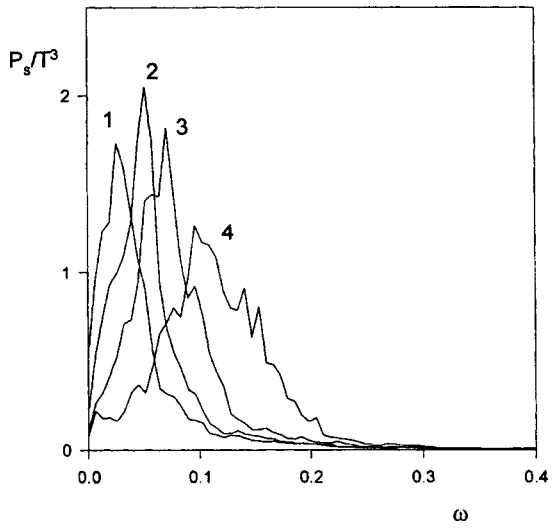

FIG. 3. Ratio of the spectral density $P_s(\omega)=|s_\omega|^2$ to T^3 for $\Delta=0$, $\gamma=0.005$, and $\Gamma=0.005$. The curves *1–4* are presented for $T=0.0002$, 0.0005, 0.001, and 0.0025, respectively.

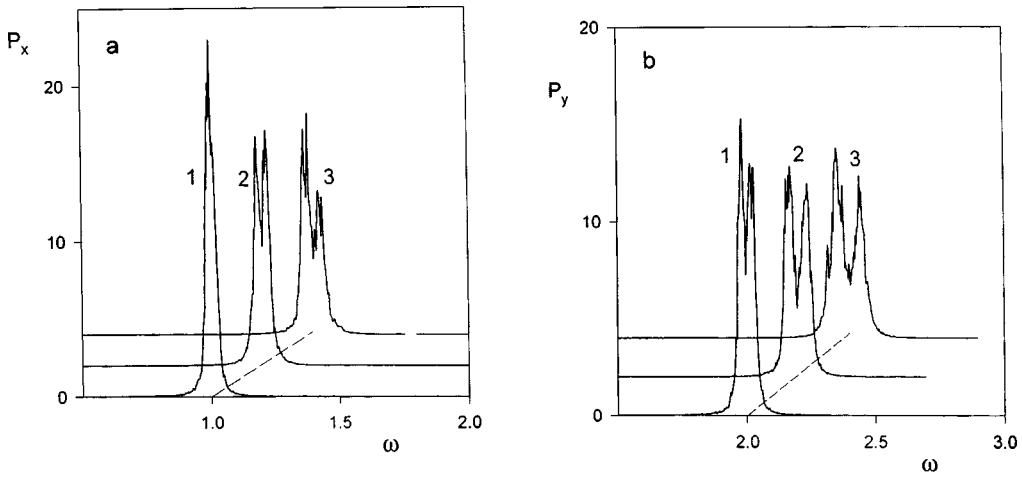

FIG. 4. Spectral densities $P_x(\omega)=|x_\omega|^2$ and $P_y(\omega)=|y_\omega|^2$ normalized to 1 for $\Delta=0$, $\gamma=0.005$, and $\Gamma=0.005$. The curves *1–3* are presented for $T=0.001$, 0.0025, and 0.005, respectively. For convenience the coordinate origin of the curves *2* and *3* is shifted.

As the noise intensity increases (the temperature increases), the ''resonance'' frequency increases and the resonance itself broadens. To determine the temperature behavior of the effects under discussion, the spectral density, made dimensionless by normalizing to the characteristic thermal-noise level T^3, is presented in Fig. 3. The intensity of the peak changes nonmonotonically with increasing T, which demonstrates the ''constructive'' role of noise in its formation. This behavior is a characteristic feature of SR.[2] It follows from our calculations that the picture remains unchanged in the entire range of frequency detunings Δ where synchronization exists at all ($\Delta \leqslant 0.1\omega_0$ for the dampings chosen), while the characteristics of SR (determined from the Fourier spectrum) are essentially independent of Δ.

The Fourier spectra for the coordinates x and y (Fig. 4) demonstrate splitting of the main peaks, which is strictly the analog of a Fermi resonance.[5] Our calculations with no dissipation and no random forces agree with the analytical results of Ref. 7 on the dependence of the intensity of the ''upper'' and ''lower'' peaks on the initial conditions. In the presence of noise averaging over the initial conditions occurs and both peaks are always present.

In conclusion, we note that in our opinion the stochastic resonance phenomenon demonstrated here between limit cycles could be quite general . It requires the presence of more than one limit cycle, corresponding to phase synchronization, which, as one can see, occurs even in such a simple and natural model as a spring pendulum. With an eye toward the possible application of the results obtained to the Fermi resonance in the vibrational spectra of molecules and the phonon spectra of metals, it would be interesting to study the behavior of the system in the quantum case. In the semiclassical approximation the latter is described by color (so-called blue) noise in a Langevin type equation.[12] Unfortunately, only ''weak'' methods[12] have been used to simulate such systems numerically, while ''strong'' systems have not even been developed. The question of the specific nature of the phenomena related to phase synchronization and SR in quantum

systems is of great interest and could be studied by such methods.

This work was supported by the Russian Fund for Fundamental Research, Project 98-02-16219.

[1] J.-P. Eckmann, Rev. Mod. Phys. **53**, 643 (1981); H. G. Schuster, *Deterministic Chaos* (Physik-Verlag, Weinheim, 1984; Mir, Moscow, 1988).
[2] L. Gammaitoni, P. Hänggi, P. Jung, and F. Marchesoni, Rev. Mod. Phys. **70**, 223 (1998).
[3] V. S. Anishchenko, A. B. Neĭman, F. Moss, and L. Shimanskiĭ-Gaĭer, Usp. Fiz. Nauk **169**, 7 (1999).
[4] A. A. Andronov, A. A. Witt, and S. É. Khaĭkin, *The Theory of Oscillations* (Fizmatgiz, Moscow, 1959); *Strange Attractors*, edited by Ya. G. Sinaĭ and L. P. Shil'nikov (Mir, Moscow, 1981); V. I. Arnol'd, V. S. Afraĭnovich, Yu. S. Il'yashenko, and L. P. Shil'nikov, *The Theory of Bifurcations* (VINITI, Current Problems in Mathematics, Vol. 5, Moscow, 1986).
[5] M. P. Lisitsa and A. M. Yaremko, *The Fermi Resonance* (Naukova Dumka, Kiev, 1984).
[6] M. I. Katsnel'son and A. V. Trefilov, Zh. Éksp. Teor. Fiz. **97**, 1891 (1990) [Sov. Phys. JETP **70**, 1061 (1990)].
[7] A. A. Vitt and G. S. Gorelik, Zh. Tekh. Fiz. **3**, 294 (1933).
[8] Yu. N. Gornostyrev, M. I. Katsnel'son, A. P. Platonov, and A. V. Trefilov, Zh. Éksp. Teor. Fiz. **107**, 925 (1995) [JETP **80**, 525 (1995)].
[9] N. G. Van Kampen, *Stochastic Processes in Physics and Chemistry* (Elsevier, New York, 1983) [Russian translation, Vysshaya shkola, Moscow, 1984].
[10] G. N. Milshtein and M. V. Tret'yakov, Preprint, IAAS No. 102, Weierstrass–Institut für Angewandte Analysis und Stochastik, Berlin, 1994.
[11] Yu. N. Gornostyrev, M. I. Katsnel'son, and A. V. Trefilov, JETP Lett. **56**, 529 (1992); Yu. N. Gornostyrev, M. I. Katsnelson, A. V. Trefilov, and S. V. Tretjakov, Phys. Rev. B **54**, 3286 (1996).
[12] U. Eckern, W. Lehr, A. Mentzel-Dorwath *et al.*, J. Stat. Phys. **59**, 885 (1990).

Translated by M. E. Alferieff

Fluctuations with a $1/f^{\alpha}$ spectrum in film boiling

V. N. Skokov, V. P. Koverda, and A. V. Reshetnikov
Institute of Thermal Physics, Ural Branch of the Russian Academy of Sciences, 620219 Ekaterinburg, Russia

(Submitted 25 March 1999)
Pis'ma Zh. Éksp. Teor. Fiz. **69**, No. 8, 590–593 (25 April 1999)

$1/f$ and $1/f^2$ noise were observed experimentally in film boiling of water on vertically oriented platinum heater. Fluctuations with a $1/f^{\alpha}$ spectrum were observed in a wide range of controlling parameters and seen over five orders of magnitude in frequency. It was noted that the process investigated is similar to the phenomenon of self-organized criticality. © *1999 American Institute of Physics.*
[S0021-3640(99)01208-6]

PACS numbers: 05.40.Ca, 68.60.Dv

Stochastic processes with a spectrum inversely proportional to the frequency (flicker or $1/f$ noise) are observed in systems of different nature and have long been the subject of intensive investigations.[1–5] Interest in random processes with divergent spectral characteristics has revived in recent years in connection with the discovery of self-organized criticality.[6] In self-organized criticality the system arrives at critical behavior in the course of its evolution and fine tuning of the controlling parameters is not required. The concept of self-organized criticality is extremely general and can be used to describe the behavior of dynamical systems of different nature,[7] but experimental investigations have been performed only on the model sandpile system. A characteristic feature of a system in a state of self-organized criticality is the presence of fluctuations of dynamical variables with a spectral density of the type $1/f$ or $1/f^2$. Fluctuations of two types have been observed experimentally in the sandpile model system[6,8] and are predicted by the continuum theory.[9]

In Refs. 10–12 we reported the experimental observation of thermal pulsations with a $1/f$ spectrum during Joule heating of a superconductor in a boiling coolant. The distinguishing feature of these experiments is that only one source of stochastic signals with a $1/f$ spectrum was present in the system and the system could be regarded as lumped. The origin of the intense thermal pulsations with the spectral density inversely proportional to frequency is due to the interaction of nonequilibrium phase transitions in nonlinear subsystems — a superconductor with the current and the boiling coolant. A mathematical model of concurrent nonequilibrium phase transitions, which consists of a system of stochastic nonlinear differential equations which convert white noise into two modes of oscillations with spectral densities proportional to $1/f$ and $1/f^2$, was proposed in Refs. 11 and 12. This model satisfactorily describes the experimental results of Refs. 10–12 on the observation of $1/f$ noise, but the accompanying $1/f^2$ spectrum predicted by theory was not observed experimentally.

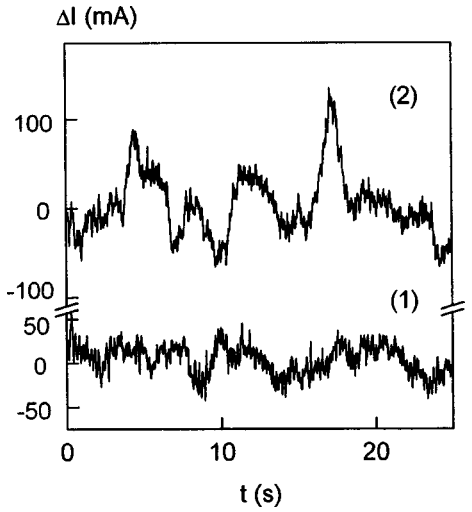

FIG. 1. Oscillograms of transport-current fluctuations for two regimes of film boiling on a vertical heater. *1* — Regime with a $1/f$ spectrum, *2* — regime with a $1/f^2$ spectrum.

In the present Letter we report the results of an experimental study of fluctuations accompanying nonequilibrium phase transitions where it was possible to observe stochastic oscillations with the spectral densities $1/f$ and $1/f^2$.

Film boiling on a Joule-heated wire heater was chosen as the object of investigation. The transition from bubble to film boiling (crisis of boiling) is a typical nonequilibrium first-order phase transition. The dynamics of the transition to crisis of boiling depends strongly on the spatial orientation of the heater. For a horizontal arrangement of the heater the transition from bubble to film boiling occurs in the form of autowave propagation of a vapor film along the heater.[13,14] For a vertically oriented heater domain instability arises, which under certain conditions leads to the appearance of traveling domain structures.[13,14] The dependence of the observed picture on the spatial orientation is due to the fact that for a vertical heater there exists an additional longitudinal temperature gradient caused by convective removal of vapor along the heater.

The experiments were performed with distilled water, into which a 100 μm in diameter and about 2 cm long platinum wire heater was inserted. The measurements were performed with a fixed source voltage. The oscillations of the transport current in the circuit which are associated with boiling were recorded in the experiments.The spectral densities were determined from the measured realizations by the Fourier-transform method.

When film boiling arose on a horizontally arranged heater, a vapor film propagated over a distance of about 1.5 cm. In contrast to experiments with superconducting heaters,[10–12] the heating zone is not localized so that the direct and reverse transitions from bubble to film boiling occurred under different loads, since the external perturbation due to the irregularity of the vapor removal is not enough to give a reversible transition between the two boiling regimes. The spectral densities of the oscillations of both bubble

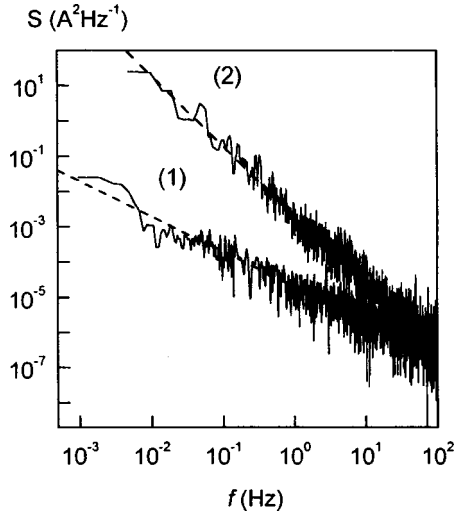

FIG. 2. Frequency dependences of the spectral density of fluctuations for two regimes of film boiling. Dashed lines — $1/f$ (*1*) and $1/f^2$ (*2*) dependences.

and film boiling on a horizontal heater were of a Lorentzian form with a characteristic horizontal shelf at low frequencies.

A different picture was observed for a vertical heater. The source of film boiling arising at a weak location of the wire rapidly propagated upwards over a distance of 1–1.5 cm. The transition to film boiling was accompanied by a large increase in temperature. The process was observed through a microscope. A cone-shaped vapor jet rose along the wire from the bottom boundary of the hot zone. The length of the hot zone fluctuated appreciably.

Oscillograms of the transport current were recorded on an S9-8 oscillograph using a time step from 1 ms to 0.5 s with 2048-point realizations, which made it possible to cover the frequency range from 10^{-3} to 10^2 Hz. The spectral densities calculated from the experimental oscillograms of film boiling had the form $1/f^{\alpha}$ in a wide range of input power. The values of α depended on the input heat power. When film boiling was quite stable, α was close to 1, i.e. $1/f$ noise was observed in the system in a wide range of controlling parameters. As the power decreased, the picture changed near the instability of film boiling. The amplitude of the fluctuations of the hot zone increased. Outwardly, the picture resembled an inverted sandpile, and the fluctuations of the length of the hot zone resembled the descent of an avalanche. The exponent α in the region of instability of film boiling was close to 2.

Figure 1 shows typical oscillograms for the two regimes described above. The oscillogram 1 in Fig. 1 corresponds to relatively stable film boiling on a vertical heater, and the oscillogram 2 corresponds to instability of the film regime. The distribution functions for the amplitudes of the oscillations in the first case were approximately symmetric with a maximum near zero and resembled Gaussian distributions. In the second case the distribution functions near zero split into two peaks and had longer ''tails.'' Longer realizations are required for quantitative analysis of the distribution functions and

to determine whether the behavior of the distribution of ''avalanches'' in the region of large outbursts is exponential or power-law.

Figure 2 shows the spectral densities of fluctuations for two film-boiling regimes in the experimental frequency range. The densities were obtained by ''joining'' the spectra for individual oscillograms with a different time step. The dashed line in Fig. 2 shows $1/f$ and $1/f^2$ curves. One can see from this figure that the $1/f^\alpha$ behavior is observed over five orders of magnitude.

It should be underscored that the $1/f^\alpha$ behavior of the spectral density of the fluctuations was observed for all oscillograms in the region of film boiling and in a wide range of input powers. The low-frequency limit of the indicated behavior was observed only when the input power was too high and the upper limit of the hot zone reached the end of the wire. In other words, the critical behavior indicated by the $1/f^\alpha$ spectra is maintained in a wide range of and without adjustment of the controlling parameters.

In summary, in the present work wideband $1/f^\alpha$ noise was observed during film boiling of a liquid. The behavior of the spectra in a wide range of external parameters and the general picture of the process suggest that the process investigated is similar to the phenomenon of self-organized criticality.

[1] Sh. M. Kogan, Usp. Fiz. Nauk **145**, 285 (1985) [Sov. Phys. Usp. **28**, 170 (1985)].
[2] R. O. Zaĭtsev, JETP Lett. **58**, 915 (1993).
[3] Yu. L. Klimontovich, *Statistical Theory of Open Systems, Vol. 1: A Universal Approach to Kinetic Description of Processes in Active Systems* (Kluwer Academic Publishers, Dordrecht–Boston, 1995) [Russian original, TOO ''Yanus,'' Moscow, 1995].
[4] Yu. E. Kuzovlev, Zh. Éksp. Teor. Fiz. **111**, 2086 (1997) [JETP **84**, 1138 (1997)].
[5] G. P. Zhigal'skiĭ, Usp. Fiz. Nauk **167**, 623 (1997).
[6] P. Bak, C. Tang, and K. Wiesenfeld, Phys. Rev. A **38**, 364 (1988).
[7] S. L. Ginzburg and N. E. Savitskaya, Pis'ma Zh. Éksp. Teor. Fiz. **68**, 688 (1998) [JETP Lett. **68**, 719 (1998)].
[8] G. F. Held, D. H. Solina, D. T. Keane *et al.*, Phys. Rev. Lett. **65**, 1120 (1990).
[9] A. Mehta, J. M. Luck, and R. J. Needs, Phys. Rev. E **53**, 92 (1996).
[10] V. P. Koverda, V. N. Skokov, and V. P. Skripov, JETP Lett. **63**, 775 (1996).
[11] V. P. Koverda, V. N. Skokov, and V. P. Skripov, Zh. Éksp. Teor. Fiz. **113**, 1748 (1998) [JETP **86**, 953 (1998)].
[12] V. P. Koverda and V. N. Skokov, Physica A **262**, 376 (1999).
[13] S. A. Zhukov, L. F. Bokova, and V. V. Barelko, Int. J. Heat Mass Transf. **26**, 269 (1983).
[14] V. V. Barelko and S. A. Zhukov, Teplofiz. Vys. Temp. **33**, 73 (1995).

Translated by M. E. Alferieff

ERRATA

Erratum: Experimental evidence for Coulomb charging effects in submicron Bi-2212 stacks [JETP Lett. 69, No. 1, 84–90 (10 January 1999)]

Yu. I. Latyshev, S.-J. Kim. and T. Yamashita

Pis'ma Zh. Éksp. Teor. Fiz. **69**, No. 8, 594–595 (25 April 1999)

[S0021-3640(99)01308-0]

PACS numbers: 85.25.Cp, 74.50.+r, 99.10.+g

For technical reasons, the reproduction quality of the oscillograms was unsatisfactory.

The editorial board apologizes to the authors and readers and reproduces the figures here. These same figures can be seen at cond-mat./9903134.

Translated by M. E. Alferieff

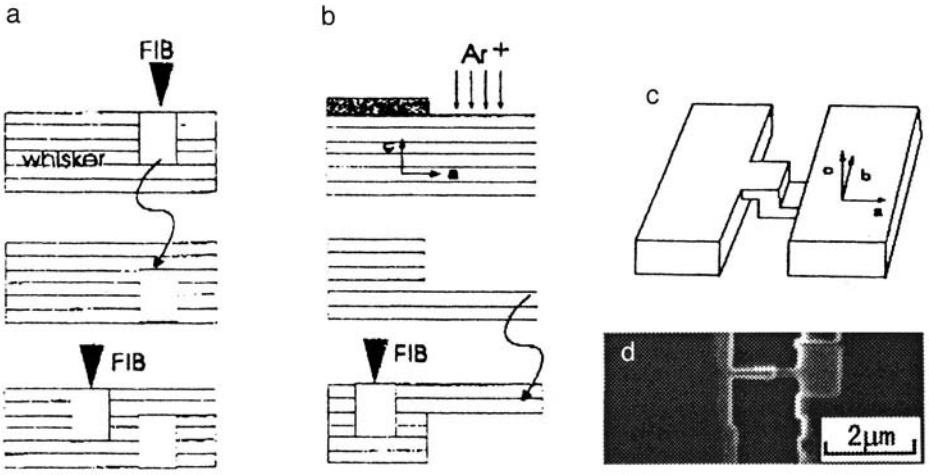

FIG. 1. Stages of the stack fabrication with FIB (a), FIB combined with ion milling (b), a schematic view (c), and a micrograph of the submicron Bi-2212 stacked junction (d).

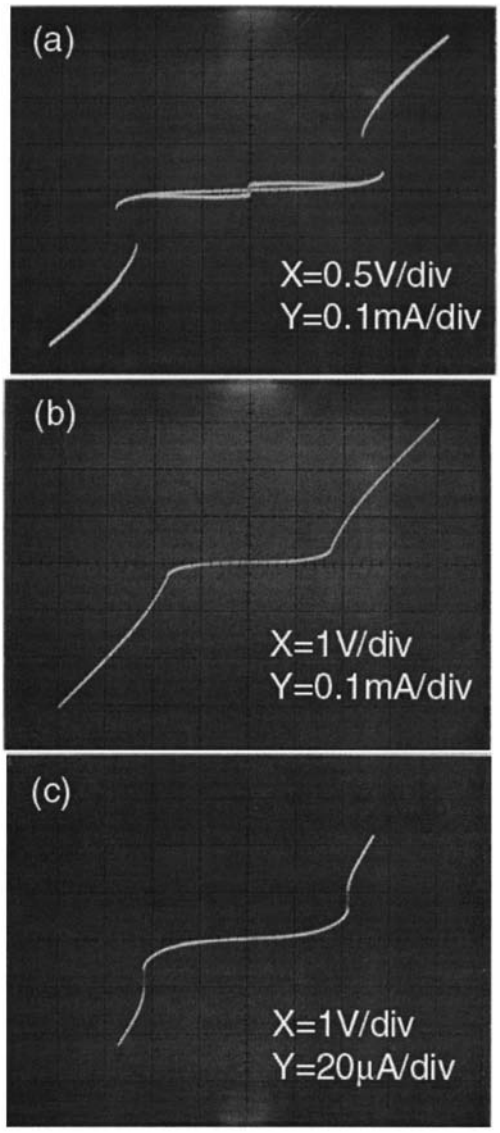

FIG. 2. The I–V characteristics of the Bi-2212 stacks on a large current and voltage scale: (1) #2, $S=2\ \mu m^2$; (b) #4, $S=0.6\ \mu m^2$; (c) #6, $S=0.3\ \mu m^2$. $T=4.2$ K.

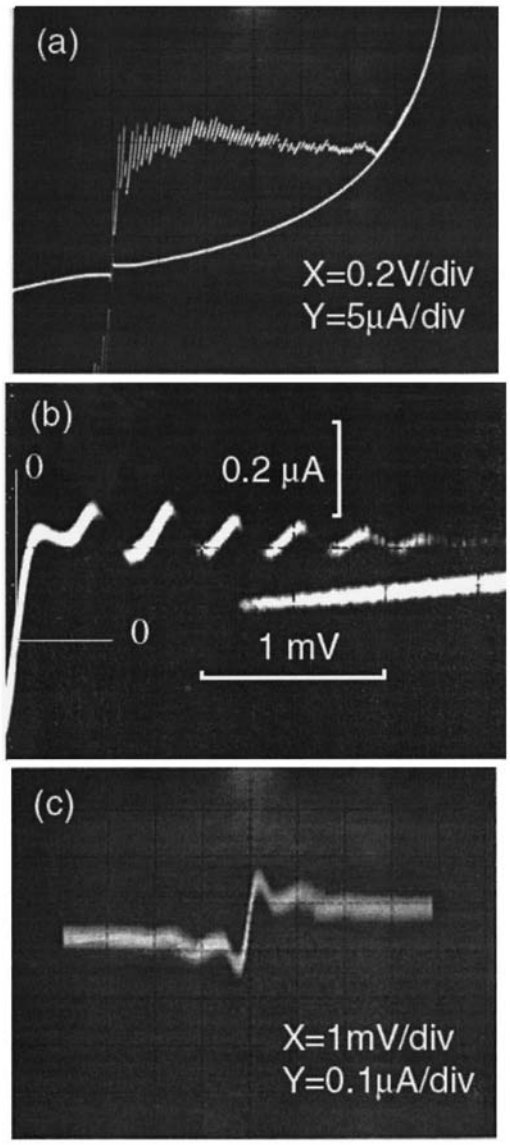

FIG. 3. The I–V characteristics of the Bi-2212 stacks on a small current and voltage scale: (1) #2, $S=2\ \mu m^2$; (b) #4, $S=0.6\ \mu m^2$; (c) #6, $S=0.3\ \mu m^2$. $T=4.2$ K.

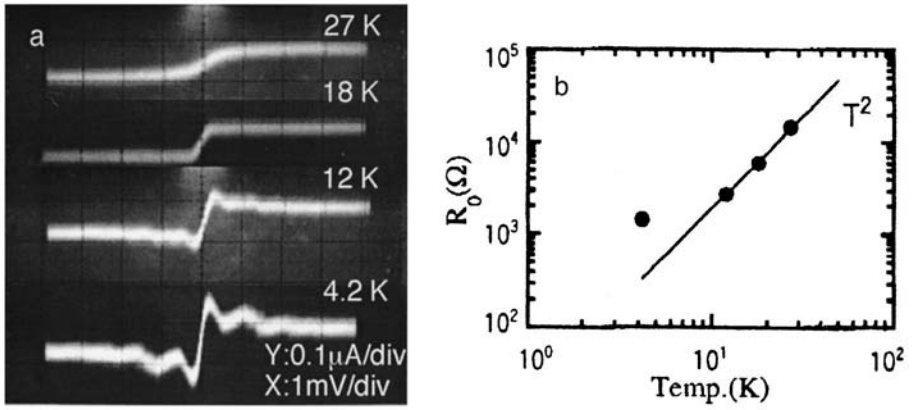

FIG. 4. Temperature evolution of the periodic structure on the I–V characteristics (a) and the temperature dependence of the zero-bias resistance R_0 (b) of Bi-2212 stack #6, $S = 0.3\ \mu\text{m}^2$.